

Dear Editor,

first of all, we would like to thank you for giving us the opportunity to further prove the scientific robustness of our study.

As you have requested, we have performed new simulations, where changes in key atmospheric components (namely: chemical species, tropospheric ice and differences between our sulfate distribution and that of CCSM-CAM4) and their radiative effects are coupled on-line with surface temperature perturbations. In the responses to Reviewers 2 and 3 and in the revised manuscript we explain in detail how this was made.

Furthermore, as you requested, we have responded to all the objections posed by the new reviewers. Considering a specific suggestion of the Reviewers, we have further expanded the evaluation of our model's output with ERA5 and MLS data.

A point by point response to the reviews is attached below, together with a marked-up copy of the manuscript with all the changes tracked.

Daniele Visioni on behalf of all authors

**Response to Reviewer #2.**

Referee comments are in black, **author responses are in blue.**

**I appreciate the authors' time in a careful revision of the manuscript, but I am unable to recommend publication in ACP for this paper.**

**I am still not convinced that the method the authors have chosen is appropriate, and the authors attempts to convince me of this are insufficient.**

**I do not think that you can impose SST perturbations from one model on another model, and expect that they will not have an impact. Because the models are different, the CCSM state applied to ULAQ is going to create imbalances that are not realistic, and would not be seen in CCSM4. Furthermore, CCSM4 itself does not have a realistic stratospheric circulation, so that any SST response to sulfate geoengineering is approximate. This would be fine, except there is a more sophisticated version of that model available with a stratosphere, and several papers have been written using fully coupled (to an ocean) versions of this model.**

**I think you are attempting to attribute changes that may be affected by the method and have nothing to do with a response to geoengineering.**

**I do not see how the present study adds to the literature, except to confuse the issues, and do not see how the authors would be able to get around this point. I am sorry, but I think this method is ill posed.**

We understand the Reviewer's point and decided to explicitly calculate SG-driven changes in surface temperatures in the ULAQ-CCM at any grid point and time step. This is done by superimposing to the background RCP4.5 surface temperatures calculated in the CCSM-CAM4 model (and used as prescribed boundary condition in the ULAQ-CCM itself) the SG-driven surface temperature perturbation associated with the ULAQ-CCM radiative flux changes produced by SG with an injection of 8 Tg-SO<sub>2</sub>/yr. These radiative flux changes are those produced by stratospheric sulfate aerosols and upper tropospheric ice particles, as well as those produced by changes of greenhouse gases directly and indirectly affected by stratospheric geoengineering aerosols (i.e., O<sub>3</sub>, H<sub>2</sub>O, CH<sub>4</sub> and CO<sub>2</sub> from changing methane oxidation). The ULAQ-CCM calculated SG effects on these greenhouse gases were documented in Pitari et al. (2014) and Visioni et al. (2017). Details on the ULAQ-CCM calculation of SG aerosol microphysics, size distribution, optical thickness, transport, strat-trop exchange and radiative impact are given in Visioni et al. (2018), as well as in Pitari et al. (2014).

In order to minimize the approximation introduced from a missing explicit ocean module in the ULAQ-CCM, the procedure adopted in the calculation of the SG perturbation on surface temperatures is described below.

- (a) As a first approximation, we use in our G4 experiment the CCSM-CAM4 predicted surface temperatures with inclusion of the radiative impact of geoengineering aerosols (with injection of 8 Tg-SO<sub>2</sub>/yr); this ocean-atmosphere coupled simulation does not include chemistry and upper tropospheric ice particle changes induced by SG. As discussed in Tilmes et al. (2016), the stratospheric aerosol distribution used in CCSM-CAM4 is sufficiently robust and validated. As clearly shown in Table 3 of the revised

manuscript, the net tropopause RF from these aerosols represent by far the largest contribution to the net SG RF.

- (b) However, as the Reviewer points out, the aerosol distribution calculated on-line in the ULAQ-CCM (which is based on a well-tested microphysics scheme and detailed stratosphere) may be different from the one in CCSM-CAM4, thus introducing a potentially significant inconsistency in the modeling scheme. To correct for this undesired effect, the ULAQ-CCM radiative-climate module has been modified for calculating on-line (in a fully coupled approach) the surface temperature perturbation produced by radiative flux changes due to the sulfate aerosol imbalance with respect to the CCSM-CAM4 distribution. In addition, we also include in the radiative balance the SG-driven indirect perturbation of greenhouse gases (see above), as well as upper tropospheric ice particles (which are the focus of the present study). Table S1, Fig. S2 and Fig. 6 of the revised manuscript document the effects of these radiative flux changes on the calculated surface temperatures.
- (c) Surface temperature changes due to the above discussed indirect SG effects are calculated from the instantaneous perturbation of radiative fluxes, which is of course an exact procedure over continents and polar ice caps, whereas is only approximate over the oceans. On the other hand, as well explained above and clearly visible in Table S1, Fig. S2 and Fig. 6, the radiative perturbation additive to the dominant one (that is the one produced by stratospheric sulfate aerosols in the CCSM-CAM4 simulation) is normally small, both globally and locally. Only the ice induced changes of surface temperatures may be comparable in magnitude to those from the stratospheric aerosols, but limited to tropical continental surfaces, where UT ice may have a significant optical depth. On the other hand, the SST calculated changes due to chemistry and ice indirect effects of SG are usually smaller, so that the impact of our approximation may be expected to be negligible.

## References:

- Pitari, G., Aquila, V., Kravitz, B., Robock, A., Watanabe, S., Cionni, I., De Luca, N., Di Genova, G., Mancini, E., and Tilmes, S.: Strato- spheric ozone response to sulfate geoengineering: Results from the Geoengineering Model Intercomparison Project (GeoMIP), *Journal of Geophysical Research: Atmospheres*, 119, 2629–2653, 2014.
- Tilmes, S., Lamarque, J.-F., Emmons, L. K., Kinnison, D. E., Marsh, D., Garcia, R. R., Smith, A. K., Neely, R. R., Conley, A., Vitt, F., Val Martin, M., Tanimoto, H., Simpson, I., Blake, D. R., and Blake, N.: Representation of the Community Earth System Model (CESM1) CAM4-chem within the Chemistry-Climate Model Initiative (CCMI), *Geoscientific Model Development*, 9, 1853–1890, doi:10.5194/gmd- 9-1853-2016, <https://www.geosci-model-dev.net/9/1853/2016/>, 2016.
- Visioni, D., Pitari, G., Aquila, V., Tilmes, S., Cionni, I., Di Genova, G., and Mancini, E.: Sulfate geoengineering impact on methane transport and lifetime: results from the Geoengineering Model Intercomparison Project (GeoMIP), *Atmospheric Chemistry and Physics*, 17, 11 209– 11 226, doi:10.5194/acp-17-11209-2017, <https://www.atmos-chem-phys.net/17/11209/2017/>, 2017.
- Visioni, D., Pitari, G., Tuccella, P., and Curci, G.: Sulfur deposition changes under sulfate geoengineering conditions: quasi-biennial oscilla- tion effects on the transport and lifetime of stratospheric aerosols, *Atmospheric Chemistry and Physics*, 18, 2787–2808, doi:10.5194/acp- 18-2787-2018, <https://www.atmos-chem-phys.net/18/2787/2018/>, 2018.

### Response to Reviewer #3.

Reviewer comments are in black, **author responses are in blue.**

The manuscript by Vioni et al. aims at investigating the impact of geoengineering by stratospheric sulfur injections on upper tropospheric cirrus formations using the ULAQ-CCM. My comments below refer only to the revised version of the manuscript. I was not involved in the review process of the first manuscript version, but from the authors' response to the Reviewer comments I understand that they reran the model simulations due to an inadequate model setup in the first round.

#### Overall comment:

My overall impression is that the study indeed targets an interesting and important side effect of sulfate geoengineering, namely changes in upper tropospheric cirrus clouds, but that the chosen methodology and the performed analysis of the model results are flawed. I am afraid that the ULAQ-CCM is simply not the right tool for such an investigation (details see below). At least from what is written in the paper I am not convinced that the results are valid and provide substantial new insights. In the present form I cannot recommend this paper for publication in ACP.

#### General comments:

1) **Model approach:** Although I agree with the authors that it is a common approach to use sea surface temperatures and sea ice coverage from coupled ocean-atmosphere models in chemistry-climate models, I think that this approach is not appropriate for all kind of research questions. In the present case I have strong doubts that the change in sea surface temperatures as simulated by CCSM-CAM4 for G4 (no chemistry, simplified ice cloud scheme) is consistent with ULAQ-CCM's G4 aerosol distributions and the change in ozone, clouds, etc. From Fig. R2\_2 and R2\_3 it is obvious that both models show substantial differences in the SG aerosol distribution and AOD. Therefore, using the SSTs from CCSM-CAM4 is as consistent as applying an artificial negative SST anomaly. In my opinion the only meaningful approach would be to use a coupled ocean-atmosphere model with aerosol scheme and interactive chemistry. Such models are in the meantime available, although probably quite expensive. Even with such models I would expect a large spread in the upper tropospheric cirrus response to SG due to uncertainties in parameterized processes.

We understand the Reviewer's point and decided to explicitly calculate SG-driven changes in surface temperatures in the ULAQ-CCM at any grid point and time step. This is done by superimposing to the background RCP4.5 surface temperatures calculated in the CCSM-CAM4 model (and used as prescribed boundary condition in the ULAQ-CCM itself) the SG-driven surface temperature perturbation associated with the ULAQ-CCM radiative flux changes produced by SG with an injection of 8 Tg-SO<sub>2</sub>/yr. These radiative flux changes are those produced by stratospheric sulfate aerosols and upper tropospheric ice particles, as well as those produced by changes of greenhouse gases directly and indirectly affected by stratospheric

geoengineering aerosols (i.e., O<sub>3</sub>, H<sub>2</sub>O, CH<sub>4</sub> and CO<sub>2</sub> from changing methane oxidation). The ULAQ-CCM calculated SG effects on these greenhouse gases were documented in Pitari et al. (2014) and Vioni et al. (2017b). Details on the ULAQ-CCM calculation of SG aerosol microphysics, size distribution, optical thickness, transport, strat-trop exchange and radiative impact are given in Vioni et al. (2018), as well as in Pitari et al. (2014).

In order to minimize the approximation introduced from a missing explicit ocean module in the ULAQ-CCM, the procedure adopted in the calculation of the SG perturbation on surface temperatures is described below.

- (a) As a first approximation, we use in our G4 experiment the CCSM-CAM4 predicted surface temperatures with inclusion of the radiative impact of geoengineering aerosols (with injection of 8 Tg-SO<sub>2</sub>/yr); this ocean-atmosphere coupled simulation does not include chemistry and upper tropospheric ice particle changes induced by SG. As discussed in Tilmes et al. (2016), the stratospheric aerosol distribution used in CCSM-CAM4 is sufficiently robust and validated. As clearly shown in Table 3 of the revised manuscript, the net tropopause RF from these aerosols represent by far the largest contribution to the net SG RF.
- (b) However, as the Reviewer points out, the aerosol distribution calculated on-line in the ULAQ-CCM (which is based on a well-tested microphysics scheme and detailed stratosphere) may be different from the one in CCSM-CAM4, thus introducing a potentially significant inconsistency in the modeling scheme. To correct for this undesired effect, the ULAQ-CCM radiative-climate module has been modified for calculating on-line (in a fully coupled approach) the surface temperature perturbation produced by radiative flux changes due to the sulfate aerosol imbalance with respect to the CCSM-CAM4 distribution. In addition, we also include in the radiative balance the SG-driven indirect perturbation of greenhouse gases (see above), as well as upper tropospheric ice particles (which are the focus of the present study). Table S1, Fig. S2 and Fig. 6 of the revised manuscript document the effects of these radiative flux changes on the calculated surface temperatures.
- (c) Surface temperature changes due to the above discussed indirect SG effects are calculated from the instantaneous perturbation of radiative fluxes, which is of course an exact procedure over continents and polar ice caps, whereas is only approximate over the oceans. On the other hand, as well explained above and clearly visible in Table S1, Fig. S2 and Fig. 6, the radiative perturbation additive to the dominant one (that is the one produced by stratospheric sulfate aerosols in the CCSM-CAM4 simulation) is normally small, both globally and locally. Only the ice induced changes of surface temperatures may be comparable in magnitude to those from the stratospheric aerosols, but limited to tropical continental surfaces, where UT ice may have a significant optical depth. On the other hand, the SST calculated changes due to chemistry and ice indirect effects of SG are usually smaller, so that the impact of our approximation may be expected to be negligible.

**2) Sect. 2.3: The description of the experimental set up is very confusing and imprecise. Do you use sea surface temperatures and sea ice coverage only or also land surface temperatures from CCSM-CAM? Is it a nudging approach or a prescribed boundary condition? There are fundamental differences. Nudging is a Newtonian relaxation technique which adds non-physical terms to the models' equations to "pull" certain variables like temperatures towards observed values. Scientific inaccuracy is a general problem throughout the whole manuscript.**

We acknowledge that our description of this part of the experimental set-up is not clear enough. The right definition, as the Reviewer suggests, is that of “prescribed boundary conditions”. CCSM-CAM4 surface temperatures are used as boundary conditions in the baseline RCP4.5 and G4 simulations (2020-2069) of the ULAQ-CCM on both sea surface and land. The historical reference case (1960-2015) has been run following the SPARC-CCMI specifications for the REF-C1 experiment (Eyring et al., 2013), i.e., sea surface temperatures and sea ice coverage from available observations and on-line explicitly calculated land temperatures. We have adjusted the manuscript to reflect a greater accuracy on this aspect. Please note the footnotes of Table 1, which clearly explain how surface temperatures are treated in Reference, Base, G4 and G4K experiments.

**3) ULAQ-CCM performance wrt ice clouds: p10, l 2-4: “...we are considering thin ice clouds...” is this because ULAQ-CCM does not consider thick ice clouds or is this because the authors did a subsampling of the model output, i.e. selected only cases with thin cirrus? In the first case I have (again) severe doubts that ULAQ-CCM is the appropriate model for this study. In the second case the evaluation does not make sense, because the authors compare apples (thin cirrus) with oranges (all ice clouds) (apart from uncertainties in the MERRA and MODIS derived quantities).**

The ULAQ-CCM does not consider thick ice clouds, as the Reviewer states, simply because the updraft velocities are calculated as a function of TKE, with typical values less than 30 cm/s, so that convective events of much stronger intensity, and leading to the formation of thicker ice clouds, are not present (see also Kärcher and Lohmann, 2002). We believe that the comparison of our results with MERRA2 and ERA5 data regarding ice water mixing ratio (see Fig. 1) is indeed meaningful, in the sense it may highlight both similarities and differences. Most of the latter may be attributed to this missing driver mechanism of thick cirrus formation (which is clearly discussed in the manuscript). Purpose of our study is to show that the largest fraction of UT ice originates from updraft in the range of approx. 10-30 cm/s and could be significantly affected by the atmospheric stabilization induced by SG.

**4) The interpretation of the model results is very much focused on the “vertical temperature gradient – homogeneous ice formation” relationship. I am not sure whether this is a remnant of the first set of simulations in which heterogeneous ice formation had been erroneously switched off, but I miss an open discussion of other potential feedback effects. For example, changes in background cloudiness or large-scale circulation changes.**

Other feedback effects have already been discussed in previous works (and referenced in the text), for example regarding circulation changes and stratospheric chemistry (Pitari et al., 2014; Vioni et al., 2017a). The background cloud cover is fixed in our model simulation. This is now clearly stated in the manuscript (P. 31, lines 4-7 in the revised manuscript). We also address the point that potential changes in background clouds may originate from the SG induced dynamical perturbation as noted by the Reviewer (thanks!), thus potentially affecting the all-sky TOA forcing of cirrus ice particles.

**Specific comments:**

**- p1, I3: Why only “homogeneous freezing”? How can you exclude SG effects on heterogeneous freezing? Or is this a remnant from the first draft, for which heterogeneous freezing was switched off in the simulations?**

Our model simulations (as well as others in the literature) show that the homogeneous freezing dominates over heterogeneous freezing (which results to produce less than 10% of the overall ice OD). Therefore, changes in heterogeneous freezing impact the overall changes in a limited way. To better pose the problem, however, we have removed “homogeneous”: “The goal of the present study is to better understand the SG thermodynamical effects on the freezing mechanisms leading to ice particle formation.”

**- p1, I6: How do you define “longwave” radiation? Aerosols also absorb incoming radiation in the near IR.**

The “longwave” term (LW as short name, throughout the manuscript) is used for the whole spectrum of the terrestrial blackbody radiation. The shortwave term (SW as short name, throughout the manuscript) is used for the whole spectrum of the incoming solar radiation. We are well aware that aerosols absorb both in the terrestrial spectrum and in the solar NIR. To avoid misunderstanding we now write “terrestrial and solar near infrared radiation”.

**- p3, I24: Again – why only “homogeneous freezing”?**

Changed, see above.

**- p4, I6: ... help to explain...**

Corrected.

**- p4, I9-11: To design SG experiments which meet certain climate targets it is, at least in my view, crucial to consider all aspects and feedback processes in a self-consistent manner, which is not done in the present study. So this argument is counterproductive.**

Our goal was not to design a SG experiment such as that, and we agree with the comments of the Reviewer regarding the self-consistency. We believe however (and we make this clear in the conclusions of this study) that highly idealized experiments, such as ours, can still shed light on the physical processes that might be affected by SG, and this was our goal all along.

**- Sect. 2.1: Are the CCSM-CAM4 simulations ensemble runs or only one realization for each scenario? And what is the climate sensitivity of the model?**

The ensemble size for both CCSM-CAM4 scenarios is 2 (see Visioni et al., 2017b, Table 2). The equilibrium climate sensitivity of the model is 2.9 °C (Bitz et al., 2012), considering an idealized 2 x CO<sub>2</sub> scenario. Further specifications are given in the above-mentioned study.

- **Table 1: equatorual -> equatorial; footnote 3 not used; do you use surface temperatures or SEA surface temperatures from CCSM-CAM4 in Base, G4 and G4K? That's an important difference and needs clarification!**

The Reviewer is correct. The third footnote is meant to go together with the second one in row 6, column 3. We have specified better in the manuscript that we always refer to surface temperatures and not just sea surface temperatures. The footnotes have now been changed to better explain our updated modeling strategy.

- **p7, l17: This represents...**

Corrected.

- **p8, l5: What is an ice mass fraction? I guess you mean ice mass mixing ratio?**

Yes, we have corrected accordingly.

- **p8, l23: What is  $Q_{ext}$ ? Extinction efficiency coefficient?**

Yes, we now specify this in the manuscript.

- **p8, l24: How is upper troposphere defined? Which altitude range?**

The sum is over all vertical layers (but cirrus ice is only found in the upper troposphere, and this is why we specified it). We have therefore removed UT from the phrase.

- **p8, l25: remove ij after rij**

Done.

- **p8, Fig.1: Do you use MERRA or MERRA-2? I assume MERRA-2. Please use a consistent nomenclature throughout the manuscript.**

Yes, we use MERRA-2 and have corrected this everywhere.

- **p9, l5: Again - ice mass fraction?**

Corrected.

- **Fig. 3: What's the purpose of showing this figure? I do not see the link to the present study, neither for model evaluation nor for the SG effects.**

The previous review (referee #1) deemed important to know the fraction of heterogeneous freezing, so we added this figure to his suggestion.

**- Fig. 3: Add explanation of dashed and dash-dotted lines in panel b) to the caption.**

Done.

**- Fig. 4c): Again - what's the purpose of showing this figure?**

The probability of ice formation is crucial in the scheme we use to determine when and where freezing may occur for a given ice supersaturation threshold.

**- Fig. 3, 4 and 7: Which seasons are shown (tropopause)? My year has 4 seasons, but only there are only two lines.**

By seasonal variability, we mean 1 standard deviation from the average height. We have better clarified this in the new caption, the first time it appears (Fig. 3).

**- Table 2: caption: homogenous -> homogeneous, row 2: (ULAQ-CCM) missing bracket; row 5: (HET) missing**

Corrected.

**- Sect. 2.3: As mentioned above Sect. 2.3 needs clarification, especially with respect to the treatment of surface or sea surface temperatures, nudging or prescribed lower boundary condition.**

We have further clarified the aspects pointed out by the Reviewer (from P. 16, line 34 to P. 18 line 6 plus the revised Fig. 6, Table S1 and Fig. S2).

**- p14, l32: Does G4 assume 5 Tg(SO<sub>2</sub>)/yr or 8 Tg(SO<sub>2</sub>)/yr, as stated 2 lines above?**

G4 normally assumes 5 Tg-SO<sub>2</sub>/yr, at °0. We have clarified this.

**- p15, l3: (Fig. 4-5) should read (Fig. 5-6)**

Corrected.

**- Fig 5: Wouldn't it make more sense to show temperature anomalies from ULAQ-CCM instead from CCSM-CAM4 as this is the basis for the study? As far as I understand surface temperatures over land are calculated by the ULAQ-CCM?**

We better clarify that we use for the reference case CCSM-CAM4 surface temperature, and not just SST temperatures. Considering the changes we have made to the simulations, we have however added to Fig. 6 the

changes in the surface temperatures calculated by ULAQ-CCM, due to online calculated indirect effects of SG aerosols.

- Fig. 6 and following: Why do you show averages for 2030-2039 when the simulations cover 2020-2069 (at least according to Table 1)?

We simply wanted to show changes in a specific selected decade, and because the injection starts at 2020, by 2030 the SG perturbation may have reached a quasi-steady state condition. Analyzing 10 years, allows us to remove time-dependent effects in the distribution of the stratospheric aerosols (such as the QBO), but results do not change significantly by averaging one or more decades. To follow the Reviewer suggestion, anyway, we now present all results as an average over 2030-69, i.e., simply skipping the first 10 years of SG when the stratospheric aerosols (and surface temperature anomalies G4-Base) may have not reached equilibrium.

- Fig. 7a,b: A  $\Delta T = 0$  contour line would be helpful to clearly identify regions with positive and negative temperature changes. Alternatively, a better color scale. And I would prefer to see the temperature changes starting at the surface.

In the revised figure, we added a contour line for  $\Delta T = 0$ , as suggested by the Reviewer. We attach here the figure with altitude starting 0 km instead of 3 km, but in the manuscript we have decided to keep it at 3 km in order to focus on changes happening in the troposphere. Now, however, Fig. 6 focuses more on surface temperature changes, so that the reader can see both tropospheric and surface changes in the two figures.

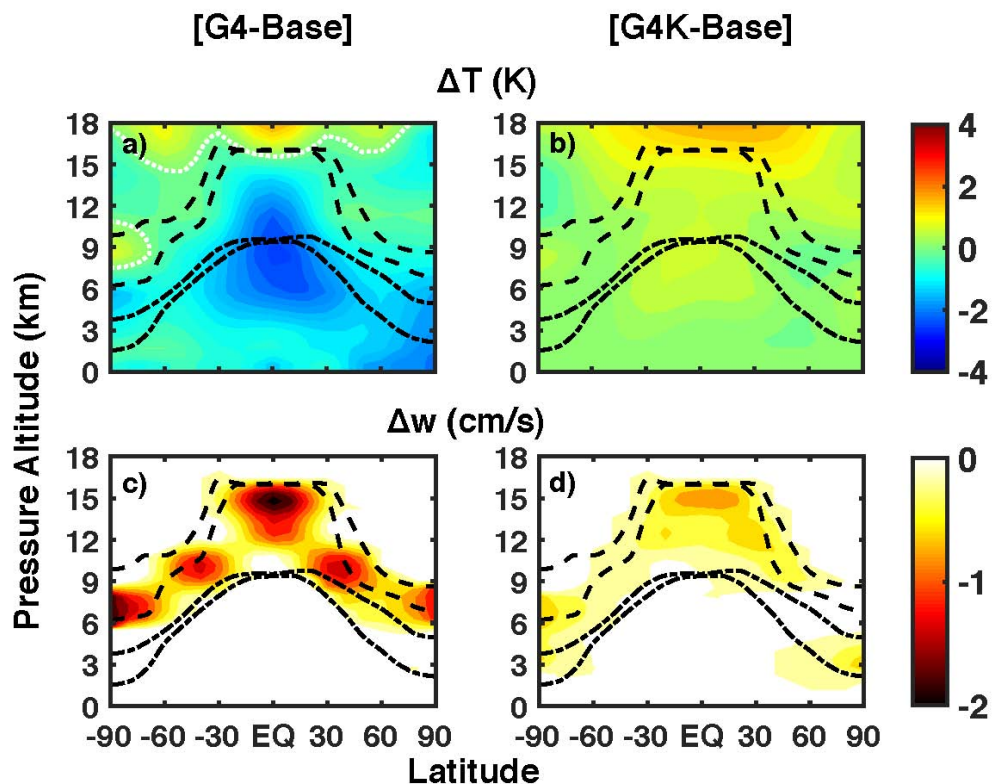


**Fig. R3\_1.** Zonally and time-averaged changes of temperature (panels a,b) and vertical velocity (panels c,d) in experiments G4 (panels a,c) and G4K (panels b,d) with respect to the Base case (years 2030–69). The dashed lines show the mean tropopause height (with seasonal variability). The dash-dotted lines show the mean height (with seasonal variability) at which the temperature reaches 238 K, thus enabling homogeneous freezing. The dotted white line highlights where  $\Delta T=0$  K.

**- Discussion of Fig. 7a,b:** The difference in surface temperatures between G4 and G4K has effect on the outgoing longwave energy and therefore the IR absorption by the SG aerosols. Furthermore I would expect general changes in cloudiness which also affect emission of terrestrial radiation. These aspects are not at all mentioned in the study.

The Reviewer is right, in fact the results in terms of aerosol optical depth and RFs are not the same between simulations G4 and G4K (a brief discussion is now made in the manuscript). For what concerns the background cloudiness, this is kept fixed in the ULAQ model at climatological values and no effect of SG is present on clouds. This is beyond the purposes of the present study and could be considered in future studies. This is now specified in the manuscript (P. 31, lines 4-7 in the revised manuscript).

**- p18, l16ff:** The authors state here that vertical motions caused by synoptic scale disturbances and gravity waves dominate the updraft velocities. Furthermore, they state that in G4 the vertical updrafts are reduced due to a reduced vertical temperature gradient, but how about the impact of changes in the meridional temperature gradient and subsequent changes in zonal winds and gravity waves?

As clearly discussed in Kärcher and Lohmann (2002) the updraft velocities in the UT may span of 2-3 orders of magnitude, due to different dynamical drivers (synoptic scale motions, gravity waves, convection). Our calculation is based on the TKE approach and  $w$  values do not normally exceed  $\sim 30$  cm/s. TKE is a function of the vertical temperature gradient and mean zonal wind shear. Dynamical changes produced by the SG aerosol radiative perturbation produce changes (including those cited by the Reviewer) that end up modifying the temperature gradient and zonal wind shear and then the TKE. This is the reason why we write: “The vertical velocity is reduced in G4 with respect to the Base case...due to the atmospheric stabilization caused by a reduction in the temperature vertical gradient”. It is a short summary of what we explain above and which also appears in various parts in the manuscript discussion. For example, few lines below, we write (referring to Fig. 9): “They help explain how the SG sulfate changes act as drivers for dynamical changes in the UT, with significant effects on ice particle formation”. To follow the Reviewer suggestion, we have modified this last sentence as follows: “They help explain how the SG sulfate changes act as drivers for dynamical changes in the UT (vertical and meridional temperature gradients, as well as vertical, horizontal winds and wave amplitude), with significant effects on ice particle formation” (P. 20, line 24-26 in the revised manuscript).

**- p18, l23:** I assume the authors mean SO<sub>4</sub> in the particulate phase, not in the gas phase.

Yes, we have better clarified this.

**- Discussion of Fig. 9:** First of all, I do not understand why the LW heating rates in Fig. 9b) have been

calculated with temperatures fixed at Base values as written in the caption? Furthermore, the authors do not mention potential changes in adiabatic heating rates due to a change in the Brewer-Dobson-Circulation (“decreased wave activity and a consequent decrease in poleward mass fluxes”) and their effects on lower stratospheric temperature changes. What is meant by “tropospheric convective cooling”? And how do the authors explain the neg. LW anomalies in G4 above ~26 km?

In order: (a) LW heating rates are shown as “instantaneous” heating rates (as it is normally done in the middle atmosphere) because the stratosphere is in quasi-radiative-equilibrium, so that the results of a non-adiabatic warming (or cooling) is a quick adjustment (positive or negative, respectively) of the temperature field. Except of course for the small departure from the radiative equilibrium, which produces changes in the residual vertical motion. In order to quantify the non-adiabatic radiative forcing of the SG aerosols is then necessary to show (in addition to the solar heating rates) the instantaneous LW heating rates (i.e., with fixed temperature in the calculation of the longwave radiative fluxes). As specified above, we are talking here of LW heating rates in the planetary blackbody spectrum, while SW heating rates result from both the solar NIR absorption by the aerosols and from UV absorption by ozone (including the effects of both SG-produced ozone changes and increased radiation scattering by the aerosols). (b): adiabatic heating rates are an indirect effect of the changing tropical upwelling. We are focusing on the direct radiative forcing by the aerosols, i.e. the diabatic heating rates. The latter will then perturb the atmospheric radiative budget and induce circulation changes and finally an adiabatic response of the atmosphere. Circulation changes (tropical upwelling, wave activity, poleward mass fluxes, strat-trop exchange have been fully covered and discussed in Pitari et al. (2014), Vioni et al. (2017), Vioni et al. (2018). (c) Tropospheric convective cooling refers to the decreased latent heat exchange due to less intense deep convection in a cooler SG atmosphere (the rather confusing statement in the original manuscript has been changed in a clearer way). (d) The discussion relative to the negative LW anomalies of heating rates above ~25 km was already given in the revised manuscript: “All features of the SW and LW heating rate anomalies in Fig. 9b can be fully explained taking into account the aerosol-O<sub>3</sub> coupled effects (Pitari et al. (2014)). The sign of tropical ozone changes under the SG conditions depends on altitude. The O<sub>3</sub> decreases below ~25 km and increases above this height; this helps explain the positive/negative heating anomalies in SW and LW components above 25 km altitude”. In other words: O<sub>3</sub> increases above ~25 km due to increasing NO<sub>x</sub> and increasing tropical upwelling, so that the LW cooling rates in the 9.6 μm O<sub>3</sub> band increases as well.

**- Fig. 7/8: Are the displayed changes in vertical velocities statistically significant? The  $\pm 1\sigma$  range (for which scenario? Base?) in Fig. 8 seems to be pretty wide compare to the differences between Base and G4.**

We report here part of our previous response to Reviewer #2, who expressed similar doubts. We note that the variability of  $w$  in Figure 8 is essentially due to seasonal changes and non-zonal asymmetries of the TKE. But if we isolate a given month in the time series, the vertical velocity change due to SG is more comparable to the  $w$  variability in the time series. We attach a figure below showing this quantity, to show what we mean.

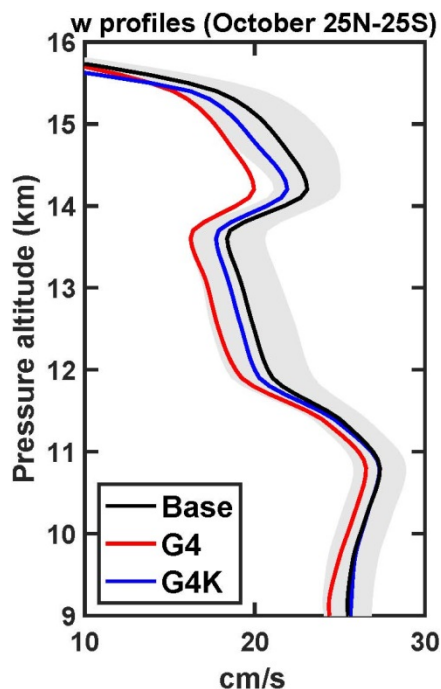
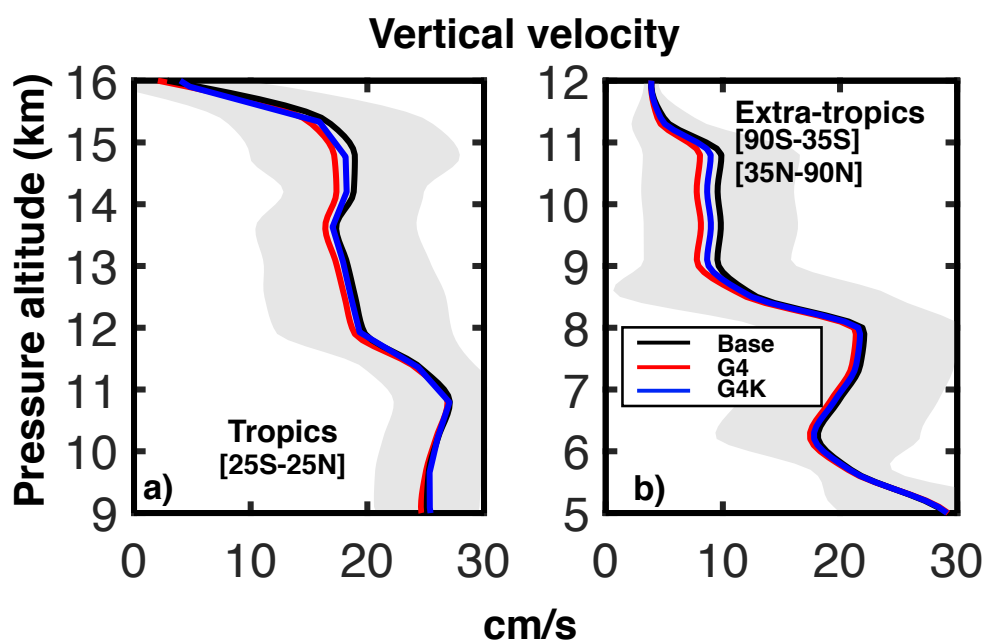


Fig. R3\_2. October monthly mean of the upper tropospheric tropical profiles of vertical velocity (cm/s) in G4, G4K and Base experiments (years 2030-39). Shaded areas represent  $\pm 1\sigma$  for the ensemble over the October month in the 40 year period 2030-69.

- Fig. 8: Why are the respective results for G4K not included?

Since they are intermediate between Base and G4 results, and the lines are already close together, we have decided to omit them in this figure, to improve readability. We attach here the figure with all three profiles, but all things considered in the manuscript, we would like to keep the figure with only the Base and G4 lines.



**Fig. R3\_3.** Average upper tropospheric profiles of the vertical velocity (cm/s) in G4, G4K and Base experiments (years 2030–69). Panels (a) and (b) are for the tropics and extratropics, respectively (see legends). The vertical velocity  $w$  is obtained as the sum of the large-scale value and that calculated as a function of the turbulent kinetic energy (see Lohmann and Kärcher, 2002 and Eq. 5), which essentially accounts for the synoptic scale and gravity wave motions. The shaded areas represent  $\pm 1\sigma$  for the ensemble over the 40-year period 2030-69.

- p23, l2-4: **As mentioned above I think the authors have to provide a more thorough evaluation of the model performance with respect to cirrus clouds.**

Following the suggestions of the Reviewer (and also of Reviewer #4), we have added further evaluations. We now add ERA5 reanalysis to all plots and discussions where MERRA2 was shown, and in the supplementary materials (Fig. S1) we also show the ice mass mixing ratio in the layer between 150 and 200 hPa for MLS.

- **Fig. 11, 12, 13, 14: Please include  $\pm 1\sigma$  range as done in other figures.**

Done. When the shaded areas overlap too much, we only left the one for the Base case. Regarding RF changes in Fig. 14, we have added uncertainties to the table rather than to the figure for better readability.

- **Discussion of Fig. 12: What is the reason for the double-peak-structure of the change in ice extinctions shown in panel a), i.e. a more pronounced decrease in ice extinctions at 11 and 13 km, and a less pronounced signal at 12 km. This feature is similar in G4 and G4K.**

The double peak can be explained by looking at Fig. 4c. Since the changes in TKE affect the probability of ice formation (because it is less probable to have vertical velocities high enough to obtain the right RH threshold), these changes are more evident not where there is the peak of probability (around 12 km in the tropical region), but where the probability is already minor to begin with, so right below (11 km) and above (13 km).

- **Sect. 3.2.2: How are the changes in RF calculated? Online during the model simulations or offline using the identical radiative transfer code as in ULAQ-CCM? In the first sentence it is written “online”, but it is not clear to me how the authors in that case distinguish between ice and background clouds. Furthermore, I miss a discussion of cloud changes in general and how they affect SW and LW radiation.**

The radiative transfer code is used on-line in the model, but to assess the changes due to ice clouds and background clouds we have repeated the calculations offline with the same code. We now better clarify this. As specified above, background clouds are kept fixed in our simulations. This is now specified in the discussion (P. 29, line 7-9 in the revised manuscript).

- **Fig. 16: Geoengineered case: In my opinion the arrow “more planetary radiation to space (ice)” is a bit misleading, because in that case the SG aerosols will absorb more IR radiation, and consequently emit more IR by themselves (upward and downward). So the sketch is overly simplified.**

The Reviewer remark is correct in principle, but not precise in the details. It is true that the aerosols upset the SW radiative budget by increasing the solar radiation scattering to space (i.e., negative TOA forcing; this is indeed shown in Fig. 16 for the SG case). It is also true that the SG-produced decrease of UT ice particles lowers the amount of trapped LW radiation (i.e., negative TOA forcing; this is also shown in Fig. 16 for the SG case). As the Reviewer correctly observes, the stratospheric aerosols also upset the LW radiative budget. But they are increasing in SG conditions, so that the amount of trapped blackbody radiation increases (i.e., positive TOA forcing (as in Table 3), only partially mitigated by the stratospheric temperature adjustment due to the positive NIR and LW aerosol heating rates). For this reason, the net effect of the stratospheric aerosols is to decrease the amount of the LW radiation to space, unless a very pronounced warming in the tropical lower stratosphere is produced, thus changing the sign of the instantaneous TOA forcing. But this is not the case, as many studies point out for explosive tropical volcanic eruptions (see for example: Hansen et al., 2005). By the way, ice particles also interact with solar radiation with increasing scattering, so that their decrease under SG conditions produces a positive TOA forcing (see again Table 3). We have slightly modified the cartoon of Fig. 16, by writing in one case “More solar (& less planetary) radiation to space (aerosols)” and in the other case “More planetary (& less solar) radiation to space (ice).

#### References:

- Bitz, C.M., K.M. Shell, P.R. Gent, D.A. Bailey, G. Danabasoglu, K.C. Armour, M.M. Holland, and J.T. Kiehl, 2012: Climate Sensitivity of the Community Climate System Model, Version 4. *J. Climate*, **25**, 3053–3070, <https://doi.org/10.1175/JCLI-D-11-00290.1>
- Eyring, V., Lamarque, J.-F., Hess, P. et al.: Overview of IGAC/SPARC Chemistry-Climate Model Initiative (CCMI) Community Simulations in Support of Upcoming Ozone and Climate Assessment, SPARC Newsletter, 40, 48–66, 2013.
- Hansen, J., M. Sato, R. Ruedy, L. Nazarenko, A. Lacis, G.A. Schmidt, G. Russell, I. Aleinov, M. Bauer, S. Bauer, N. Bell, B. Cairns, V. Canuto, M. Chandler, Y. Cheng, A. Del Genio, G. Faluvegi, E. Fleming, A. Friend, T. Hall, C. Jackman, M. Kelley, N.Y. Kiang, D. Koch, J. Lean, J. Lerner, K. Lo, S. Menon, R.L. Miller, P. Minnis, T. Novakov, V. Oinas, J.P. Perlwitz, J. Perlwitz, D. Rind, A. Romanou, D. Shindell, P. Stone, S. Sun, N. Tausnev, D. Thresher, B. Wielicki, T. Wong, M. Yao, and S. Zhang, 2005: Efficacy of climate forcings. *J. Geophys. Res.*, **110**, D18104, doi:10.1029/2005JD005776.
- Pitari, G., Aquila, V., Kravitz, B., Robock, A., Watanabe, S., Cionni, I., De Luca, N., Di Genova, G., Mancini, E., and Tilmes, S.: Stratospheric ozone response to sulfate geoengineering: Results from the Geoengineering Model Intercomparison Project (GeoMIP), *Journal of Geophysical Research: Atmospheres*, 119, 2629–2653, 2014.
- Tilmes, S., Lamarque, J.-F., Emmons, L. K., Kinnison, D. E., Marsh, D., Garcia, R. R., Smith, A. K., Neely, R. R., Conley, A., Vitt, F., Val Martin, M., Tanimoto, H., Simpson, I., Blake, D. R., and Blake, N.: Representation of the Community Earth System Model (CESM1) CAM4-chem within the Chemistry-Climate Model Initiative (CCMI), *Geosci. Model Dev.*, 9, 1853-1890, <https://doi.org/10.5194/gmd-9-1853-2016>, 2016.
- Visioni, D., Pitari, G., and Aquila, V.: Sulfate geoengineering: a review of the factors controlling the needed injection of sulfur dioxide, *Atmos. Chem. Phys.*, 17, 3879–3889, doi:10.5194/acp-17-3879-2017, <http://www.atmos-chem-phys.net/17/3879/2017/>, 2017a.

Visioni, D., Pitari, G., Aquila, V., Tilmes, S., Cionni, I., Di Genova, G., and Mancini, E.: Sulfate geoengineering impact on methane transport and lifetime: results from the Geoengineering Model Intercomparison Project (GeoMIP), *Atmospheric Chemistry and Physics*, 17, 11 209– 11 226, doi:10.5194/acp-17-11209-2017, <https://www.atmos-chem-phys.net/17/11209/2017/>, 2017b.

Visioni, D., Pitari, G., Tuccella, P., and Curci, G.: Sulfur deposition changes under sulfate geoengineering conditions: quasi-biennial oscillation effects on the transport and lifetime of stratospheric aerosols, *Atmos. Chem. Phys.*, 18, 2787-2808, <https://doi.org/10.5194/acp-18-2787-2018>, 2018.

Response to Reviewer #4.

Reviewer comments are in black, **author responses are in blue.**

This is a valuable contribution to the underrepresented topic of cirrus responses to stratospheric sulphur injections. While I think the authors did a good job in explaining the main physical mechanism behind the observed changes, I am pointing out a few more issues, which would need to be addressed before the paper can be published in final form.

Major comments

1.) Is detrained moisture/ice water content from convection included in the cirrus formation mechanisms? How did you include it?

You mention on page 7 that upper tropospheric ice can be formed only by homogeneous or heterogeneous freezing. However, a large part of the cirrus, in particularly in the tropics, is formed by detrainment of ice crystals from deep convective cores. Such ice crystals formed either by homogeneous nucleation of cloud droplets or in mixed phase by heterogeneous nucleation; their formation is therefore significantly different from the in-situ cirrus.

Did you include such detrained ice crystal sources in your model? I think the strength and level of maximum detrainment is probably modulating the responses of in-situ formed cirrus in the tropics, i.e. in the region where most of your cirrus cloud radiative effect comes from.

Most of your ice mass comes from heterogeneous freezing at lower elevations in the tropics. This is in a zonal average perspective not realistic, as most of it should be a result of detrainment from deep convection, at least near the location of the intertropical convergence zone.

Detrainment from deep convective clouds is an important source of cirrus clouds and therefore needs to be mentioned/commented in the manuscript.

No, we do not include detrained ice in our cirrus formation mechanism, we only consider in-situ formation. As the Reviewer suggested, we have clarified the lack of this mechanism in our model, and we also discuss its importance.

2.) Model evaluation with MERRA2/MODIS data

I. Please state which version of MODIS data you use. You cite Yang et al., 2007, which is a reference for the V5. I assume you either use V5 or V6, please add this as the retrievals changed between several product versions. Do you use level 3 1x1° gridded data?

II. I would suggest removing the use of MODIS IC radius due to the following reasons:

- MODIS derived IC radius is valid only for cloud tops of optically thicker clouds and not representative of the whole cloud distribution. In a thick cloud, the MODIS IC effective radius would correspond to the upper portion of the thick(er) cloud, until the optical depths of about 1.2, at least for the case of detrained anvil

clouds as shown in Hong et al., 2012. The retrieval would give more weight to the radius closer to cloud top also for the case of intermediately thick cirrus (COD between 1 and 5, Zhang et al., 2010).

- MODIS cannot see the thinnest of the cirrus clouds. Its approximate detection limit is close to COD of 0.4 (Ackerman et al., 2008). I assume you include clouds of any optical depth in your analysis.
- MODIS is a passive instrument and detects cloud properties only during daytime, while I assume you take both day and night data from the model output. To summarize my point, the comparison of IC radius and the derived IC number concentration is based on too many very shaky assumptions and needs to be removed from the manuscript. If you would like to keep it, you may use the MODIS satellite simulator, which takes into account MODIS retrieval limitations and therefore ensures an apple-to-apple comparison.

After evaluating the Reviewer comment, we have decided to remove MODIS from our comparisons as suggested. In all plots regarding IC number concentration and optical depth, where we combined MERRA2+MODIS, we have removed the MODIS radius and calculated these quantities using the radius from our model instead.

**III. MERRA2** MERRA2 has a very simplistic treatment of ice clouds, leading to large biases (e.g. large biases in cloud radiative effect noted in Bosilovich et al., 2015). Using a reanalysis dataset is anyway not the best, but if you already went for one, ERA5 would be a more appropriate choice, as it compares better with CALIPSO-CloudSat datasets (DARDAR, 2C-ICE) as shown for instance by Duncan and Eriksson, 2018. Nevertheless, considering this is the second phase of review, I can accept the comparison used in Figure 1 as good enough due to large IWC retrieval uncertainty (as you also pointed out in the manuscript). Yet, I think you should remove from the paper your optical depth estimates from MERRA+MODIS in figure 2, as the assumptions behind that plot are too large and you are mixing up reanalysis, satellite retrieval, and model output without making sure this is an “apple-to-apple” comparison (i.e. you don’t take into account the satellite retrieval limitations and the issue of collocation of data in space and time).

See above, regarding the removal of MODIS data. In the revised manuscript, we have also added further evaluation, both ERA5 as the Reviewer suggests (for Fig. 1) and MLS satellite data for Fig. S1. The optical depth estimates are now performed using MERRA2 and ERA5 data for ice water content together with the radius calculated in our model.

#### Minor comments

- please add uncertainty estimates (e.g. +/- 1 st. dev.) to the results you show, at least in the tables. This would give the reader a better feeling for the significance of your radiative forcing anomalies.

We have now added uncertainty estimates wherever necessary.

**Abstract:** After line 15 the abstract clarity becomes challenging for the reader as you are making very fast transitions from effects of cirrus clouds which cool the climate, to comparing all-sky with clear-sky forcing, and saying that the all-sky has a positive effect on the radiative balance. I would just qualitatively mention the effect of a positive (total) cloud radiative effect -> dimming the sun that reaches the cloud tops indeed

**has to decrease the amount of reflected SW radiation. Moreover, do you really need to always mention 2 significant numbers after the decimal point, considering all the uncertainties?**

As the Reviewer suggests, in the abstract we now mention only 1 significant number for most of the quantities listed. The solar dimming mechanism is already explained in the study, and we do not feel like there's room to briefly explain it also in the abstract, where we would like to keep some key quantitative results.

**page 2, line 21-24: The current best knowledge of cirrus microphysics does not show much support of the predominance of homogeneous nucleation in in-situ cirrus cloud. Your extensive answer to Reviewer #1 unfortunately does not help in changing that view. I think the uncertainty in cirrus formation mechanisms is high enough to accept your modelling results related to the freezing mechanisms as plausible.**

**What does it mean that homogeneous processes dominate the heterogeneous? Do you refer to the relative radiative forcing difference, the ice water content, ice crystal number concentration, frequency of occurrence of nucleation events?**

**Moreover, I am not sure whether figures from the latest ECHAM-HAM studies (e.g. Gasparini and Lohmann 2016, Gasparini et al., 2018) confirm your homogeneous vs. heterogeneous nucleation arguments. Homogeneous freezing seems to dominate only near the tropopause and over mountains.**

**You could also cite Barahona et al., 2017, which shows somewhat consistent results with Gasparini and Lohmann 2016 in terms of homogeneous vs. heterogeneous freezing importance.**

Responding to the Reviewer question, what we mean when we talk about homogeneous freezing "dominating" over heterogeneous freezing is that the ice crystals formed homogeneously are formed in a much larger quantity than those formed heterogeneously. In the revised manuscript, we now include Barahona et al. (2017) as suggested.

**page 2, line 33/34 (and on page 33): I don't think Sanderson et al., 2008 is looking at radiative balance of upper tropospheric clouds, but rather at the sensitivity of climate feedback to tuning parameters. Also, Mitchell et al., 2008 look at differences in simulated climate by changing the particle shape distributions, affecting the fall velocities, and finally the radiative effects of clouds.**

We have removed Sanderson et al. (2008). Our reference to Mitchell et al. (2008) points however to how changes in optical properties and other parameters might affect the radiative effect of clouds, so we believe it to be an appropriate reference in that phrase.

**page 3, line 5 Liquid (or more precisely aqueous) sulphuric acid droplets CANNOT act as ice nucleating particles for heterogeneous freezing. The increase in IC number concentration in Cirisan et al., 2013 is related to the presence of large sulphuric acid particles, which makes homogeneous freezing more favourable. Sulphuric particles at  $r < 0.1 \mu\text{m}$  only hardly nucleate ice crystals homogeneously due to the strong Kelvin effect. Stratospheric perturbations shift this distribution closer to sulphuric aerosol radii between 0.6 and 0.8, which were shown to be most susceptible for homogeneous freezing (see paragraph 2.3 of Cirisan et al.).**

We are aware that liquid sulphuric acid droplets cannot act as ice nucleating particles, and we have further modified the phrase so as to better reflect this. Furthermore, we have better explained the findings by Cirisan et al. (2013) as suggested.

**page 4, lines 5-10** The discussion seems to clearly highlight the thinning of cirrus in presence of a volcanic forcing. I think that by our current best knowledge we cannot give a conclusive answer on the influence of volcanic eruptions on cirrus clouds frequency, microphysics, or radiative properties (e.g. Meyer et al., 2015 has a different conclusion from the study you cited).

We added the suggested reference and made it clearer that no conclusive answer can be given regarding the influence of aerosols on cirrus ice.

**page 7, line 18** Homogeneous freezing threshold is not constant, but should have some temperature (or, more precisely, water activity) dependence. Many parameterizations follow the Koop et al., 2000 results/formula. You have to therefore mention that important shortcoming, which might lead in most places to some overestimation of your homogeneous freezing probability, and the opposite at temperatures close to the homogeneous freezing temperature of water.

We now mention this aspect of our parametrization in the revised manuscript (P. 7, line 18-19 in the revised manuscript).

**page 7, line 32-33:** Again, I don't think there is much evidence for the dominant role of homogeneous freezing. At most, you can mention that the relative importance of homogeneous vs. heterogeneous freezing is currently still very uncertain. The cited study with the message: "beware of the coating of dust, which decreases the ability to nucleate ice of several ice nucleating particles" (i.e. Cziczo et al., 2009) is not a proof of your statement!

We have removed the reference that the Reviewer did not deem appropriate. We now specify that our model sees a dominant role of homogeneous freezing, but that this is not a general conclusion.

**page 10, line 8-10:** That's surprising; I would expect that the IWC at the lowest levels is dominated by detrained sources. Indeed, you might be just looking at IWChet/IWChom, which is OK, but you need to mention in this case the missing and probably large convective IWC source in the tropics below about 12 km.

Following also the first comment of the Reviewer, when discussing the differences between our model and reanalyses we discuss the lack of detrained ice in our model (P. 10, line 5-7 in the revised manuscript).

**page 11, line 9-15:** I do not see much value in the comparison of your globally averaged ice crystal number concentration with a randomly picked study from a field campaign (which is, moreover, likely affected by the pre early 2000s retrieval problems due to ice crystal shattering, see Cziczo et al., 2014). Again, I also do not see any reason to trust the MERRA+MODIS derived IC number concentrations on Figure 4.

We MERRA+MODIS quantity has been modified as discussed above. We have also removed the comparison in the text.

**Figure 12 and related text: Again, the derived extinction from MERRA+MODIS does not add much of scientific value. Same for Figure 13 b.**

We have removed this as discussed above.

**page 30, line 3-5: Background clouds have a positive cloud radiative effect. That means they reflect less (if we assume all comes from SW), and not more! If the solar radiation reaching top of the clouds decreases by, say, 1%, the amount of reflected SW radiation has to also decrease by the same relative value to first order (1% in this example).**

Our sentence in the manuscript (“...due to the mere presence of background clouds, whose increased reflectivity enhances the downward scattered solar radiation by the stratospheric aerosol layer”) may indeed originate confusion; in this aspect, we agree with the Reviewer. However, he is referring the decreasing reflectivity of the background cloud layer when the SG aerosols are included and then are subtracting part of the incoming solar radiation, with respect to a background atmosphere without SG aerosols. On the other hand, the cloud adjustment we are quantifying here, is the net effect of clouds below the SG aerosol layer with respect to clear sky conditions. The net effect of cloudiness is to decrease the magnitude of the TOA forcing. This is a well-documented effect in the literature, so that we decided to change our unclear sentence in the following way: “...due to the mere presence of background clouds, which substantially alter the radiative fluxes (see also Kuebbeler et al., 2012; Shulz et al., 2006; Stier et al., 2013)”.

**Figure 14: Why is the background cloud effect plotted only once? I guess it does change between the two cases.**

To increase the readability of Fig. 14, we decided to show with the black solid line only the net cloud adjustment due to background clouds (i.e., SW+LW) for the G4 case (the net adjustment for G4k is rather similar). For the sake of completeness and clarity, we have modified Fig. 14 including also the net adjustment for the G4K case. In addition, we have also included a new figure in the supplementary material (Fig. S3), presenting the latitudinal behavior of the SW and LW adjustments, separately, for both G4 and G4K.

**Figure 15: You never show that there is reduced water vapour transport to the upper troposphere? Prove it or remove it! Also, I would like to see some evidence for the “convectively driven tropospheric cooling” before putting that in your summary sketch! In summary, your schematic is a bit too complicated to be easily digested by an average reader. I think you can drop a few of the points, unless you prove them to be crucial in delivering your message.**

We have modified Figure 15 by writing in the central box: “Atmospheric stabilization: reduced TKE and updraft velocities”. The evidence for convectively driven tropospheric cooling is indeed given in Fig. 7a and discussed in the text (tropospheric convective cooling refers to the decreased latent heat exchange due to less intense deep convection in a cooler SG atmosphere). To avoid mix-up of too many thermodynamics effects in a summary sketch, we have now simply written “Tropospheric cooling” as a consequence of the SG aerosol produced “Surface cooling”.

**page 31, lines 27-28: Or maybe simply the water cycle slows down due to decrease of surface temperature, following Clausius-Clapeyron?**

The Reviewer is correct in his remark. In lines 27-28 we are however pointing out that the tropospheric cooling actually might counterbalance (partially) the effect pointed out before (see also Kuebbeler et al., 2012).

**page 33, lines 14-16: This is not really a good explanation of the SW adjustment. It is rather confusing to the reader. I thought you do not include cirrus in the “background clouds” effects based on your Figure 14, which shows the background effect separately from the effect on ice clouds.**

In Tables 3 and 4 and in Figure 14 we actually separate the two effects. As explained above, the background clouds (that we keep fixed, and thus are not affected by SG) are separated from the cirrus clouds. So, the effect in the SW and LW adjustment is twofold: partly it comes from background clouds (and we can calculate this effect alone by not considering changes in cirrus ice) and partly from changes in ice clouds. Also following suggestions from Reviewer #3, we have updated the discussion in Section 3.2.2 to better clarify how we calculate the two separate effects: this way, it is easier to understand the point in the final discussion that the Reviewer deems unclear.

#### **References:**

Barahona, D., Molod, A., and Kalesse, H.: Direct estimation of the global distribution of vertical velocity within cirrus clouds, *Scientific Reports*, 7, 6840, doi:10.1038/s41598-017-07038-6, <https://doi.org/10.1038/s41598-017-07038-6>, 2017.

Cirisan, A., Spichtinger, P., Luo, B. P., Weisenstein, D. K., Wernli, H., Lohmann, U., and Peter, T.: Microphysical and radiative changes in cirrus clouds by geoengineering the stratosphere, *Journal of Geophysical Research: Atmospheres*, 118, 4533–4548, doi:10.1002/jgrd.50388, <http://dx.doi.org/10.1002/jgrd.50388>, 2013.

Kuebbeler, M., Lohmann, U., and Feichter, J.: Effects of stratospheric sulfate aerosol geo-engineering on cirrus clouds, *Geophysical Research Letters*, 39, doi:10.1029/2012GL053797, <http://dx.doi.org/10.1029/2012GL053797>, l23803, 2012.

Meyer, K., Platnick, S., and Zhang, Z.: Simultaneously inferring above-cloud absorbing aerosol optical thickness and underlying liquid phase cloud optical and microphysical properties using MODIS, *Journal of Geophysical Research: Atmospheres*, 120, 5524–5547, doi:10.1002/2015JD023128, <https://agupubs.onlinelibrary.wiley.com/doi/abs/10.1002/2015JD023128>, 2015.

Mitchell, D. L., Rasch, P., Ivanova, D., McFarquhar, G., and Nousiainen, T.: Impact of small ice crystal assumptions on ice sedimentation rates in cirrus clouds and GCM simulations, *Geophysical Research Letters*, 35, n/a–n/a, doi:10.1029/2008GL033552, <http://dx.doi.org/10.1029/2008GL033552>, l09806, 2008.

Sanderson, B. M., Piani, C., Ingram, W. J., Stone, D. A., and Allen, M. R.: Towards constraining climate sensitivity by linear analysis of feedback patterns in thousands of perturbed-physics GCM simulations, *Climate Dynamics*, 30, 175–190, doi:10.1007/s00382-007-0280-7, <https://doi.org/10.1007/s00382-007-0280-7>, 2008.

Schulz, M., C. Textor, S. Kinne, Y. Balkanski, S. Bauer, T. Berntsen, T. Berglen, O. Boucher, F. Dentener, S. Guibert, I.S.A. Isaksen, T. Iversen, D. Koch, A. Kirkevåg, X. Liu, V. Montanaro, G. Myhre, J.E. Penner, G. Pitari, S. Reddy, Ø. Seland, P. Stier, and T. Takemura, 2006: Radiative forcing by aerosols as derived from the AeroCom present-day and pre-industrial simulations. *Atmos. Chem. Phys.*, 6, 5225-5246, doi:10.5194/acp-6-5225-2006.

Stier, P., Schutgens, N. A. J., Bellouin, N., Bian, H., Boucher, O., Chin, M., Ghan, S., Huneeus, N., Kinne, S., Lin, G., Ma, X., Myhre, G., Penner, J. E., Randles, C. A., Samset, B., Schulz, M., Takemura, T., Yu, F., Yu, H., and Zhou, C.: Host model uncertainties in aerosol radiative forcing estimates: results from the AeroCom Prescribed intercomparison study, *Atmos. Chem. Phys.*, 13, 3245-3270, <https://doi.org/10.5194/acp-13-3245-2013>, 2013.

# Upper tropospheric ice sensitivity to sulfate geoengineering

Daniele Visionsi<sup>1,2</sup>, Giovanni Pitari<sup>1</sup>, Glauco di Genova<sup>2</sup>, Simone Tilmes<sup>3</sup>, and Irene Cionni<sup>4</sup>

<sup>1</sup>Department of Physical and Chemical Sciences, Università dell'Aquila, 67100 L'Aquila, Italy

<sup>2</sup>CETEMPS, Università dell'Aquila, 67100 L'Aquila, Italy

<sup>3</sup>National Center for Atmospheric Research, Boulder, CO 80305, USA

<sup>4</sup>ENEA, Ente per le Nuove Tecnologie, l'Energia e l'Ambiente, 00123 Rome, Italy

**Abstract.** Aside from the direct surface cooling that sulfate geoengineering (SG) would produce, the investigation of the possible side effects of this method is still ongoing, such as, for instance, on upper tropospheric cirrus cloudiness. The goal of the present study is to better understand the SG thermo-dynamical effects on the ~~homogeneous-freezing-ice-formation process~~freezing mechanisms leading to ice particle formation. This is done by comparing the SG model simulations against a Representative Concentration Pathway 4.5 (RCP4.5) reference case. In one case, the aerosol-driven surface cooling is included and coupled to the stratospheric warming resulting from the aerosol absorption of ~~longwave-terrestrial and solar near infrared~~ radiation. In a second SG perturbed case, the surface temperatures are kept unchanged with respect to the reference RCP4.5 case. Surface cooling and lower stratospheric warming, together, tend to stabilize the atmosphere, thus decreasing the turbulence and updraft velocities (-10% in our modelling study). The net effect is an induced cirrus thinning, which may then produce a significant indirect negative radiative forcing (RF). This would go in the same direction as the direct effect of solar radiation scattering by the aerosols, thus influencing the amount of sulfur needed to counteract the positive RF due to the greenhouse gases. In our study, given an 8 Tg-SO<sub>2</sub>/yr equatorial injection into the lower stratosphere, an all-sky net tropopause RF of ~~-1.54~~-1.46 W/m<sup>2</sup> is calculated, of which ~~-0.37~~-0.3 W/m<sup>2</sup> (~~24~~20%) is from the indirect effect on cirrus thinning (~~5.26~~5.26% reduction in ice optical depth). When the surface cooling is ignored, the ice optical depth reduction is lowered to ~~3.13~~3.13%, with an all-sky net tropopause RF of ~~-1.42~~-1.4 W/m<sup>2</sup>, of which ~~-0.18~~-0.14 W/m<sup>2</sup> (~~12~~10%) is from cirrus thinning. Relative to the clear-sky net tropopause RF due to the SG aerosols (~~-2.06~~-2.1 W/m<sup>2</sup>), the cumulative effect of the background clouds and cirrus thinning accounts for ~~+0.52~~+0.6 W/m<sup>2</sup>, due to the ~~close~~partial compensation of large positive shortwave (~~+1.56~~+1.6 W/m<sup>2</sup>) and negative longwave adjustments (~~-1.04~~-1.0 W/m<sup>2</sup>). When the surface cooling is ignored, the net cloud adjustment becomes ~~+0.74~~+0.8 W/m<sup>2</sup>, with the shortwave contribution (~~+1.51~~+1.5 W/m<sup>2</sup>) almost twice as much as that of the longwave (~~-0.77~~-0.7 W/m<sup>2</sup>). This highlights the importance of including all of the dynamical feedbacks of the SG aerosols.

## 1 Introduction

Sulfate geoengineering (SG) is one of the methods that have been proposed in the scientific community (Budyko (1974); Crutzen (2006); Niemeier and Tilmes (2017)) to cool our planet for a limited amount of time, in response to the warming caused by the increasing greenhouse gases of anthropogenic origin. SG proposes the injection of SO<sub>2</sub> into the tropical lower

stratosphere in order to produce an optically active cloud of  $\text{H}_2\text{SO}_4\text{-H}_2\text{O}$  supercooled liquid aerosols that would reflect part of the incoming solar radiation back to space. These aerosols, however, would at the same time warm the lower stratosphere by a few degrees. The idea stems from the cooling effect of past explosive volcanic eruptions in the tropical region (the last being Pinatubo in 1991). These major eruptions injected large amounts of  $\text{SO}_2$  into the lower stratosphere and increased the planetary albedo. The resulting cooling effect has been clearly observed (Robock (2000)), although its magnitude is still being discussed (Canty et al. (2013)).

In the case of past volcanic eruptions, both the direct and indirect effects of episodic large injections of sulfur into the stratosphere have been observed and documented; this is obviously not possible for planned sustained sulfur injections in the SG experiments. Because of this, the scientific community mainly relies on simulations using climate models and comparisons of the results among them, such as, for instance, under the GeoMIP project (Kravitz et al. (2011); Kravitz et al. (2013)). Different injection scenarios have been proposed and adopted in modelling experiments, the most used being the one with a constant sulfur injection rate at the Equator for a certain number of years to understand the climate response to such an atmospheric perturbation. Simulations have also been performed to identify the optimal magnitude and location of the stratospheric sulfur injection and to obtain the highest ratio between the radiative forcing (RF) and the injection magnitude (Niemeier and Schmidt (2017); Tilmes et al. (2017); Kleinschmitt et al. (2017)).

Amongst various side effects of SG, those with non-negligible impacts on the RF were analysed and summarized in Visionsi et al. (2017a). These are related to an enhancement of stratospheric ozone destruction (Tilmes et al. (2008); Pitari et al. (2014); Xia et al. (2017)), an increase in the concentration and lifetime of methane (Visioni et al. (2017b)), an increase of stratospheric water vapour due to a tropical tropopause layer (TTL) warming (Pitari et al. (2014)) and, most importantly, to a change in the probability of the formation of cirrus ice particles in the upper troposphere (UT) (Kuebbeler et al. (2012)). Regarding this latter effect, some studies have appeared in the recent literature that propose ways in which SG could affect the UT cirrus ice number density and optical depth. We will discuss them below and try to expand some aspects further in the present work.

In an unperturbed atmosphere, the formation of UT ice particles may take place either by homogeneous or heterogeneous freezing (Karcher and Lohmann (2002); Hendricks et al. (2011)), with the former process normally dominating over the latter, at least in model simulations (Storelvmo and Herger (2014); Gasparini and Lohmann (2016); Gasparini et al. (2017); Barahona et al. (2017)). Cziczo et al. (2013), however, reported that, in some areas, in-situ measurements show that heterogeneous freezing dominates over homogeneous freezing. Homogeneous freezing takes place when the ice saturation ratio is relatively high (typically above  $\sim 1.5$ ), local temperatures are below the threshold for atmospheric ice particle formation ( $\sim 238$  K) and supercooled solution droplets are present, namely, sulfate aerosols or sulfate-coated aerosols. Supersaturation conditions are maintained by intense vertical motions controlling the adiabatic cooling rate and bringing water vapour from the lower to the upper troposphere. Ice crystals formed in this way both reflect part of the incoming solar radiation (negative RF) and trap part of the outgoing planetary radiation, contributing to the greenhouse effect (positive RF). The sign of the combined effects could not easily be determined in a variety of atmospheric conditions. Normally, it has been shown that the net UT ice contribution to the RF is positive (Chen et al. (2000); Fusina et al. (2007); Gasparini et al. (2017)). This is, however, a rather

delicate balance and strongly depends on the humidity, cloud cover and optical properties (Sanderson et al. (2008); Mitchell et al. (2008)), so that a robust atmospheric perturbation, such as the one that the SG could produce, may significantly affect it. The perturbation to the UT ice could be twofold. On one hand, Cirisan et al. (2013) studied how the H<sub>2</sub>SO<sub>4</sub>-H<sub>2</sub>O droplets resulting from the sulfur injection would interact with cirrus clouds, both microphysically and radiatively. An upper tropospheric increase of the sulfate aerosol number concentration is expected under the SG conditions due to gravitational sedimentation and the large-scale transport of the particles below the tropopause from the lower stratosphere (LS). However, sulfuric acid liquid supercooled droplets ~~are very inefficient cannot act as~~ ice nuclei (IN) for heterogeneous freezing. At the same time, the background number concentration of the UT aerosols acting as nuclei for homogeneous freezing is already much higher with respect to the ice particle number density. For this reason, a negligible increase of the active IN population would be found in the UT ~~and the~~ (mainly due to a shift in the distribution of sulfate particles towards radii where homogeneous freezing is more favorable); the same would hold true for the positive RF associated with a possible increase of ice particles from this effect, as Cirisan et al. (2013) concluded in their study.

Kuebbeler et al. (2012), on the other hand, analysed the effects produced by dynamical changes due to the modification of the tropospheric thermal gradient produced by stratospheric geoengineering aerosols. In particular, the LS warming, caused by increasing heating rates in the optically thick sulfate cloud, tends to decrease the tropospheric lapse rate. A subsequent decrease in the available turbulent kinetic energy (TKE) would follow and translate in a slowing down of the updraft and of the adiabatic cooling rate, thus reducing the probability for sufficiently high supersaturation values capable of producing ice crystals formation via homogeneous freezing. Their study found a resulting large net RF reduction in magnitude with respect to clear-sky conditions, where only the direct aerosol forcing is considered (-0.93 W/m<sup>2</sup> against -1.53 W/m<sup>2</sup>). They concluded that this forcing reduction results not only from the mere (passive) presence of background clouds that affect the atmospheric radiative transfer but also from the cirrus cloud thinning produced by the SG aerosols. This may obviously have clear implications regarding the potential of the SG to counterbalance global warming.

The aforementioned study, however, lacked an important part of the possible dynamical feedback of the SG, that is, the changes in sea surface temperatures (SSTs) that would result from the decreased incoming solar radiation. The goal of the present study is to study the impact on cirrus ice particles formed via homogeneous freezing of a stratospheric sulfate injection and to understand how both the local stratospheric warming and the surface and tropospheric cooling can affect this process; to do this, we will use the composition-climate coupled model developed at the University of L'Aquila (ULAQ-CCM). We performed an SG simulation with an 8 Tg-SO<sub>2</sub>/yr injection, using surface temperatures (T<sub>s</sub>) calculated in the atmosphere-ocean coupled model CCSM-CAM4 (Community Climate System Model - Community Atmospheric Model version 4), operated with the same sulfur injection (thus resulting in a general surface cooling, with respect to atmospheric unperturbed conditions). This perturbed experiment (named G4, according to the convention of Kravitz et al. (2011), regardless of the time constant magnitude of the injection) is compared against a baseline simulation without SG and using a background anthropogenic emission scenario corresponding to the Representative Concentration Pathway 4.5 (RCP4.5) (Taylor et al. (2012)) (named Base case in

our study). To properly compare our results with those of Kuebbeler et al. (2012), a third simulation was performed with the same geoengineering sulfur injection of G4 but with the surface temperatures fixed at the Base case values (named G4K).

The effects of the SG ~~surface-temperature- $T_s$~~  changes on the lower stratospheric dynamics were already discussed in Visioni et al. (2017b); this time, we focus on their impact in the upper troposphere. Unlike other side effects of sulfur injection into the stratosphere, a comparison between the effects of a volcanic eruption and the SG on cirrus ice is difficult to draw. This is mainly because in a volcanic eruption episode (contrary to SG), a large amount of solid ash particles is injected into the lower stratosphere together with  $SO_2$ . Part of these particles, after settling down below the tropopause, may contribute to increasing the number density of IN available for heterogeneous freezing in the UT. This could help to explain some observed increases in UT ice particles after the Pinatubo eruption (Sassen et al. (1995)). More recently, Friberg et al. (2005) showed that cirrus cloud reflectance and optical depth are reduced in the Northern Hemisphere in periods with more pronounced volcanic activity. However, other studies such as Meyer et al. (2015) dispute this effect, and no conclusive answer can be given. Understanding the RF contribution of the UT ice perturbation in a SG scenario is particularly crucial if the scientific community wants to design experiments whose goal is to meet a given climate target, as proposed in Kravitz et al. (2017) and MacMartin et al. (2017).

This paper is structured in three subsequent sections plus the conclusions: in Section 2, we describe the CCSM-CAM4 and ULAQ-CCM models and the setup of the numerical experiments. Furthermore, in Section 2 we try to evaluate the ULAQ-CCM skill in simulating the formation of the cirrus ice clouds, using re-analysis and satellite data. In Section 3, we discuss the model-calculated changes in the thermo-dynamical properties of the atmosphere and in cirrus cloudiness (size distribution, extinction, optical depth, number concentration) produced by the SG, and finally, we show how these perturbations translate into tropopause radiative forcing terms.

## 2 Model descriptions and setup of numerical experiments

### 2.1 CCSM-CAM4

The Community Climate System Model - Community Atmospheric Model version 4 (CCSM-CAM4) is an atmosphere-ocean coupled model that was used in this experiment to calculate the evolution of ~~surface-temperature- $T_s$~~  for both the Base case (RCP4.5 scenario) and a geoengineering case with the same sulfur injection as the ULAQ-CCM model, described in Tilmes et al. (2015). For these simulations, the model was run without interactive chemistry. The resolution of the model is  $1.9^\circ \times 2.5^\circ$  with 26 vertical levels and the top of the model is at 3 hPa. The model has been fully described in Neale et al. (2013) and Tilmes et al. (2016) and has been shown to compare well against observations in the stratosphere in Lamarque et al. (2012). Ice clouds are diagnosed from a purely relative humidity-based formulation (Neale et al. (2013)). The results of an 8 Tg- $SO_2$ /yr injection on ~~the~~ surface temperatures and the effects of the inclusion of the perturbed ~~SSTs- $T_s$~~  in the ULAQ-CCM model have

been already discussed in Visioni et al. (2017b).

## 2.2 ULAQ-CCM

The University of L'Aquila composition-climate coupled model was described in its first version in Pitari et al. (2002); subsequent model versions were documented in modelling intercomparison campaigns (Eyring et al. (2006); Morgenstern et al. (2010); Morgenstern et al. (2017)). Model updates in the horizontal and vertical resolution, photolysis cross sections, the treatment of Schumann-Runge bands and radiative transfer code were described and tested in Pitari et al. (2014) and Chipperfield et al. (2014). The shortwave radiative module has been documented and tested for tropospheric aerosols in Randles et al. (2013) and for volcanic stratospheric aerosols in Pitari et al. (2016a). It makes use of a two-stream delta-Eddington approximation and is on-line in the model for ~~both photolysis and solar heating rate~~ photolysis, solar heating rates and radiative flux calculations. A companion broadband, k-distribution longwave radiative module is used for the heating rate and ~~the top-of-atmosphere radiative forcing~~ radiative flux calculations in the planetary infrared spectrum (Chou (2001)).

A critical atmospheric region in the SG studies is the upper troposphere and lower stratosphere (UTLS). An extensive model evaluation based on specific physical and chemical aspects was made in Gettelman et al. (2010) and Hegglin et al. (2010)). Subsequent model improvements in this region were discussed in Pitari et al. (2016b). The treatment of ~~surface temperatures~~ Ts, and their importance for the lower stratospheric dynamics and species transport under a geoengineering scenario, has been discussed in Visioni et al. (2017b). Another very important aspect to be taken into account for large-scale species transport in the lower stratosphere is the role of the quasi-biennial oscillation (QBO) in SG studies. It has been discussed from different points of view in some recent studies (Aquila et al. (2014); Niemeier and Schmidt (2017); Visioni et al. (2018)). A nudging procedure for the QBO is adopted in the ULAQ-CCM, based on an observed historical data series of equatorial mean zonal winds (Morgenstern et al. (2017)).

For the sake of completeness, we discuss in the following two sub-headings some of the model features, in particular, those relevant for stratospheric sulfate aerosols and upper tropospheric cirrus ice particle formation.

**Table 1.** Summary of ULAQ-CCM features and numerical experiments for the present study.

Years of simulation	1960-2015	2020-2069
Type of simulation	Reference	Base (RCP4.5) + G4 + G4K
Ensemble size	2	1 + 2 + 2
Horizontal and vertical resolution	5° × 6°, L126 log-pressure top: 0.04 hPa	
Chemistry	On-line (strat & trop)	
Dynamics	Calculated <sup>1</sup>	Calculated <sup>2</sup>
QBO	Nudged (from eqt. wind obs.)	Nudged (iteration of observed cycles of eqt. winds)
Altitude of equatorial injection of SO <sub>2</sub> in G4 (8 Tg-SO <sub>2</sub> /yr)	-	18-25 km (Gaussian Distribution)

<sup>1</sup> Sea surface temperatures from observations; on-line explicitly calculated land temperatures.

<sup>2</sup> Surface temperatures from CCSM-CAM4 (land, ocean, sea ice coverage), separately for Base and G4 (Visioni et al. (2017b)); Base values also used for G4K. Indirect effects of SG aerosols on surface temperatures are calculated on-line in the ULAQ-CCM radiative module (due to UT ice, GHGs and SO<sub>4</sub> imbalance relative to CCSM-CAM4); see text in section 2.3.

### 2.2.1 Stratospheric sulfate aerosols

In SG experiments G4 and G4K, SO<sub>2</sub> is injected at the Equator (0° longitude) throughout the altitude range 18-25 km with a Gaussian distribution centred at 21.5 km. The OH oxidation of SO<sub>2</sub> starts the production of supercooled H<sub>2</sub>O-H<sub>2</sub>SO<sub>4</sub> particles, whose size distribution is calculated in an aerosol microphysics module with a sectional approach, starting from gas-particle interaction processes (nucleation, H<sub>2</sub>SO<sub>4</sub> condensation and H<sub>2</sub>O growth) and then including aerosol particle coagulation. Removal processes are included via gravitational settling across the tropopause and evaporation in the upper stratosphere (Visioni et al. (2018)).

In the troposphere, the ULAQ-CCM includes sulfate production from the dimethyl sulfide (DMS) and SO<sub>2</sub> emissions, with gas phase and aqueous/ice SO<sub>2</sub> oxidation (by OH and H<sub>2</sub>O<sub>2</sub>, O<sub>3</sub>, respectively) to produce SO<sub>4</sub> (Feichter et al. (1996); Clegg and Abbatt (2001)). The tropospheric and stratospheric SO<sub>x</sub> budget in the ULAQ-CCM (for unperturbed background conditions) was recently discussed in Pitari et al. (2016c), with a focus on the role of non-explosive volcanic sulfur emissions, and in Visioni et al. (2018), in connection with the SG.

Aerosol extinction, optical thickness, single scattering albedo and surface area density are calculated on-line at all model grid-points every hour. This allows the interactive calculation of up/down diffuse radiation and absorption of solar near-infrared and planetary radiation by SG aerosols, with explicit full coupling of the aerosol, chemistry and radiation modules in the ULAQ-CCM. This justifies the 'composition-climate' name for this coupled model, which is more general than the usual 'chemistry-climate' model name.

The ULAQ-CCM ability to produce the correct confinement of sulfate aerosols in the tropical stratosphere has already been documented in the literature, with a comparison against SAGE II data following the Pinatubo eruption or looking at the SG

conditions (see Pitari et al. (2014); Pitari et al. (2016a); Vioni et al. (2017b)).

### 2.2.2 Upper tropospheric ice

The formation of UT ice particles may take place via heterogeneous and homogeneous freezing mechanisms. In the latter  
5 case, the ULAQ-CCM adopts the approach initially described in Karcher and Lohmann (2002), which assumes ice crystals  
formed only via homogeneous freezing of solution droplets as a function of local UT temperatures and updraft velocities, also  
including the effects of a variable aerosol size distribution. These updraft velocities are obtained as the sum of a dominant  
term related to the TKE and a much smaller contribution from the large-scale tropospheric circulation (Lohmann and Karcher  
(2002)). Typical vertical velocity net values are on the order of 10-20 cm/s (see Section 3.1) and allow the formation of thin  
10 cirrus.

For the ice supersaturation ratio, we adopt a simplified probabilistic approach, starting from the knowledge of climatolog-  
ical frequencies of the UT relative humidity ( $RH_{ICE}$ ), from which a mean value and a standard deviation can be calculated,  
assuming a normal distribution. Local ice super-saturation conditions ( $RH_{ICE} > 100\%$ ) are a result of turbulent ascent and can  
15 be found in the UT, in the vertical layer below the tropopause (where turbulent updraft conditions may be found) and above  
an altitude where  $T < 238$  K (i.e., the assumed threshold for the spontaneous freezing of solution droplets). Here, the condi-  
tions for ice formation are met and we may calculate the probability that  $RH_{ICE} > 1.5$  ( $P_{HOM}$ ). This represent the assumed  
threshold for homogeneous freezing to be activated (in our model this threshold does not depend on local temperature or  
water activity conditions), which is considerably higher with respect to the threshold for heterogeneous freezing to take place  
20 ( $RH_{ICE} > \sim 1.3$ ) (Hendricks et al. (2011)). This represents the probability that an ice particle could be formed via heterogeneous  
freezing ( $P_{HET}$ ) on a pre-existing population of ice condensation nuclei ( $P_{HET} N_{IN}$ ), typically mineral dust or BC particles  
transported from the surface ( $N_{TN}$ ).

The size distribution and number density  $n_{HET}$  of ice particles formed via heterogeneous freezing is calculated starting from  
25 the formulation of Hendricks et al. (2011) using the ULAQ microphysical scheme adopted for polar stratospheric ice particle  
formation (Pitari et al. (2002)).  $N_{IN}$  is the sum of grid-point model-predicted concentrations of mineral dust and black carbon  
aerosols ( $N_{DU}$  and  $N_{BC}$ , respectively) and is used as the population of available condensation nuclei, with  $P_{HET} P_{HET}$  being  
the probability that  $RH_{ICE} > 1.3$  at any model grid point. The problem in this case is on the actual availability of solid ice  
nuclei. A low fraction of activated IN is suggested in the literature ( $f_{DU}=1\%$  for mineral dust and  $f_{BC}=0.25\%$  for BC) because  
30 the large majority of IN will rapidly be coated by sulfate (Hendricks et al. (2011)). The number density  $n_{HET}$  is then obtained  
as:

$$n_{HET} = (f_{BC} N_{BC} + f_{DU} N_{DU}) P_{HET} \quad (1)$$

The specification of the active ice fraction for both mineral dust and BC represents the major source of uncertainty for UT ice particle formation via heterogeneous freezing. With the above assumptions ~~and under typical UT conditions,~~, in the ULAQ-CCM homogeneous freezing normally dominates ice particle formation, with respect to the heterogeneous freezing mechanism ~~(Cziczo et al. (2009); Hendricks et al. (2011))~~. However, this may not be considered a general conclusion, assumed to be valid in all thermodynamics conditions and any local atmospheric composition, as it has been shown for instance in Cziczo et al. (2013), where a predominance of heterogeneous freezing over homogeneous may be found. In general, which freezing mechanism dominates in the atmosphere is still very uncertain.

The calculated mass ~~fraction-mixing ratio~~ of ice formed in the ULAQ-CCM through both ~~freezing-freezing~~ mechanisms is shown in Fig. 1ac for two pressure layers, 150-200 hPa and 350-400 hPa, where the ice formation is greater in the tropics and mid-high latitudes, respectively. These calculations are compared against the ~~MERRA data (Bosilovich et al. (2017); Gelaro et al. (2017))~~, MERRA-2 (Bosilovich et al. (2017); Gelaro et al. (2017)) and ERA5 reanalyses (Stephens et al. (2000)), all averaged over the same decade ~~(Fig2003-2012)~~. For the upper layer (150-200 hPa), we also show in Fig. S1 the MLS satellite retrieval (Wu et al. (2008)), which compares very closely to the ERA5 reanalysis. 1bd) Tropical ice formation shows a strong land-ocean asymmetry due to significantly higher  $P_{HOM}$  and  $P_{HET}$  values over land. For both pressure layers, the magnitude and spatial distribution of the ice mass mixing ratio are comparable between the ULAQ-CCM and MERRA. Regarding the datasets used ~~in this work~~ to compare against our model results, note that there is a large spread amongst retrievals (such as MODIS or CALIPSO) and amongst reanalyses (Zhang et al. (2010); Duncan and Eriksson (2018)). In particular, MERRA-2 appears to be in the lower end of the spectrum in ~~regards-regard~~ to some quantities, such as ice water path. Considering that the dataset only considers non precipitating ice (Duncan and Eriksson (2018)), this quantity might be however closer to the one simulated in our model, and thus allow for a more correct comparison.

While the probability of homogeneous ice formation is defined as above, the number density and size of the ice particles formed this way is determined by the local temperatures and vertical velocities, in addition to the competing ice formation mechanism via heterogeneous freezing. The lower the temperature, the faster the nucleation rate; thus, more ice crystals can be formed. On the other hand, higher vertical velocities increase the saturation ratio, leading to more ice crystals formed before water deposition on ice crystals reduces supersaturation below the threshold. The spatial distribution of the cirrus ice optical depth (OD) in the model is calculated as:

$$\tau_{ice} = \Delta z \sum_i \sum_j Q_{ext} \pi r_{ij}^2 n_{ij}(r) \quad (2)$$

where the extinction efficiency coefficient  $Q_{ext} \sim 2$  at all visible wavelengths for ice particle sizes on the order of 5-50  $\mu\text{m}$ ;  $i$  is an index for the vertical layers, and the sum is over all the vertical layers in the UT;  $j$  is an index for the particle size bins, and the sum is over the whole size distribution;  $r_{ij}$  is the particle radius at the  $i$ -th layer and  $j$ -th bin; and  $n_{ij}$  is the corresponding

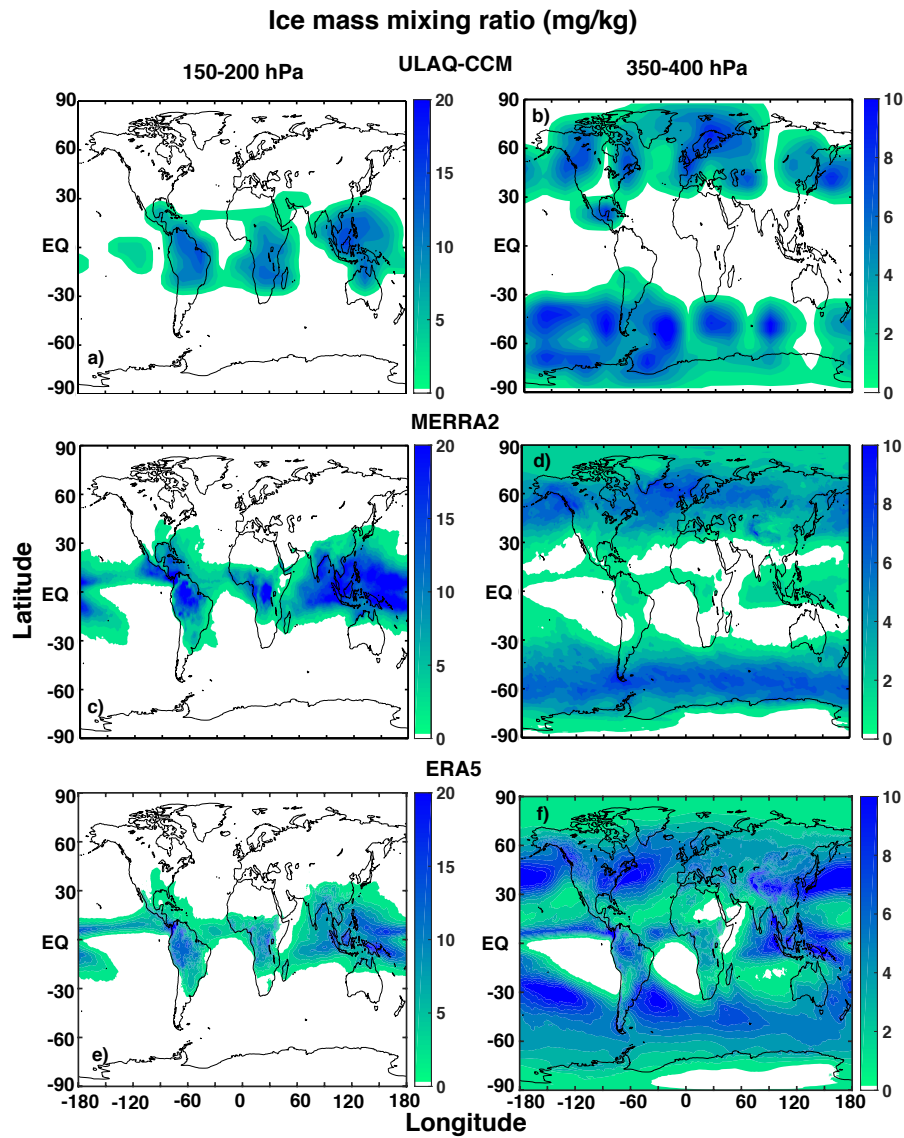


**Figure 1.** Lat/lon maps of the ice mass mixing ratio (mg/kg-air) for pressure layers representative of tropical (panels a,b,c,e) and extratropical (panels e,b,d,f) upper troposphere. Panels (a,e,b) are for the ULAQ-CCM; panels (b,c,d) are for ~~MERRA~~ MERRA-2 data (Bosilovich et al. (2017)); panels (e,f) are for ERA5 data (Stephens et al. (2000)). Time average is on years 2003-2012.

ice number density.

Equation 2 can easily be applied to the model, and the results are shown in Fig. 2a. An evaluation can be made again using the ice mixing ratio from [MERRA-MERRA-2 and ERA5](#) (shown in Fig. 1bc for two specific pressure layers), together with the [MODIS-derived ULAQ-CCM](#) values of the ice particle effective radius (<https://giovanni.gsfc.nasa.gov>) (Yang et al. (2007)). [Intrinsic limitations regarding the retrieval of this quantity are discussed in Delanoe and Hogan \(2008\) and Zhang et al. \(2010\)](#)

5 ~~With these two products quantities~~ we have indirectly derived  $\tau_{ice}$  at every horizontal grid point in Eq. (2), using the hydrostatic equation:

$$\tau_{ice} = Q_{ext} \frac{3}{2} \frac{\Delta p}{g} \frac{1}{\rho_{ice}} \sum_i \frac{\chi_i}{r_i} \quad (3)$$

where the sum is, again, over all the vertical layers (constant  $\Delta p=50$  hPa),  $g$  is the acceleration of gravity,  $\rho_{ice}$  is the ice bulk density,  $r_i$  is the [MODIS effective radius](#),  $r_i$  is the [ULAQ-CCM effective radius at the  \$i^{th}\$  layer](#); and  $\chi_i$  is the [MERRA ice mass fraction at the  \$i^{th}\$  MERRA-2 and ERA5 ice mass mixing ratio at the  \$i^{th}\$  layer](#). Doing so, we obtain [an optical depth shown the optical depth values](#) in Fig. 2b. ~~The two bc.~~ The ODs are comparable in terms of spatial distribution, with the highest values in the tropics over land. The absolute values in the ULAQ-CCM, however, are significantly smaller over the tropics. ~~This should not surprise, in principle, because we are considering thin ice clouds, with~~ [The reason is that updraft velocities result in a relatively narrow interval for updraft velocities \( \$w < \(w < 30\$  cm/s\) so that events leading to when calculated only as a function of TKE \(as in the ULAQ-CCM\), while thick cirrus formation are not considered takes place from strong \(and less frequent\) convective events \( \$w < 100\$  cm/s\). This detrained ice originating in deep convection is not included in our model formulation.](#)

15

In Fig. 3, we show the model-predicted fraction of ice formed through heterogeneous freezing in terms of optical depth (Fig.3a) and zonally averaged extinction (Fig.3b). In both panels, we see that a large part of the ice particles formed through heterogeneous freezing is located in the tropical band at lower altitudes, where a higher concentration of mineral dust and BC ice nuclei can be transported from the surface. In those regions, the fraction of ice formed this way can be as much as 80% of the total.

20

In Fig. 4ab we show the model calculated vertical profiles of ice particle number density averaged over the tropics (Fig. 4a) and the extratropics (Fig. 4b), with superimposed the time variability produced by changing conditions of vertical velocity, temperature and  $P_{HOM}$ ,  $P_{HET}$ . The ice number density maxima are located at rather different altitudes in the two latitude bands, close to 13 km in the tropics and 8 km elsewhere. This is clearly expected from the latitudinal variability of the tropopause height.

25

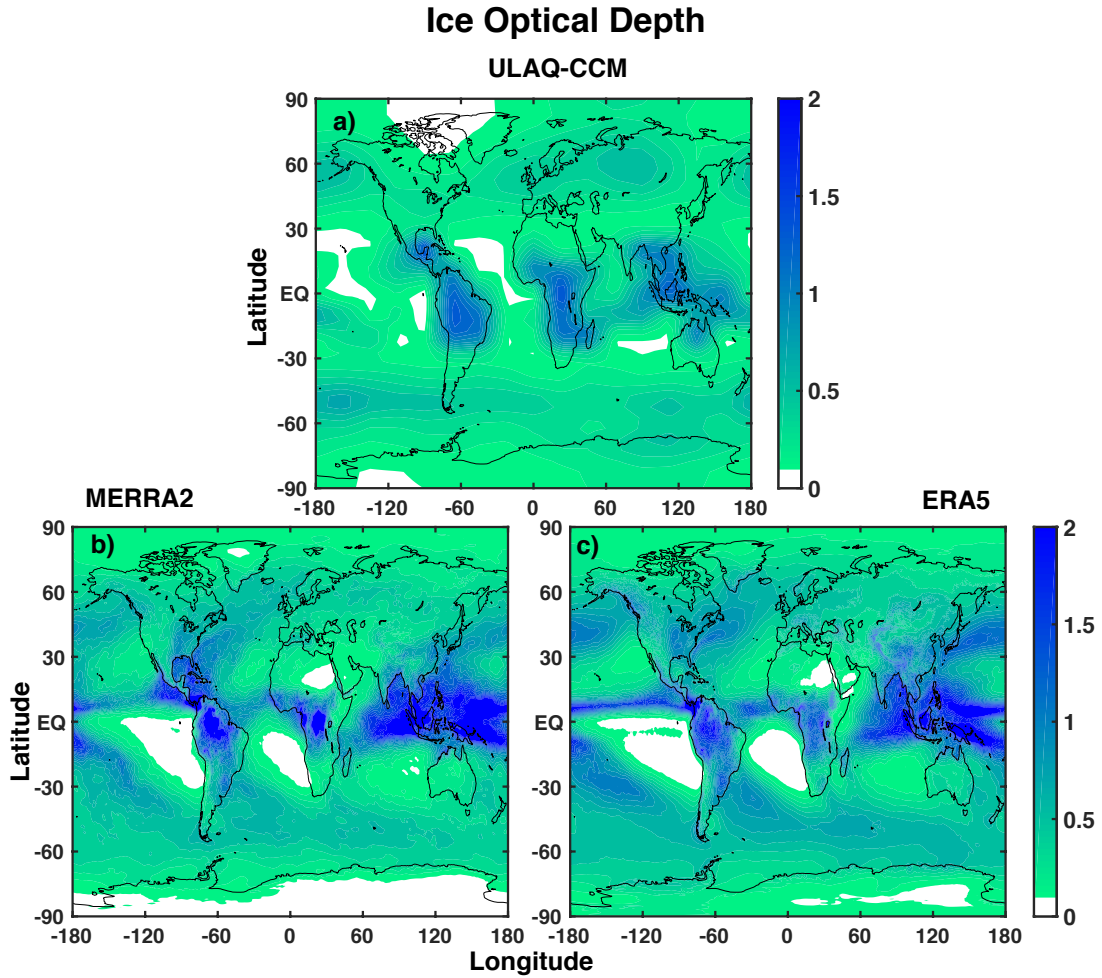


**Figure 2.** Ice optical depth at  $\lambda=0.55 \mu\text{m}$ , from ULAQ-CCM calculations (a) and from the [MERRA-MERRA-2](#) (b) and [ERA5](#) (c) ice mass fractions-mixing ratio ( $100 <<p<< 450 \text{ hPa}$ ) ([Bosilovich et al. \(2017\)](#)), with [MODIS-ULAQ-CCM](#) particle effective radius (b). Time is averaged over the years 2003-2012 ([MODIS data downloaded from https://giovanni.gsfc.nasa.gov, version MOD08M3v6](#)).

With a procedure similar to the one described above for the ice OD, we may derive a first order approximation of the ice number density from the [MERRA-MERRA-2](#) and [ERA5](#) ice mass mixing ratio and [MODIS-ULAQ-CCM](#) radii. Similar to Eq. 3, for the ice number density  $n_i$  at each vertical layer we obtain the following expression:

$$n_i = \frac{3}{4\pi} \frac{1}{\rho_{ice}} \frac{1}{r^3} \chi_i \quad (4)$$

5 The results from Eq. 4 ([red-circles in Fig. 4ab](#)) show that while the model and the indirectly derived [points-values from the reanalyses](#) agree in terms of the general vertical distribution and localization of the [vertical-maxima in the extratropics](#), the

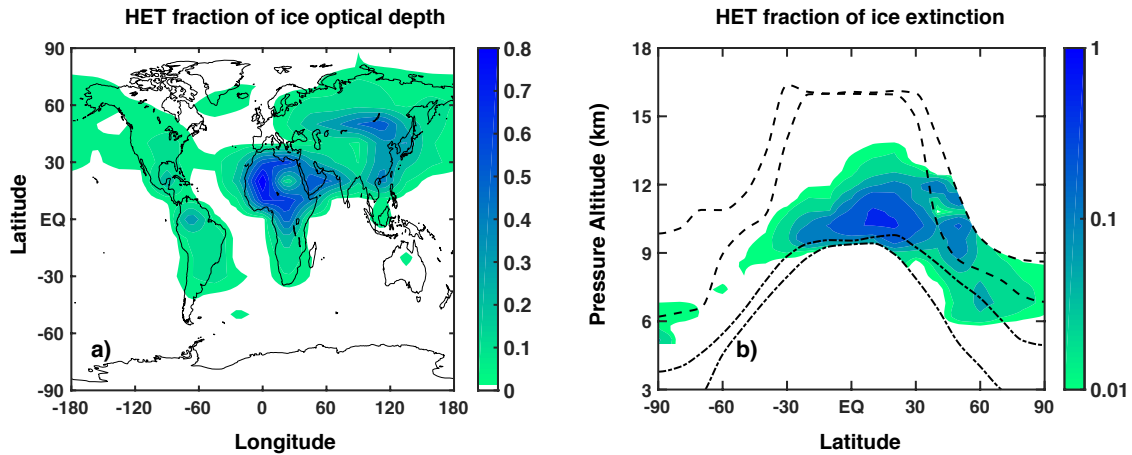


**Figure 3.** Fraction of total ice formed through heterogeneous freezing in ULAQ-CCM averaged over the years 2003-2012, as a function of latitude and longitude for the total optical depth (a) and as a function of altitude and latitude for the zonally averaged extinction (b). In panel (b), the colour scale is logarithmic, starting at 0.01 (i.e., 1% of total ice extinction) up to 1 (100%). The dashed lines show the mean tropopause height with seasonal variability (where seasonal variability is defined as  $\pm 1 \sigma$  of the average height). The dash-dotted lines show the mean height (with seasonal variability) at which  $T=238$  K (freezing is allowed for colder temperatures).

ULAQ-CCM tends, however, to have smaller number densities in the tropics in the 10-13 km layer. Again, this should not surprise in light of the fact that we are focusing on a specific type of cirrus cloud particles.

Figure 4c shows the model-calculated values of  $P_{HOM}$ , as a 2D zonally averaged distribution. Using these  $P_{HOM}$  values, it is possible to scale a  $n_i$  value measured in the mid-latitude airborne campaign of Strom et al. (1997) during a young cirrus formation, to derive an average climatological value to be considered consistent with our modelling approach. They measured a mid-latitude ice concentration value  $n=0.3 \text{ cm}^{-3}$  in a young cirrus cloud at  $T=220 \text{ K}$  and  $p=320 \text{ hPa}$ . If we scale this result with our corresponding  $P_{HOM}=12\pm 3\%$ , a 'climatological-mean' value  $n=0.025\pm 0.005 \text{ cm}^{-3}$  is obtained, close to our model prediction value of  $0.031\pm 0.008 \text{ cm}^{-3}$  (Fig. 4b).

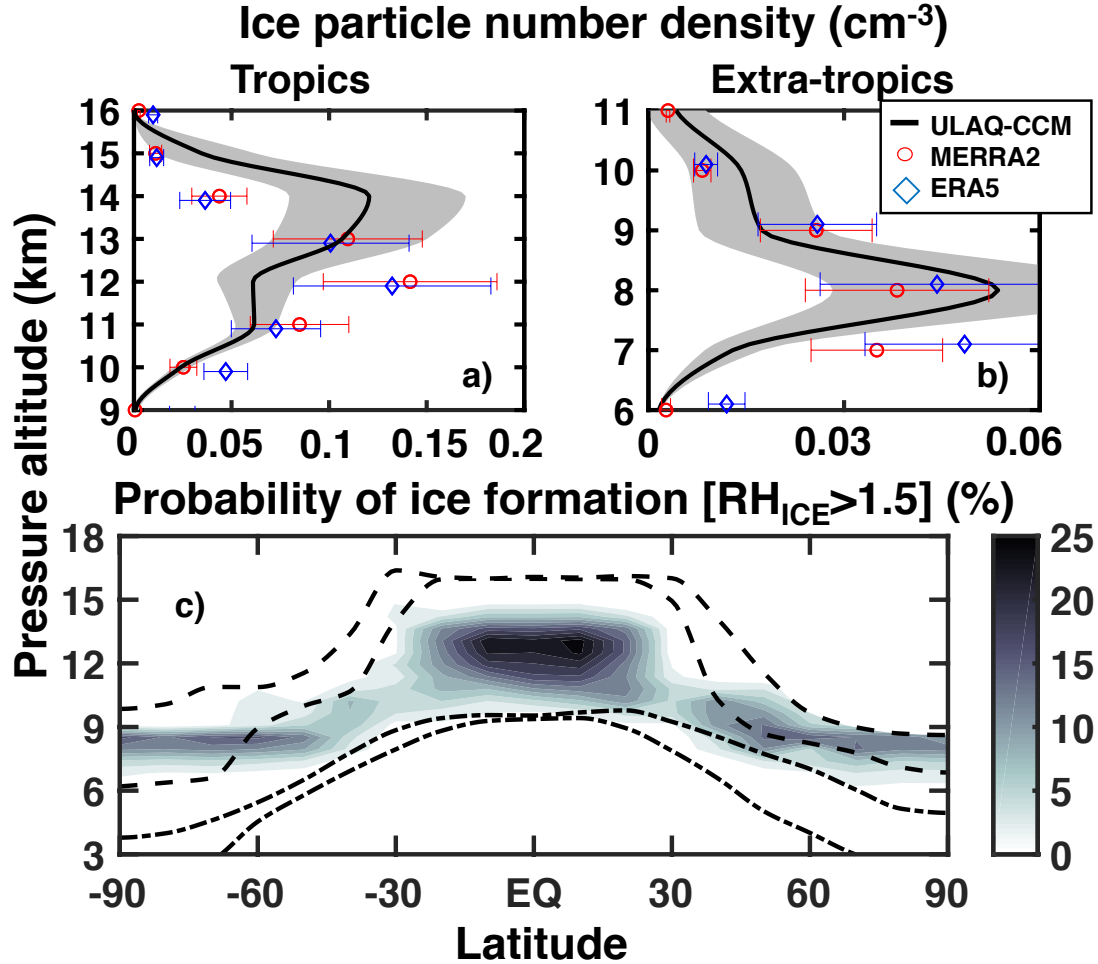


**Figure 4.** Average upper tropospheric profiles of ice particle number density ( $\text{cm}^{-3}$ ), for the tropics (25S-25N) and extratropics (35S-90S, 35N-90N), in panels (a) and (b), respectively. Time is averaged over the years 2003-2012. Shaded areas represent  $\pm 1\sigma$  for the ensemble over the 10-year period. The red circles show indirectly derived values from the [MERRA-MERRA-2](#) and [ERA5](#) ice mass mixing ratio and [MODIS-ULAQ-CCM](#) effective radius (see text). Panel (c) shows the zonally averaged probability of ice formation via homogeneous freezing (percent), as a function of altitude and latitude. The dashed lines show the mean tropopause height (with seasonal variability). The dash-dotted lines show the mean height (with seasonal variability) at which  $T=238\text{ K}$  (homogeneous freezing allowed for colder temperatures with seasonal variability).

**Table 2.** Summary of globally and time-averaged sulfate aerosol and cirrus ice particle related quantities, as calculated in the ULAQ-CCM and compared with available satellite observations and reanalyses data. Sulfate aerosols: sectional approach (Pitari et al. (2002); Pitari et al. (2014)). Cirrus ice particles: parameterization for homogenous (HOM) and heterogeneous (HET) freezing are summarized in the text and based on the formulation of Karcher and Lohmann (2002) (HOM), but including the effects of the aerosol size distribution, and Hendricks et al. (2011) (HET); a probabilistic approach is adopted for the ice supersaturation ratio. Standard deviations are calculated over the time series of globally averaged monthly mean values. On the global average, our model predicts a 90% fraction of the ice optical depth formed via homogeneous freezing.

Stratospheric sulfate optical depth [post-Pinatubo conditions] [reference (September 1991 - August 1992)]	0.11 ± 0.02 (ULAQ-CCM) 0.13 ± 0.02 (SAGE II) 0.13 ± 0.02 (AVHRR)
Sulfate $r_{eff}$ ( $\mu\text{m}$ ) (30-100 hPa, 25S-25N) [post-Pinatubo conditions] [reference (September 1991 - August 1992)]	0.54 ± 0.06 (ULAQ-CCM) 0.58 ± 0.06 (SAGE II)
Sulfate $r_{eff}$ ( $\mu\text{m}$ ) (30-100 hPa, 25S-25N) [volcanic unperturbed conditions] [reference (1999 - 2000)]	0.19 ± 0.02 (ULAQ-CCM) 0.22 ± 0.02 (SAGE II)
Ice mass mixing ratio (mg/kg) (150-200 hPa) [reference (2003 - 2012)]	3.3 ± 0.2 (ULAQ-CCM) (HOM) 0.1 ± 0.1 (ULAQ-CCM) (HET) 3.5 ± 0.4 (MERRA-MERRA-2) <u>3.2 ± 0.4 (ERA5)</u>
Ice mass mixing ratio (mg/kg) (200-300 hPa) [reference (2003 - 2012)]	3.8 ± 0.5 (ULAQ-CCM) (HOM) 0.6 ± 0.2 (ULAQ-CCM) (HET) 5.5 ± 0.8 (MERRA-MERRA-2) <u>5.7 ± 0.9 (ERA5)</u>
Ice mass mixing ratio (mg/kg) (350-400 hPa) [reference (2003 - 2012)]	2.4 ± 0.4 (ULAQ-CCM) (HOM) 0.1 ± 0.1 (ULAQ-CCM) (HET) 2.6 ± 0.5 (MERRA-MERRA-2) <u>2.7 ± 0.7 (ERA5)</u>
<del>Upper tropospheric</del> Tropospheric ice $r_{eff}$ ( $\mu\text{m}$ ) [reference (2003 - 2012)]	31.3 ± 3.1 (ULAQ-CCM) (HOM) 34.6 ± 3.8 (ULAQ-CCM) (HET) 33.4 ± 2.1 (MODIS)
<del>Upper tropospheric ice optical depth</del> <u>Tropospheric ice optical depth</u> [reference (2003 - 2012)]	0.37 ± 0.03 (ULAQ-CCM) (HOM) 0.04 ± 0.01 (ULAQ-CCM) (HET) 0.62 ± 0.04 (MERRA+MODIS MERRA-2) <u>0.65 ± 0.06 (ERA5)</u>

Relevant aerosol and ice quantities calculated in the ULAQ-CCM are summarized in Table 2 in comparison with available satellite observations. The first two rows in Table 2 compare the ULAQ-CCM results for stratospheric sulfate optical depth (OD) and the tropical effective radius ( $r_{eff}$ ) against SAGE-II and AVHRR satellite observations (Thomason et al. (1997); Long and Stowe (1994)), under post-Pinatubo conditions (Pitari et al. (2016a)). This is done to highlight the realistic representation of the gas-particle conversion and aerosol microphysics processes in the model, along with the aerosol large-scale transport in the lower stratosphere in case of a major tropical volcanic eruption, which may be used as a proxy for SG with an equatorial SO<sub>2</sub> injection. A comparison of the aerosol effective radii under volcanic and background conditions (see rows 2 and 3 in Table 2) clearly shows the effects of the sulfuric acid condensation on the size extension of the aerosol accumulation mode and how this is represented in the model.

The bottom 5 rows in Table 2 compare the global budget calculations for upper-tropospheric ice particles with values obtained from the ~~MERRA-MERRA-2 and ERA5~~ reanalyses (ice mass mixing ratio) and ~~MODIS-retrieval~~ (ULAQ-CCM effective radius (compared in row 7 with the ice effective radius as retrieved by MODIS)). The simultaneous use of these two products (reanalysis values for ice mass mixing ratio and model calculated radius) allows an indirect calculation of the ice optical depth (row ~~7 of Table 28 of Table 2~~), as previously discussed. The ULAQ-CCM OD underestimation is mostly related to the ice mass mixing ratio lower values in the largest portion of the upper troposphere (see row 5 of Table 2 ) and may be, in part, explained with the inclusion of a relatively narrow interval for updraft velocities ( $w < 30$  cm/s).

The values are given separately for the ice formed through homogeneous and heterogeneous freezing.

### 2.3 Setup of the numerical experiments and role of perturbed SSTs

The use of a composition-climate coupled model, such as the ULAQ-CCM model, offers multiple advantages in this type of study: (a) the on-line inclusion of interaction between aerosol and ice particles microphysics with chemistry, radiation, climate, dynamics and transport; (b) the stratosphere-troposphere explicit interactions for the large-scale transport of gas and aerosol species (the model adopted high vertical resolution is important across the tropopause region); (c) the sufficiently detailed chemistry both in the stratosphere and troposphere, with a robust design for heterogeneous chemical reactions on sulfuric acid aerosols, polar stratospheric cloud particles, and upper tropospheric ice and liquid water cloud particles. This allows us to account for the atmospheric circulation changes produced by sulfate geoengineering. The ULAQ-CCM model has many times proven to be capable of producing sound physical and chemical responses to both sulfate geoengineering (Pitari et al. (2014); Vioni et al. (2017b)) and for large explosive volcanic eruptions (Pitari (1993); Pitari et al. (2016b); Pitari et al. (2016a)).

In addition to a reference historical model experiment (1960-2015), we performed three sets of SG simulations: a baseline (Base) unperturbed case and two geoengineering experiments (G4 and G4K), both run with an injection of 8 Tg-SO<sub>2</sub>/yr into the equatorial stratosphere between 18 and 25 km of altitude, as described in Kravitz et al. (2011) for the GeoMIP G4 experiment with a sustained fixed injection of sulfur dioxide (5 Tg-SO<sub>2</sub>/yr in that case: while we use 8 Tg-SO<sub>2</sub>/yr, all other prescriptions such as height and latitude of the injections are the same as in the above mentioned paper). These numerical experiments

were all run between years 2020 and 2069, with analyses focusing on the 2030 to ~~2039-decade~~2069 period; all take place under the same RCP4.5 reference scenario for well-mixed greenhouse gases. The ULAQ-CCM is not an atmosphere-ocean coupled model and uses ~~a nudging technique for surface temperatures, taking them externally provided surface temperatures as prescribed boundary condition for the dynamical module.~~ These surface temperatures are taken from the CCSM-CAM4 model, which was run under the same RCP4.5 and G4 conditions (8 Tg-SO<sub>2</sub>/yr fixed injection into the equatorial lower stratosphere). In this way our main experiment G4 may account for the ~~oceanic surface temperature-T<sub>s</sub>~~ response to SG (Fig. 4-5). We acknowledge that ~~the perturbation introduced in the dynamics of ULAQ-CCM by the external SSTs changes is a first-order~~ this procedure may only be valid as a first order approximation, considering that CCSM-CAM4 has not been run with a coupled chemistry and a much simpler cirrus parametrization that produces negligible changes in the geoengineering experiment (Neale et al. (2013)). However, we believe it to be still a consistent one, considering that the main effect produced by the sulfate injection is the direct aerosol effect (Visioni et al. (2017a)) and that the prescribed stratospheric aerosol field in the SG simulation in CCSM-CAM4 (Tilmes et al. (2015)) is comparable to the one produced by the sulfate injection in ULAQ-CCM. With this in mind, in the next ~~paragraph we discuss the SSTs perturbation and their~~ paragraphs, we first discuss the T<sub>s</sub> perturbation and its significance for this study and then the approach adopted for minimizing the inconsistency introduced in ULAQ-CCM with the use of T<sub>s</sub> from a different model.

A strong inter-hemispheric asymmetry in the ~~surface temperature-T<sub>s</sub>~~ changes produced by ~~the SG with an 8 Tg-SO<sub>2</sub>/yr injection~~ SG is evident in ~~both Figs. 5-6~~ Fig. 5 (see also the annually and zonally averaged values in Fig. 6a), with a negative anomaly in the Arctic region that is approximately 1 K larger than that of the high southern latitudes. The SG cooling impact on the Arctic sea ice is such that larger negative surface temperature anomalies are favoured in the Northern Hemisphere high latitudes for several months during the year, from the fall to spring months (see Fig. 5a, Fig. 5b, Fig. 5d), thus increasing atmospheric stabilization with respect to the Southern Hemisphere. Note, however, that the dynamical effects of this enhanced atmospheric stability in the SG conditions (decreasing wave activity and turbulence) may be partially counterbalanced by the increased longitudinal variability of the induced cooling, mostly connected with positive surface temperature anomalies in the subpolar North Atlantic. These positive temperature anomalies in the North Atlantic sub-Arctic are a direct consequence of the increasing amount of polar sea ice in the SG conditions, with the southward transport of colder and saltier ocean waters in the sub-Arctic, with respect to the RCP4.5 Base conditions (Tilmes et al. (2009)). In this way, the North Atlantic subpolar downwelling of these cold surface waters to the deep ocean is favoured with respect to the Base conditions, thus producing positive anomalies in sea surface temperatures.

Although not statistically significant, the SG-induced warming on the Antarctic continent during wintertime (Fig. 5c) is a direct consequence of the geoengineering aerosol positive radiative forcing in the planetary longwave, which represents the net forcing at these high latitudes in the absence of sunlight. This radiative feature will be further discussed in Section 3. All these high-latitude positive temperature anomalies directly reflect in the large variability of the zonally averaged surface temperature

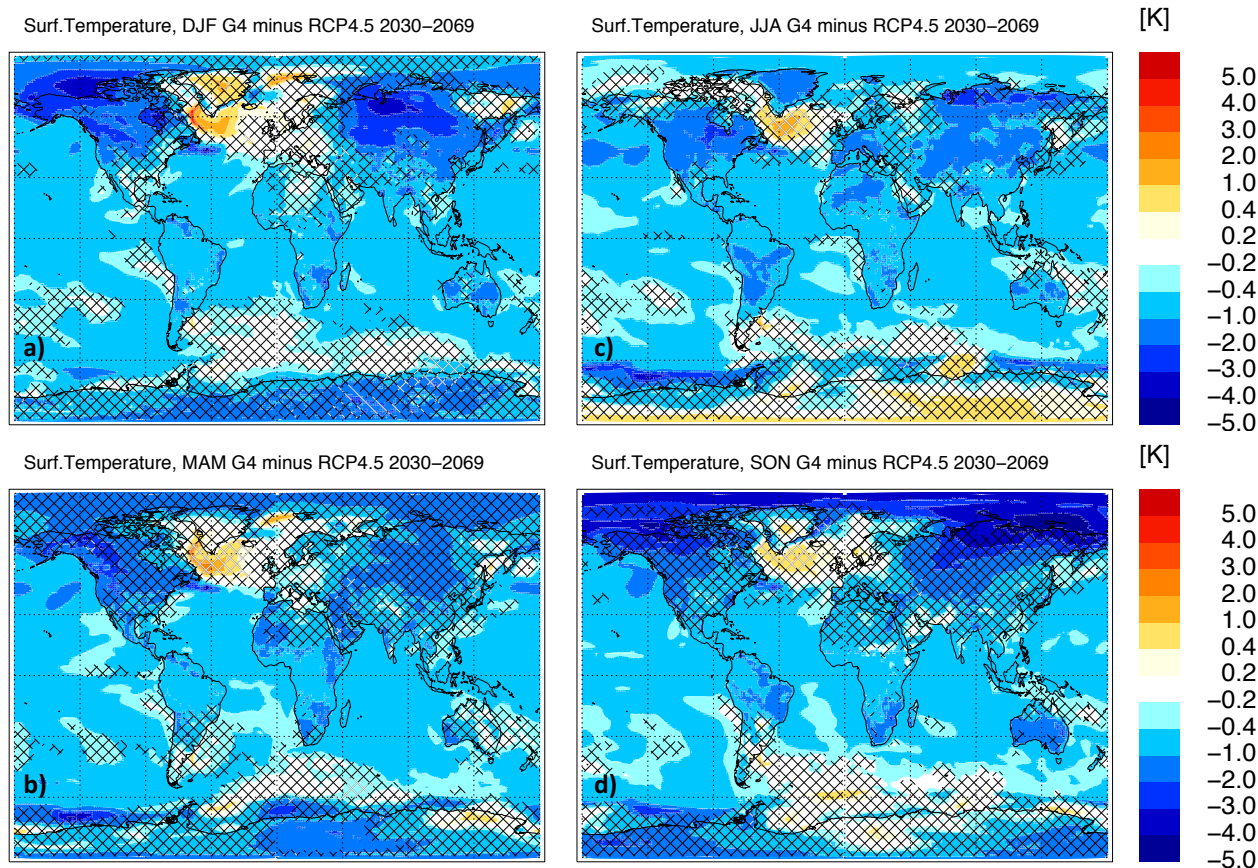


**Figure 5.** Seasonally averaged surface temperature anomalies G4-RCP4.5 (K) from the atmosphere-ocean coupled model CCSM-CAM4 (time average 2030-2069). The shaded areas are not statistically significant within  $\pm 1\sigma$ . Panels (a-d) refer to: December-January-February (a); March-April-May (b); June-July-August (c); September-October-November (d).

changes presented in Fig. 6-a.

To correct for the potentially significant model inconsistency introduced by the use of surface temperatures taken from a different model, the following procedure has been adopted. The ULAQ-CCM radiative-climate module has been modified for calculating on-line (in a fully coupled approach) the  $T_s$  perturbation produced by the radiative flux changes due to the stratospheric sulfate aerosol imbalance with respect to the CCSM-CAM4 distribution in the G4 case. In addition, we also include in the radiative balance the SG-driven indirect perturbation of greenhouse gases ( $O_3$ ,  $H_2O$ ,  $CH_4$  and  $CO_2$  from the changing methane oxidation), as well as of upper tropospheric ice particles. This on-line calculated  $T_s$  perturbation is then added to the externally provided  $T_s$  field from CCSM-CAM4 for the G4 experiment. Table S1, Fig. S2 and Fig. 6 document

these radiative flux changes and their impact on the calculated Ts.

5 Surface temperature changes due to the above discussed indirect SG effects are calculated from the instantaneous perturbation of radiative fluxes, which is of course an exact procedure over continents and polar ice caps, whereas is only approximate over the oceans. On the other hand, as explained above and clearly visible in Table S1, Fig. S1 and Fig. 6, the radiative perturbation additive to the dominant one (i.e., the one produced by stratospheric sulfate aerosols in the CCSM-CAM4 simulation) is normally small, both globally and locally (notice the different color scale between Fig. 6b and Fig. 5). Only the ice induced changes of Ts may be comparable in magnitude to those from the stratospheric aerosols, but limited to tropical continental surfaces, where UT ice may have significant optical depth values. On the other hand, the SST calculated changes due to chemistry and ice indirect effects of SG are usually smaller, so that the impact of our approximation may be expected to be negligible.

10

Together with the G4 simulation, a sensitivity case (G4K) was run, with surface temperatures fixed at the RCP4.5 Base values. Here, the experimental approach is similar to that of Kuebbeler et al. (2012) who ran a G4 simulation with a 5 Tg-  
15 SO<sub>2</sub>/yr injection and prescribed sea surface temperatures and sea ice from the RCP4.5 Base case. This is done not only to highlight the role of the tropospheric temperature perturbations in cirrus ice formation (given a certain vertical velocity change) but mostly to calculate the updraft sensitivity to different conditions of tropospheric stabilization introduced by the stratospheric sulfate aerosol injection.

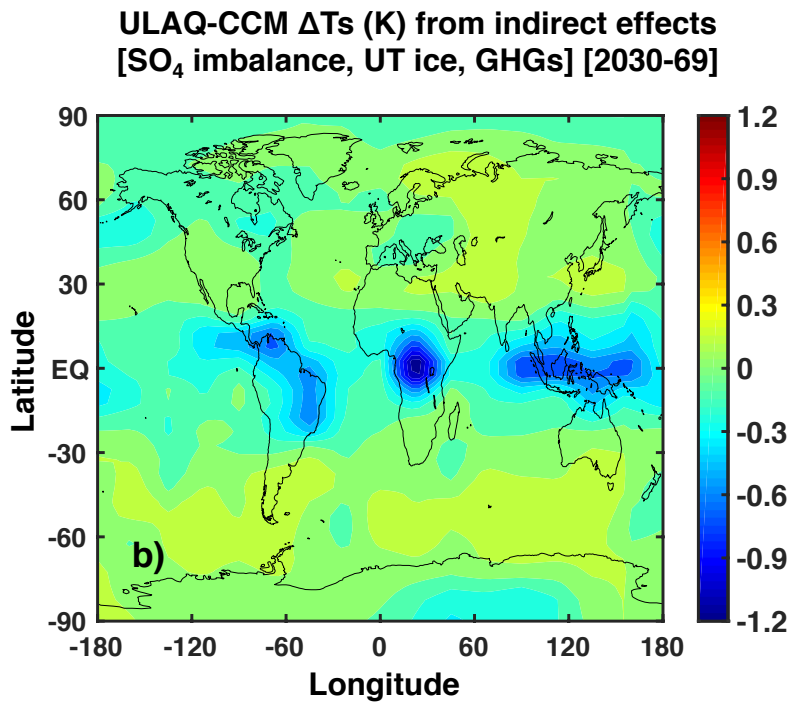
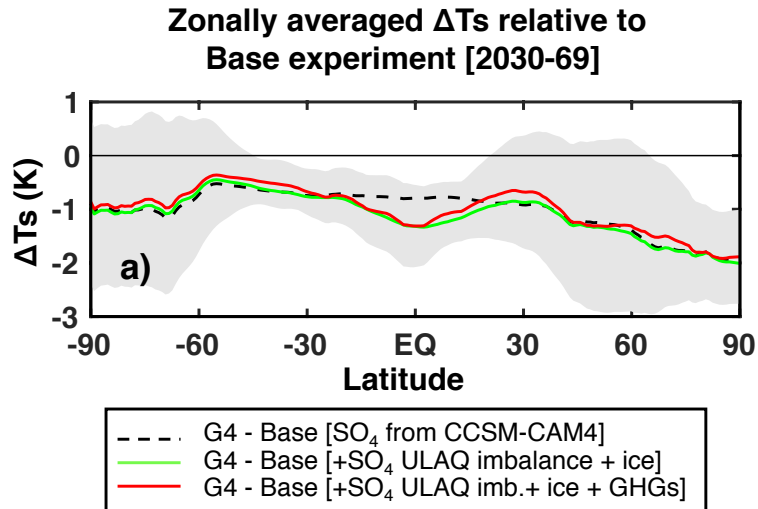


**Figure 6.** Annually- and Panel (a): zonally averaged surface temperature- $T_s$  anomalies G4-RCP4.5 (K), under different conditions for the G4 perturbed case (time average 2030-69): from the atmosphere-ocean coupled model CCSM-CAM4 (time average 2030-39) black dashed line); as above, but adding the  $T_s$  anomalies in the ULAQ-CCM with on-line coupling of cirrus ice changes and the  $\text{SO}_4$  imbalance between CCSM-CAM4 and ULAQ-CCM (green line); as above, but adding also the  $T_s$  anomalies in the ULAQ-CCM with on-line coupling of GHG changes (red line) (see text and legend). The shaded area represents  $\pm 1 \sigma$  of the zonally averaged temperature anomalies- $T_s$  over the 10-year-40-year period. b) Lat-lon distribution of the  $T_s$  anomalies (K) calculated on-line in the ULAQ-CCM model considering cirrus ice changes, the  $\text{SO}_4$  imbalance between CCSM-CAM4 and ULAQ-CCM and GHG changes (time average 2030-2069).

### 3 Model response to sulfate geoengineering

In this section, we will show the ULAQ-CCM response to the stratospheric sulfate injection. Some of the perturbations have already been discussed in previous works, in particular regarding stratospheric dynamics changes (Pitari et al. (2014); Visioni et al. (2017b)). Here, we will focus on the thermo-dynamical changes in the upper troposphere and, consequently, on changes  
5 in the formation of cirrus ice clouds.

#### 3.1 Thermo-dynamical changes in the troposphere

Figure 7 shows the differences in temperature and updraft in G4 and G4K with respect to the Base case. In G4, we observe a tropospheric cooling of  $\simeq 1-2$  K in the ice formation region throughout all latitudes, while the warming due to the sulfate  
10 aerosol absorption of shortwave and longwave radiation is confined above the tropopause (Fig. 7a). When surface temperatures are kept fixed at the RCP4.5 baseline values with the SG perturbation (G4K case), the upper troposphere and lower stratosphere temperature anomalies look very different (Fig. 7b). The tropospheric cooling is absent and the stratospheric warming produced  
15 by [longwave absorption of longwave planetary](#) and near-infrared solar radiation [absorption](#) is more uniformly spread across the lower stratosphere, with some penetration also in the UT ( $\simeq 0-1$  K). The latter is due to the sulfate aerosol cross-tropopause  
fluxes that are due to the large-scale transport (at mid-latitudes) and gravitational sedimentation (mostly relevant in the tropical region).

The updrafts responsible for the upper tropospheric ice particle formation result from the sum of a rather small large-scale vertical velocity contribution (on the order of 1-2 cm/s) and a dominant part due to motions associated with synoptic scale disturbances and gravity waves (on the order of 10-20 cm/s); the latter is calculated as a function of the TKE (Lohmann and  
20 Karcher (2002)) with the exact formulation reported in Eq. 5:

$$w_{TOT} = w_{LS} + 0.7\sqrt{TKE} \quad (5)$$

The vertical velocity is reduced in G4 with respect to the Base case by  $\simeq 1-2$  cm/s in the whole UT (Fig. 7c) (on the order of -10%, as visible in Fig. 8), due to the atmospheric stabilization caused by a reduction in the temperature vertical gradient.

Fig. 9a shows the average tropical vertical profiles of the  $\text{SO}_4$  mixing ratio ([in the particulate phase](#)), for both the Base and  
25 SG experiments (with an 8 Tg- $\text{SO}_2$  injection). The changes in zonally averaged net heating rates, temperatures and zonal winds are also shown in Fig. 89, panels (b), (c) and (d), respectively. They help explain how the SG sulfate [changes act as drivers](#)  
[perturbation may act as driver](#) for dynamical changes in the UT, with significant effects on ice particle formation.

In Fig. 9a, it is interesting to note a somewhat smaller tropical aerosol confinement in the G4K case. This is consistent with the findings of Visioni et al. (2017b): the aerosol-driven surface cooling in G4 (contrary to G4K) favours a decreased wave  
30 activity and a consequent decrease in poleward mass fluxes from the tropical reservoir, for both gas and aerosol species. On the other hand, the increased  $\text{H}_2\text{SO}_4$  tropical amount available for aerosol formation tends to produce larger particles with smaller equivalent optical thickness (see Niemeier and Schmidt (2017); Visioni et al. (2018)). In light of this, smaller stratospheric

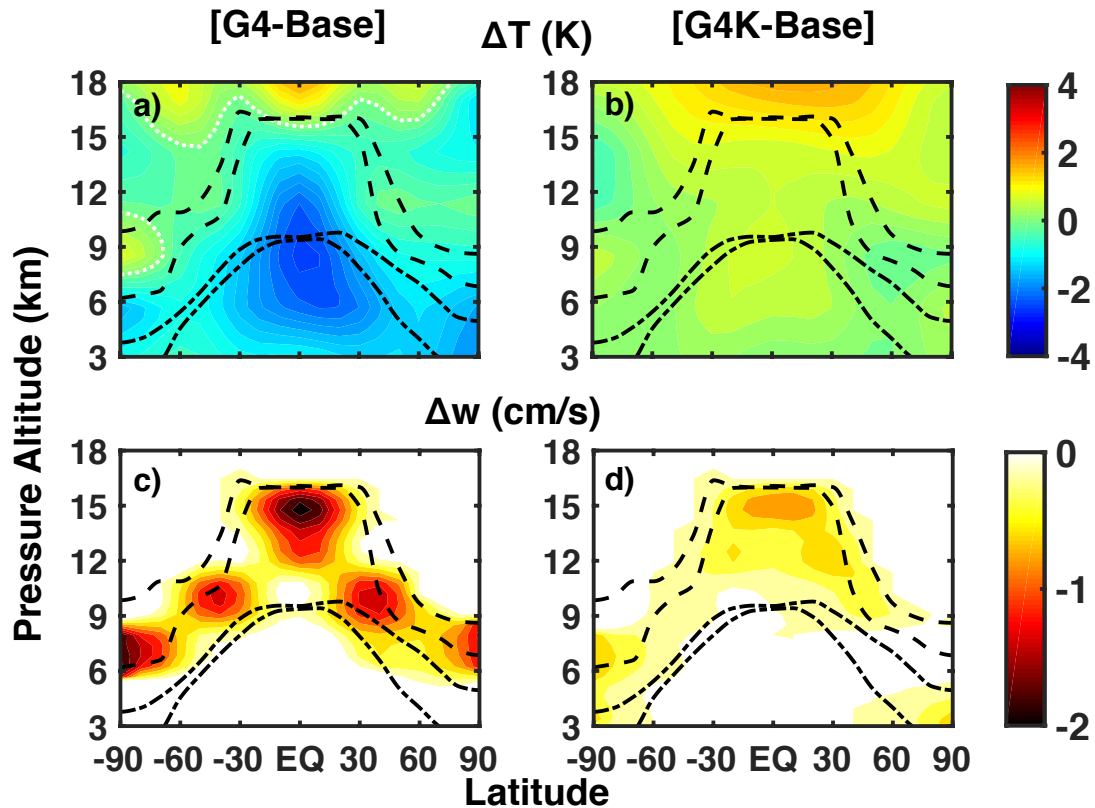


**Figure 7.** Zonally and time-averaged changes of temperature (panels a,b) and vertical velocity (panels c,d) in experiments G4 (panels a,c) and G4K (panels b,d) with respect to the Base case (years 2030-39/2030-69). The dashed lines show the mean tropopause height (with seasonal variability). The dash-dotted lines show the mean height at which  $T = 238$  K (with seasonal variability) at which the temperature reaches 238 K. The dotted white lines in panel a) highlights where  $\Delta T = 0$  K, thus enabling homogeneous freezing.

heating rate anomalies are calculated in G4 with respect to G4K (Fig. 9b): in the latter case, we then expect an enhanced temperature increase in the tropical lower stratosphere (Fig. 9c), coupled to a slight tropospheric warming due to the SG aerosol sedimentation below the tropopause. The latter, in addition, causes the on the other hand, results to be greatly overbalanced by tropospheric convective cooling produced by the aerosol-driven surface cooling-mid-upper tropospheric cooling in G4, due to less intense latent heat exchange resulting from the aerosol-driven  $T_s$  decrease (contrary to G4K). As a result, the G4 atmosphere is more efficiently stabilized with respect to G4K, and the positive/negative anomalies of  $T/u$  shears in the UT (Fig. 9cd) favour a decrease of the TKE (and updraft velocities) in G4 with respect to G4K (Fig. 7cd).

All features of the SW and LW heating rate anomalies in Fig. 9b can be fully explained taking into account the aerosol- $O_3$  coupled effects (Pitari et al. (2014)). The sign of tropical ozone changes under the SG conditions depends on altitude. The  $O_3$  decreases below  $\sim 25$  km and increases above this height; this helps explain the positive/negative heating anomalies in SW and

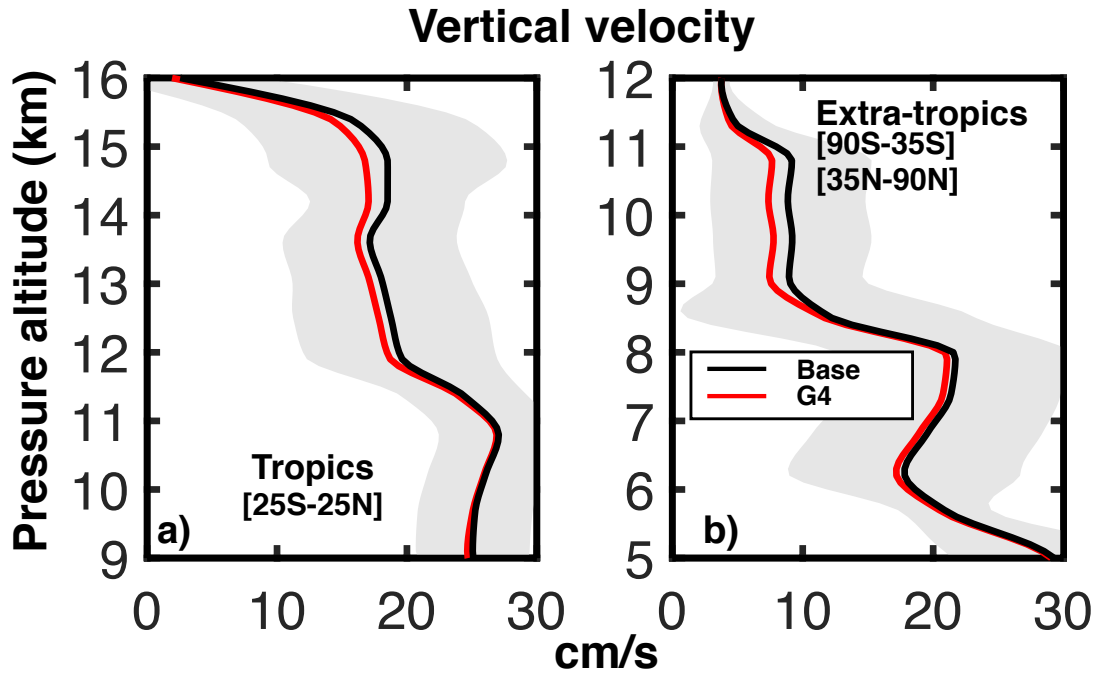


**Figure 8.** Average upper tropospheric profiles of the vertical velocity (cm/s) in G4 and Base experiments (years ~~2030-39~~2030-69). Panels (a) and (b) are for the tropics and extratropics, respectively (see legends). The vertical velocity  $w$  is obtained as the sum of the large-scale value and that calculated as a function of the TKE (see Lohmann and Karcher (2002) and Eq. 5), which essentially accounts for the synoptic scale and gravity wave motions. The shaded areas of the same color represent  $\pm 1\sigma$  for the ensemble over the ~~10-year~~40-year period 2030 to ~~39-~~69-.

LW components above 25-km altitude.

The SG induced reduction of updraft velocities is significantly smaller in the G4K case ( $\simeq 0.5$  cm/s, on the order of -3% the baseline values), as clearly visible in Fig. 7d. This will represent the major change in our approach to studying the UT ice sensitivity to SG with respect to the one adopted in Kuebbeler et al. (2012). According to our calculations, when taking into account both the main radiative effects of geoengineering stratospheric aerosols (i.e., lower stratospheric heating on one hand, surface and tropospheric cooling on the other hand), the resulting impact on tropospheric turbulence and updraft is significantly enhanced with respect to the case in which only the stratospheric warming is considered. A noticeable difference in the G4K  $w$ -anomalies with respect to those of G4 is at low altitudes over the polar regions, where the G4K negative values are larger than in G4. This may be largely explained by the increasing longitudinal variability of surface temperatures in the G4 case, mainly in the sub-Arctic region (see previous discussion relative to Fig. 5).

The tropical and extratropical average profiles of the updraft velocity are shown in Fig. 8 for both the Base and G4 conditions. The G4K curve (not shown) is intermediate between the previous two. The pronounced variability of the vertical velocity is

expected as a consequence of time, latitude and longitude fluctuations of the TKE. This will produce a significant dispersion of the ice particle size distribution (see ahead in Section 3.2).

## Tropical profiles

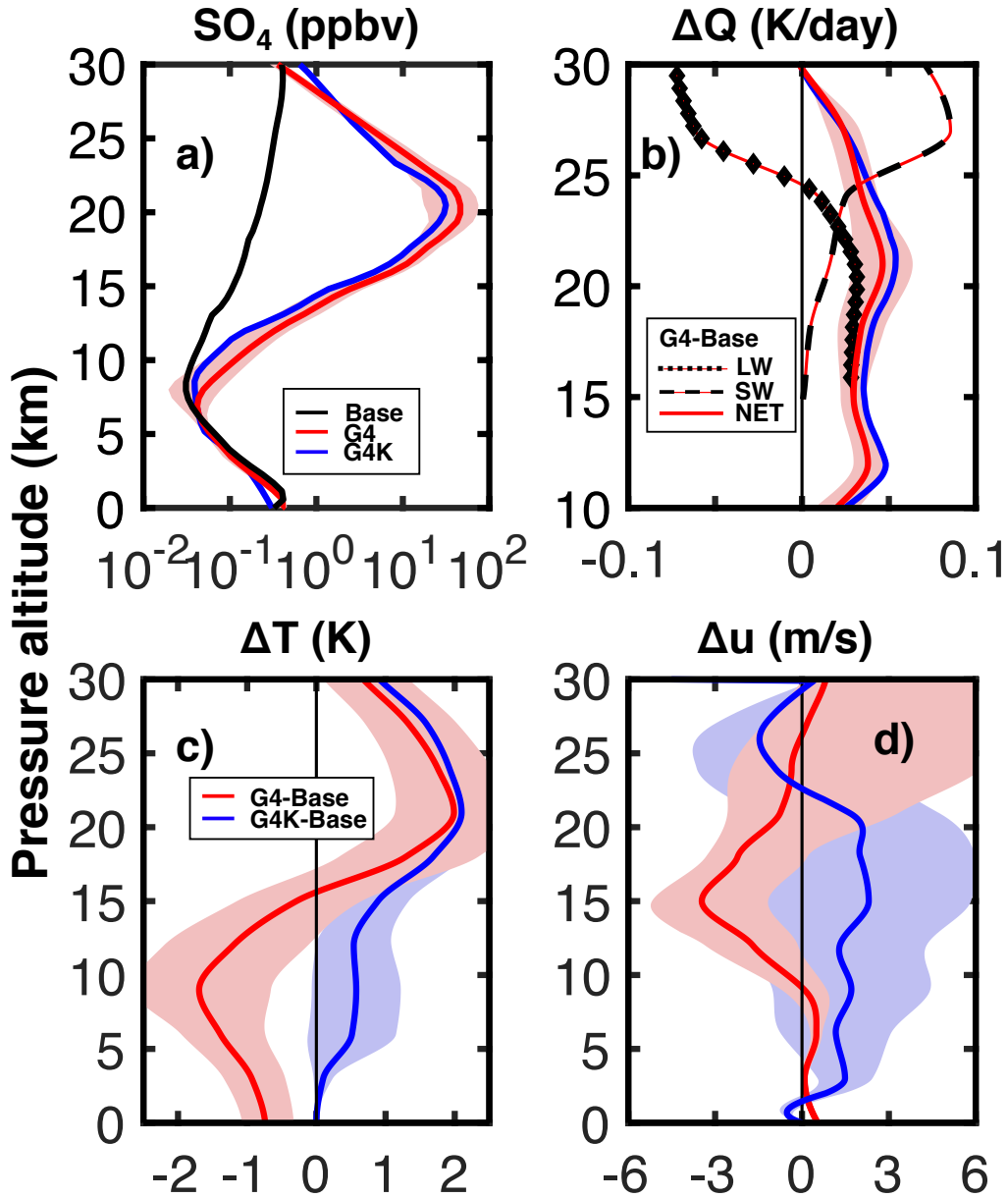


**Figure 9.** Average tropical vertical profiles (25S-25N, years 2030-39/2030-69) of the SO<sub>4</sub> volume mixing ratio for G4, G4K and Base experiments (ppbv, panel a); G4-Base changes of net, shortwave and longwave heating rates (K/day, panel b) (LW is calculated with temperature fixed at Base values) (net heating rate changes are also shown for G4K-Base, with the blue line); G4-Base and G4K-Base temperature changes (K, panel c); G4-Base and G4K-Base changes of mean zonal winds (m/s, panel d). The shaded areas of the same colour represent ± 1σ for the ensemble over the 10-year/40-year period 2030 to 39/69.

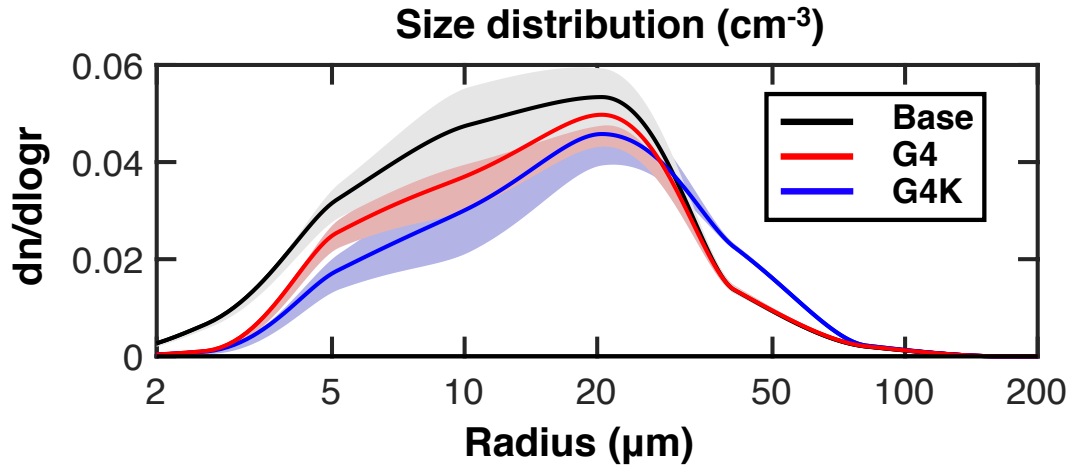


**Figure 10.** Globally and time-averaged number density values of ice crystals as a function of particle radius ( $dn/d\log r$ ,  $\text{cm}^{-3}$ ) (years ~~2030-39~~2030-69). Shaded areas of the same colour represent  $\pm 1 \sigma$  for the ensemble over the ~~10-year~~40-year period ~~2030-39~~2030-69. The calculated global mean values of the ice particle effective radius are as follows: Base  $\rightarrow$  ~~31.3~~31.2 $\pm$ ~~3.1~~3.2  $\mu\text{m}$ ; G4  $\rightarrow$  ~~33.1~~33.5 $\pm$ ~~3.4~~3.6  $\mu\text{m}$ ; G4K  $\rightarrow$  ~~36.9~~36.8 $\pm$ ~~4.0~~4.1  $\mu\text{m}$ . The reference MODIS value in Table 2 is  $33.4 \pm 2.1 \mu\text{m}$ .

### 3.2 Tropospheric ice perturbations due to sulfate geoengineering

In Section 2.2.2, we showed that the ULAQ-CCM parametrization for ice particle formation through both homogeneous and heterogeneous freezing produces a spatial distribution of the UT ice particles reasonably comparable to available data in terms of ice number concentration, OD, mass mixing ratio and effective radius. We now move to analyse the model-calculated SG perturbation of some of these quantities by comparing the G4 and G4K simulations against the Base case. As we have previously discussed and shown in Fig. 7-9, these perturbations are essentially produced and regulated by decreasing vertical velocities (-1.7 cm/s and -0.8 cm/s, in the tropical region below the tropopause, for G4 and G4K, respectively) and by changing the tropospheric temperatures (-1.2 K and +0.5 K, in the tropical UT region, for G4 and G4K, respectively).

The model-calculated globally and time-averaged size distribution of the ice particles is presented in Fig. 10 for the three experiments, along with their globally averaged effective radius. A significant change in size distribution is highlighted in Fig. 10 in both SG experiments with respect to not only the Base case, but also G4 and G4K. The common feature in both SG cases is the expected decreased particle population over the whole radial spectrum with respect to the Base experiment. This is due to the increased atmospheric stabilization forced by the SG aerosols with reduced updraft velocities and consequent decrease of the UT ice supersaturation probability.

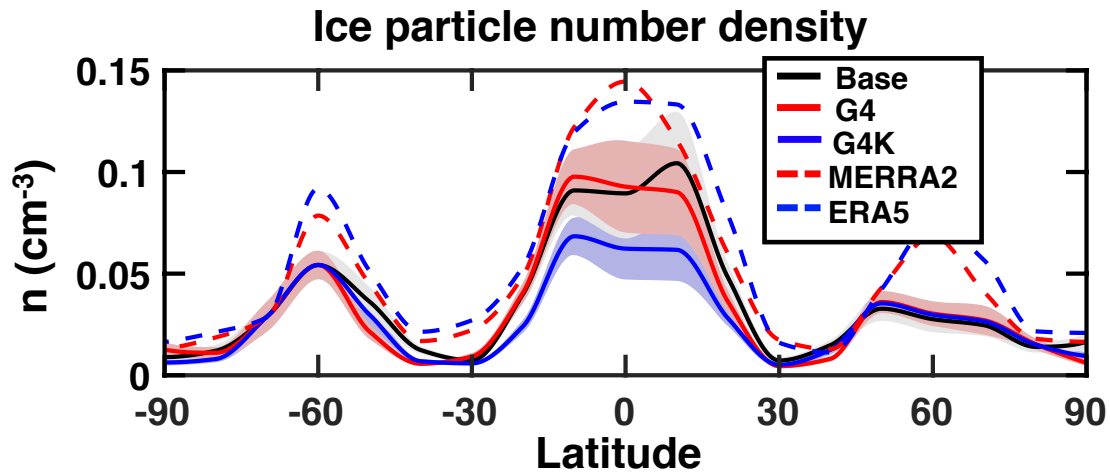


**Figure 11.** Zonally and time-averaged total number density values of ice crystals as a function of latitude ( $n$ ,  $\text{cm}^{-3}$ ) (years 2030-39/2030-69), as calculated in the ULAQ-CCM (for Base, G4, G4K experiments) and compared with indirectly derived values from the [MERRA-MERRA-2](#) and [ERA5](#) ice mass [fraction-mixing ratio](#) and [MODIS-effective-radius-ULAQ-CCM](#) (Eq. 4). Number densities are calculated at pressure layers 150-200 hPa for 25S-25N, 200-250 hPa for 25-35 (N/S), 250-300 hPa for 35-45 (N/S), 300-350 for 45-55 (N/S) and 350-400 for 55-90 (N/S).

The UT temperature anomalies, however, are very different in the two SG experiments with respect to the Base case (see Fig. 67). As a consequence of this, the tropospheric cooling produced in G4 by the [surface-temperature-Ts](#) adjustment to the stratospheric aerosol negative RF favours a number density increase of ice particles with respect to the G4K experiment but is still less than in the Base case (see also Fig. 11), due to the dominant impact of the reduced updraft. Cooler temperatures, in fact, cause a faster nucleation of the ice particles, quickly removing water vapour available for the freezing itself and limiting the condensational growth of ice particles (Kuebbeler et al. (2012); Visioni et al. (2017a)). At the same time, the velocity and temperature negative anomalies partially compensate each other also in the particle size spectrum, with a resulting effective radius in G4 larger with respect to the one in the unperturbed atmosphere ( $33.133.5 \pm 3.43.2 \mu\text{m}$  and  $31.331.2 \pm 3.13.2 \mu\text{m}$ , respectively) but smaller than that in G4K. In this latter case, the UT is slightly warmed up with respect to the Base case (see Fig. 7) so that both the velocity and temperature anomalies tend to increase the particle size ( $36.936.8 \pm 4.04.1 \mu\text{m}$ ). Globally, the ULAQ-CCM baseline values of the effective radius fall well inside the MODIS range of variability ( $33.4 \pm 2.1 \mu\text{m}$ ). As visible in Fig. 11 the calculated ice number densities follow the zonal mean behaviour of the [MERRA+MODIS-MERRA-2](#) and [ERA5](#) indirectly derived values, with the previously discussed underestimation tendency, mainly in the tropical region (see Fig. 4).

15

### 3.2.1 Optical depth

The ice extinction anomalies of G4-Base that are calculated in the ULAQ-CCM are negative in the whole UT (Fig. 12ab) due to the decreasing number density of the particles caused by the reduced vertical velocities in the SG dynamical conditions (see Fig. 7-8). Although the UT cooling in G4 tends to partially offset the effects of the updraft decrease on the ice particle number density, the overall impact is of a general decrease of the UT ice extinction and is even more pronounced than in G4K where the tropospheric cooling is not taken into account. In the latter case, however, the particle effective radius is larger than in G4, as discussed above for Fig. 10. These size distribution changes affect not only ice extinction, but also the shortwave and longwave radiative responses per unit optical depth (see ahead Section 3.2.2).

Following the procedure described in Section 2.2 (see Eq. 3), an evaluation of the model calculated ice extinction profiles is attempted (Fig. 12cd). This is made using indirectly derived values from the [MERRA-MERRA-2 and ERA5](#) ice mass mixing ratio and the [MODIS effective radii](#) [ULAQ-CCM effective radius](#), as in Eq. 6 below. Here,  $\chi_{ext,i}$  is the ice extinction at the  $i$ -th  $i^{th}$  vertical layer and  $\rho_{atm,i}$  is the atmospheric mass density at the same vertical layer:

$$\chi_{ext,i} = Q_{ext} \frac{3}{2} \frac{\rho_{atm,i}}{\rho_{ice}} \frac{\chi_i}{r} \quad (6)$$

The ULAQ-CCM tropical underestimation of the ice extinction below 13 km is consistent with that of the ice number density and is partly justified by the specific assumptions made on cirrus cloud formation in the model, as pointed out in the discussion of Fig. 4.

The net result on the ice optical depth (i.e., the vertical integral of ice extinction) is shown in Fig. 13. In general, a latitude-dependent OD reduction comparable to that found in Kuebbeler et al. (2012) is present in G4K, while in the G4 case (as expected from the extinction anomalies) a further decrease is calculated mainly in the tropics, even though the UT temperatures are cooler. The effects regarding the temperature and updraft cannot be easily separated, but the colder tropospheric temperatures in G4 with respect to G4K reduce the particle size increase respect to the Base case, producing an additional decrease in the optical depth. The coupled effects of the velocity and temperature anomalies on the ice particle number density and size produce the most relevant impact in our study, pointing out the importance of allowing surface temperatures to respond to the stratospheric aerosol radiative forcing.

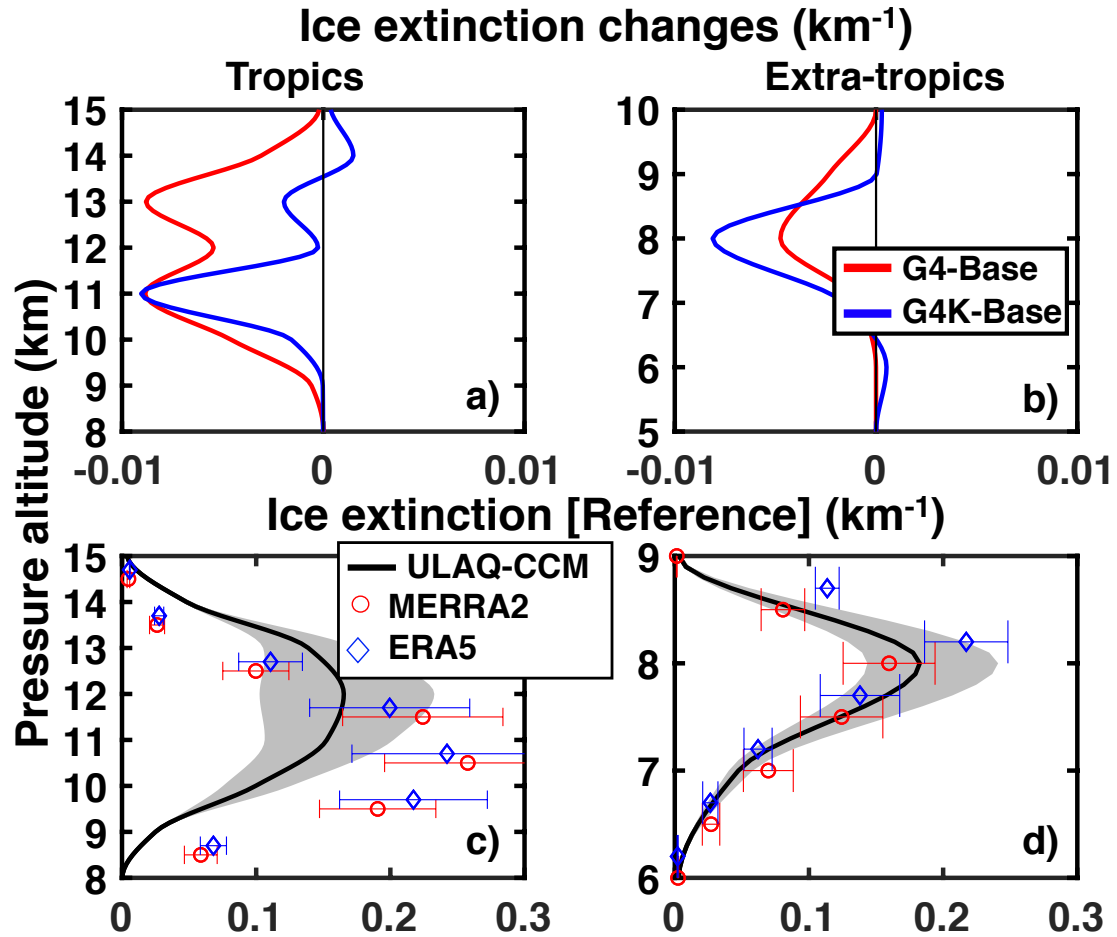


**Figure 12.** Average upper tropospheric profiles of ice particle extinction ( $\lambda=0.55 \mu\text{m}$ ) ( $\text{km}^{-1}$ ) for the tropics (25S-25N) and extratropics (35S-90S, 35N-90N) in panels (a,c) and (b,d), respectively. Panels (a,b): ice extinction changes for G4-Base (red curves) and G4K-Base (blue curves) (years [2030-39](#)[2030-69](#)). Panels (c,d): comparison of ULAQ-CCM calculated values of ice extinction with indirectly derived values from the [MERRA-MERRA-2](#) and [ERA5](#) ice mass mixing ratio and [MODIS-ULAQ-CCM](#) effective radius (red and blue circles) (see text). The time average is over the years 2003-2012. The shaded areas represent  $\pm 1 \sigma$  for the ensemble over the 10-year period.

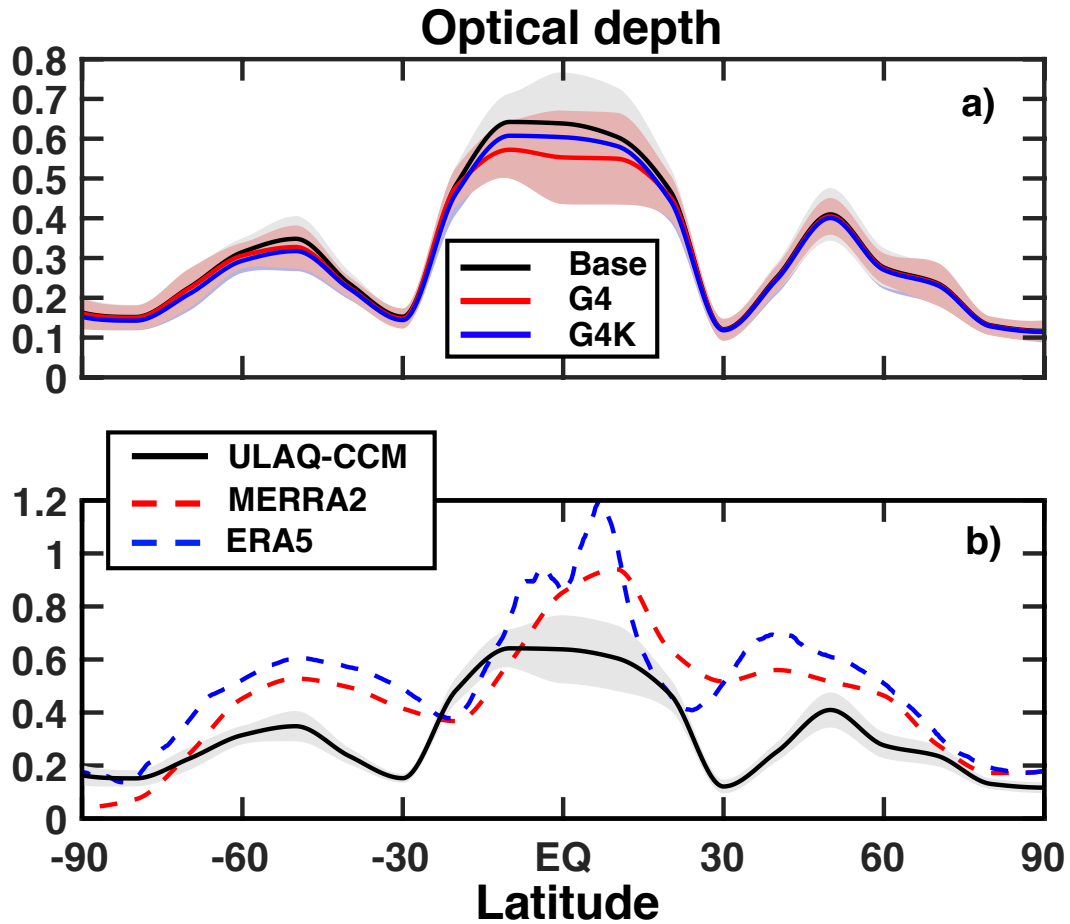


**Figure 13.** Zonally and time-averaged values of the ice optical depth ( $\lambda=0.55 \mu\text{m}$ ) for the ULAQ-CCM Base, G4 and G4K experiments (solid black, red and blue lines, respectively) (panel a) and Base case comparison with the [MERRA+MODIS-MERRA-2](#) and [ERA5](#) indirectly derived values (dashed [black-red](#) and [blue](#) line) (panel b). The model results are for years [2030-39](#)[2030-69](#); the [MERRA+MODIS-MERRA-2](#) and [ERA5](#) data are for years 2003-12. The shaded area represents  $\pm 1 \sigma$  for the ensemble over the [10-year](#)[40-year](#) period [2030-39](#)[2030-69](#).

### 3.2.2 Consequences on radiative forcing

The well-tested radiative transfer code on-line in the ULAQ-CCM (Chou (2001); Randles et al. (2013); SPARC (2013)) has been used to calculate the shortwave and longwave components of the tropopause radiative forcing due to SG aerosols (direct forcing) and to UT ice changes (indirect forcing). As discussed so far, the latter are largely produced by the SG-driven dynamical perturbations on the homogeneous freezing process for ice formation. The ice radiative effects have been calculated using up-to-date wavelength-dependent refractive index available in the literature (Warren (1984); Warren and Brandt (2008); Curtis et al. (2005)) and compared against previous results under similar conditions, such as those by Schumann et al. (2012). All the radiative calculations shown in this section have been performed off-line with the same radiative transfer code as the one present on-line in the ULAQ-CCM model, in order separate the effects of the single components analyzed.

The results are shown separately for the G4 and G4K experiments, both with respect to the RCP4.5 Base case. Following the previously discussed thinning of the UT ice clouds, a positive SW RF is calculated because of the decreased scattering of the incoming solar radiation by the ice particles. However, such an effect is largely covered by the negative LW RF due to a lessened capacity of the ice particles to trap outgoing planetary radiation; therefore, the obtained net effect on RF is negative, as shown in Table 3. This indirect negative RF is smaller but still significant when compared to the negative direct net RF due to the SG aerosols (~30% of it).

It is interesting to note that the shortwave component of the ice RF is indeed smaller than the longwave component, however, not as much as one could expect from the very different normalized RFs (i.e., forcing per unit OD) at a given particle radius. The reason is that both the SW and LW normalized RFs are decreasing with the increasing particle radius, but the relative changes of these normalized RF components are significantly different between the SW and LW. According to our radiative calculations, the SW normalized values decrease (in magnitude) from  $-12.1 \text{ W/m}^2$  to  $-5.7 \text{ W/m}^2$  (-53%) with the ice effective radius increasing from  $15 \mu\text{m}$  to  $40 \mu\text{m}$ , whereas the instantaneous LW normalized RF ~~values remain~~ remains quasi-constant on ~~average value~~ an average value of  $+53 \text{ W/m}^2$ , with a smooth 3% decrease over the same radius interval. The resulting SW RF is then controlled not only by the negative OD changes (-0.020 in G4 and -0.012 G4K) but also by the magnitude of the particle radius increase, which is larger in G4K than in G4, both with respect to the Base case (see discussion of Fig. 10).

25

**Table 3.** Top three rows: globally and time-averaged values of the upper tropospheric ice optical depth changes and RF differences ( $W/m^2$ ) between the SG perturbed experiments and the RCP4.5 Base case due to changes in ice crystal concentration and size. Middle three rows: globally averaged values of stratospheric sulfate aerosol optical depth changes and RF differences ( $W/m^2$ ) defined as above due to changes in aerosol concentration and size. Bottom three rows: total OD and RF changes (i.e., ice + sulfate). All results are for all-sky conditions (i.e., including the presence of background cloudiness) and with an 8 Tg-SO<sub>2</sub>/yr injection. The RFs are calculated at the tropopause with [temperature adjustment of stratospheric temperatures](#). The time average is over the years ~~2030-39~~[2030-69](#).

Exp [all sky]	Ice OD change	RF SW	RF LW	RF Net
G4-Base	<del>-0.020</del> <a href="#">-0.024 ± 0.003</a>	<del>+0.46</del> <a href="#">0.50</a>	<del>-0.83</del> <a href="#">-0.79</a>	<del>-0.37</del> <a href="#">-0.29 ± 0.04</a>
G4K-Base	-0.012 <a href="#">± 0.001</a>	+0.35	<del>-0.53</del> <a href="#">-0.49</a>	<del>-0.18</del> <a href="#">-0.14 ± 0.02</a>
Exp [all sky]	SO <sub>4</sub> OD change	RF SW	RF LW	RF Net
G4-Base	+0.079 <a href="#">± 0.003</a>	-2.03	+0.86	-1.17 <a href="#">± 0.06</a>
G4K-Base	+0.083 <a href="#">± 0.003</a>	-2.14	+0.90	-1.24 <a href="#">± 0.06</a>
Exp [all sky]	Total OD change	RF SW	RF LW	RF Net
G4-Base	<del>-0.020</del> <del>-0.024</del> +0.079	<del>-1.57</del> <del>-1.53</del>	<del>+0.03</del> <del>0.07</del>	<del>-1.54</del> <del>-1.46</del> <a href="#">± 0.10</a>
G4K-Base	-0.012+0.083	-1.79	<del>+0.37</del> <del>0.33</del>	<del>-1.42</del> <del>-1.38</del> <a href="#">± 0.08</a>

**Table 4.** Rearrangement of the results presented in Table 3, with the calculated cloud adjustments (bottom three rows) ~~in~~ [to](#) clear-sky RF components (top three rows). The cloud adjustments for the SW and LW RF contributions are shown separately for the mere presence of background atmospheric clouds (left) and for the cirrus thinning (right): the former is calculated as the difference between the all-sky and clear-sky aerosol RFs, with the all-sky including the background warm clouds and fixed UT ice clouds.

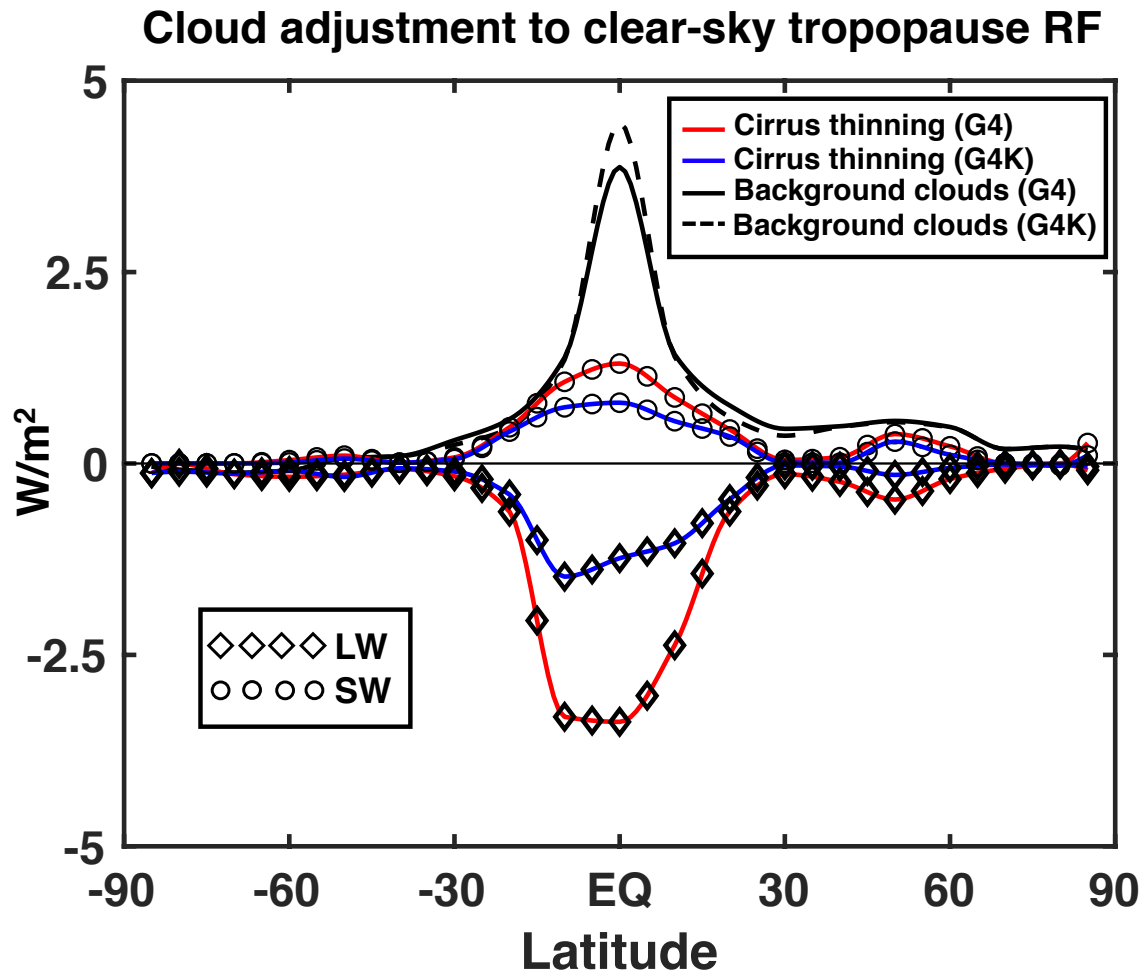
Exp [clear sky]	RF SW		RF LW		RF Net
G4-Base	-3.13		+1.07		-2.06
G4K-Base	-3.30		+1.14		-2.16
Cloud adjustment	RF SW		RF LW		RF Net
G4-Base	+1.10	<del>+0.46</del> <del>0.50</del>	-0.21	<del>-0.83</del> <del>-0.79</del>	+0.60
G4K-Base	+1.16	+0.35	-0.24	<del>-0.53</del> <del>-0.49</del>	+0.78

Table 4 presents, in a compact form, the globally and time averaged ULAQ-CCM results for the cloud adjustments of clear-sky RF components due to the SG stratospheric aerosols. The SW and LW cloud adjustments are roughly comparable to the ones calculated in Kuebbeler et al. (2012) (+1.11  $W/m^2$  and -0.51  $W/m^2$ , respectively, calculated at the top of atmosphere for an SG experiment with a 5 Tg-SO<sub>2</sub>/yr injection). These numbers could be compared with those obtained in the ULAQ-CCM

5 G4K case (although for an 8 Tg-SO<sub>2</sub>/yr injection), i.e., +1.51  $W/m^2$  and ~~-0.77~~ ~~-0.73~~  $W/m^2$  for SW and LW, respectively, with a net value of +0.52  $W/m^2$  against +0.60  $W/m^2$  in Kuebbeler et al. (2012).

In the (more realistic) G4 simulation performed by the ULAQ-CCM model, the SW cloud adjustment is only slightly smaller

than in the G4K, while a significantly larger negative LW component is calculated. This ends up in a net adjustment of +0.52 W/m<sup>2</sup> in the G4 against +0.72 W/m<sup>2</sup> in the G4K experiment. A latitude-dependent view of these results is presented in Fig. 16. The black solid line shows the net positive adjustment (SW+LW) due to the mere presence of background clouds, ~~whose increased reflectivity enhances the downward-scattered solar radiation by the stratospheric aerosol layer, which substantially~~  
5 ~~alter the radiative fluxes (see also Kuebbeler et al. (2012); Schulz et al. (2006); Stier et al. (2013)). These clouds are kept fixed in the ULAQ-CCM model, using climatological values, and thus do not present changes under the G4 scenario. An estimate of the all-sky RF contribution due to SG-driven changes of background clouds is beyond the purposes of the present study.~~ According to our model calculations, the negative LW is the dominant component of the cloud adjustment due to cirrus ice thinning, and this is particularly true for the more realistic G4 simulation. In this latter case, significantly larger values of the  
10 LW adjustment are found over the tropics with respect to G4K, consistent with the ice extinction profile changes in Fig. 12a. ~~Further informations on the model calculated RFs are shown in Fig. S3, where we show both the Clear-Sky latitudinal distribution of the sulfate aerosols RF (Fig. S3a) for both G4 and G4K and the LW and SW cloud adjustment due to the presence of background clouds for both G4 and G4K (Fig. S3b).~~



**Figure 14.** Cloud-Zonally averaged cloud adjustments in-to the clear-sky SG aerosol RF ( $W/m^2$ ), as a function of latitude (time average 2030-2069). See legends for line meaning. The positive adjustment due to (passive) background clouds (black solid line for G4, black dashed line for G4K) shows the net value (SW+LW), which is, however, largely controlled by the SW contribution (see Table 4 and Fig. S3).

## 4 Conclusions

Sulfate geoengineering is considered, amongst other solar radiation management (SRM) techniques, one of the most promising. One reason for this (and unlike other methods) is that we have a natural proxy for the stratospheric sulfate injection, i.e., past explosive volcanic eruptions in the tropical belt. This does not mean that SG does not still pose some scientific questions that need to be answered thoroughly, as pointed out by MacMartin et al. (2016). For instance, models still show many significant differences regarding the confinement of stratospheric sulfate aerosols in the tropical pipe Pitari et al. (2014).

In recent years, some experiments have been proposed where SG is used to meet different climate targets (MacMartin et al. (2017); Kravitz et al. (2017)). However, to properly do so, a clear understanding is needed of how multiple side effects of this technique can modify the net RF (Visioni et al., 2017a). While some of these effects produce a negligible difference in forcing, such as those from gas species perturbations ( $\text{CH}_4$ ,  $\text{O}_3$ , stratospheric  $\text{H}_2\text{O}$ ) (Visioni et al. (2017b)), this might not be the case for changes produced in the formation of thin cirrus ice clouds.

This latter indirect effect was already analysed in two previous works. Cirisan et al. (2013) looked at the potential impact of IN changes in the UT, finding a negligible positive TOA forcing ( $+0.02 \text{ W/m}^2$ , up to  $0.04 \text{ W/m}^2$ ) due to the number density increase of  $\text{H}_2\text{SO}_4\text{-H}_2\text{O}$  aerosols transported down in the UT from the lower stratosphere. Kuebbeler et al. (2012), on the other hand, have studied the effects of dynamical changes caused by the aerosol-induced stratospheric warming and their consequences on UT ice formation via homogeneous freezing. They found a considerable negative TOA forcing in the longwave spectrum ( $-0.51 \text{ W/m}^2$ ), greatly attributable to the SG-induced ice optical depth reduction. In the present study, we focused on these same indirect dynamical effects, adding the potential impact of the SG aerosol-induced surface cooling (G4 experiment), which was not explicitly considered in the study of Kuebbeler et al. (2012). Their approach was also included for comparison in our study, by means of a sensitivity study (G4K) conducted with the ULAQ-CCM, where we keep the surface temperature fixed at the RCP4.5 baseline values so that we can quantify more precisely the surface cooling impact on the UT thin cirrus clouds.

A compact view of the SG effects on UT ice formation is presented in Fig. 15. On one hand, the aerosol-induced stratospheric warming and surface cooling combined together produce a further atmospheric stabilization with an even larger reduction in tropospheric updraft with respect to the G4K case. This lowers the UT probability for ice supersaturation and thus, with less favourable conditions especially for homogeneous freezing. On the other hand, this ice formation limiting effect is partially counterbalanced by the convectively driven tropospheric cooling, which is not observed in the G4K case.

The resulting changes in ice particle number density and size distribution, when combined, translate into a globally averaged decrease of the ice optical depth ( $\Delta\tau = -0.020$  to  $-0.024$ , at  $\lambda = 0.55 \mu\text{m}$ ), i.e.,  $-5.2$  to  $-6\%$  of the baseline OD. This reduction is larger than the one in G4K relative to the Base case ( $\Delta\tau = -0.012$ ,  $-3.1$  to  $-3\%$ ), pointing to the dominant and controlling role of the reduced updraft velocities. According to our model results, these OD changes (coupled to increases in ice particle effective radii) translate in net tropopause RFs of  $-0.37$  to  $-0.29 \text{ W/m}^2$  and  $-0.18$  to  $-0.14 \text{ W/m}^2$ , for G4 and G4K experiments, respectively,

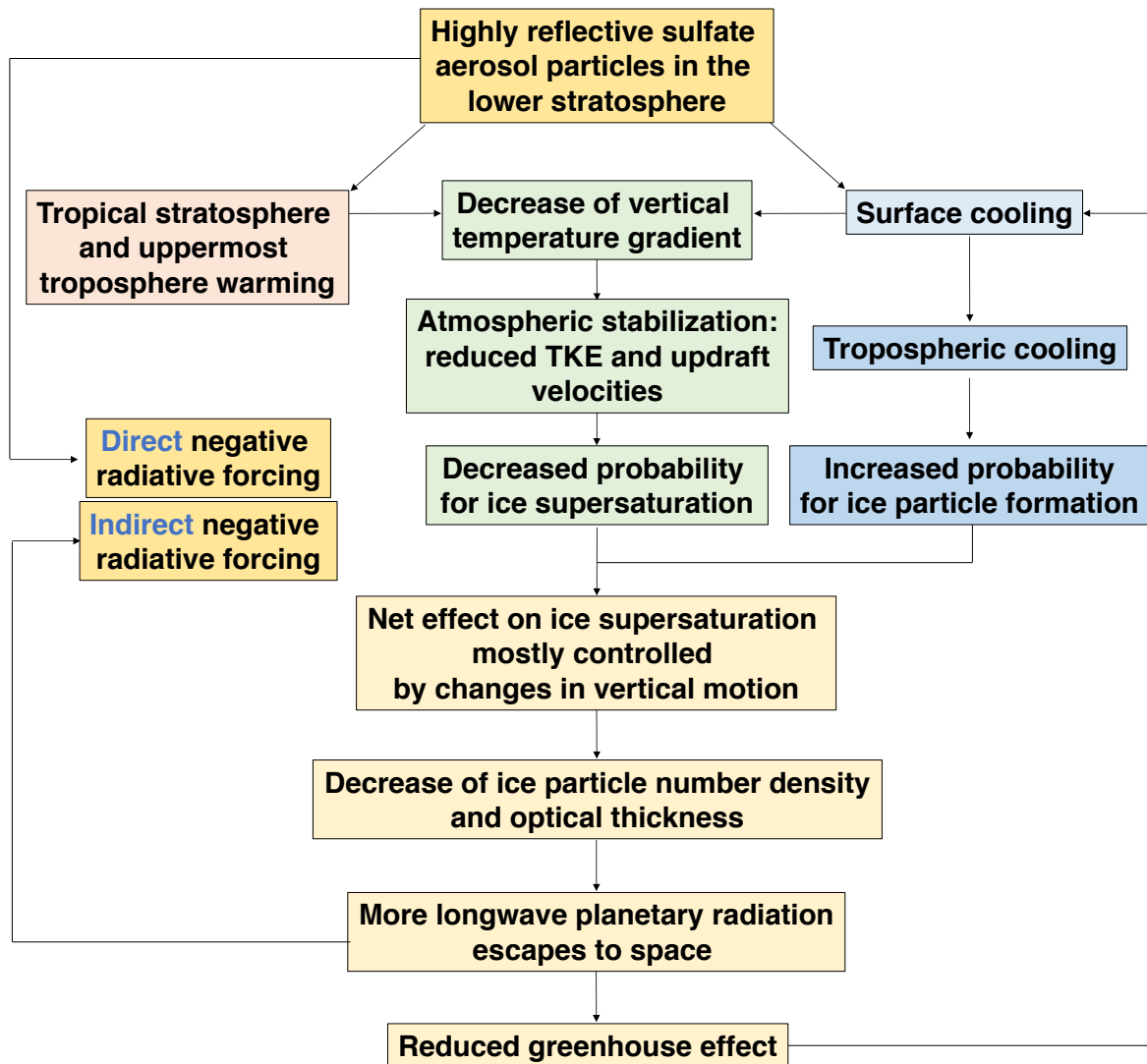


**Figure 15.** Schematic summary of the sulfate geoengineering impact on the dynamical processes driving changes of upper tropospheric ice particle formation through homogeneous freezing.

produced only by the cirrus ice thinning effect of SG. These two cloud adjustments result from a combination of the SW and LW RF contributions, which account for  $+0.46$ – $0.50$   $\text{W/m}^2$  and  $+0.35$   $\text{W/m}^2$  in the SW (for G4 and G4K, respectively) and  $-0.83$ – $0.79$   $\text{W/m}^2$  and  $-0.53$ – $0.49$   $\text{W/m}^2$  in the LW (again for G4 and G4K).

- We can compare these ice thinning forcing contributions with the net tropopause all-sky RF produced by the stratospheric SG aerosols, i.e., of  $-1.17$   $\text{W/m}^2$  and  $-1.24$   $\text{W/m}^2$ , for the G4 and G4K experiments, respectively. According to our model, the

net negative RF due to the cirrus ice cloud thinning is (in G4) close to ~~30~~25% of the direct effect of the sulfate particles themselves. This might have consequences in the definition of the sulfate injection efficiency in terms of RF per Tg-S/yr injected, especially if such efficiency is used to determine the amount of SO<sub>2</sub> that needs to be injected into the stratosphere to achieve climate targets (MacMartin et al. (2017); Kravitz et al. (2017)).

5

Fig. 16 summarizes, in a schematic way, the thermo-dynamical processes leading to the changes in cirrus ice formation and the radiative response caused by these changes in the Earth's radiative balance, as analysed in detail in this paper, together with the direct radiative effect of the sulfate particles.

10 Furthermore, one last consideration is necessary regarding the RFs in the SG scenarios and the unperturbed atmosphere, more specifically, regarding the cloud adjustment to clear-sky RFs due to the stratospheric sulfate aerosols. In our fully interactive aerosol simulation (G4), we obtain a total cloud adjustment (from both cirrus ice thinning and passive background clouds) of ~~+0.52~~-0.60 W/m<sup>2</sup> due to compensating large adjustments in the LW and SW. The SW adjustment results in part from the mere presence of (passive) background clouds and in part from the changing size distribution of UT ice particles.

15 The increasing particle size is more pronounced in the partially interactive aerosol simulation (G4K), thus producing a larger positive SW contribution (~~+0.74~~0.78 W/m<sup>2</sup>).

This latter value is comparable to that calculated in the similar experiment of Kuebbeler et al. (2012) (+0.60 W/m<sup>2</sup>, with a 5 Tg-SO<sub>2</sub> injection). It means that the lower stratospheric warming produced by the SG aerosols acts indirectly on atmospheric dynamics with a strong feedback on the UT cirrus clouds so that a simple reduction of the incoming solar radiation is not a

20 good proxy for the eventual injection of sulfate particles into the stratosphere. When the aerosol-induced surface cooling is coupled to the lower stratospheric warming, the net cloud adjustment is significantly reduced; however, the clear-sky balance of the SW and LW RF contributions is greatly altered by the presence of background clouds coupled to the UT ice thinning.

One important caveat to the conclusions of this study, is that the physical processes behind the UT ice particle formation are

25 highly idealized in our parameterization. Nonetheless, the results it produces in the reference (historical) simulation are generally comparable with the ~~MERRA~~MERRA-2 and ERA5 reanalysis and some satellite data. In addition, the calculated SG dynamical anomalies in the stratosphere are consistent with those from other modelling studies (Pitari et al. (2014); Niemeier and Schmidt (2017)). Finally, taking into account the consistency with the findings from the study of Kuebbeler et al. (2012), we may reasonably conclude that our results regarding the thinning of the UT ice clouds under SG conditions are sufficiently

30 robust. However, considering how complex is the balance between the UT ice formation changes and their radiative forcing is (~~Sanderson et al. (2008)~~; Mitchell et al. (2008)), the results in the present cannot be considered conclusive and exhaustive. Additional results using different and more complete physical parametrizations (both regarding the ice formation processes and a wider range of updraft velocities), together with an on-line ocean coupling, may help clarify the net contribution of ice clouds in a sulfate geoengineering scenario.

35

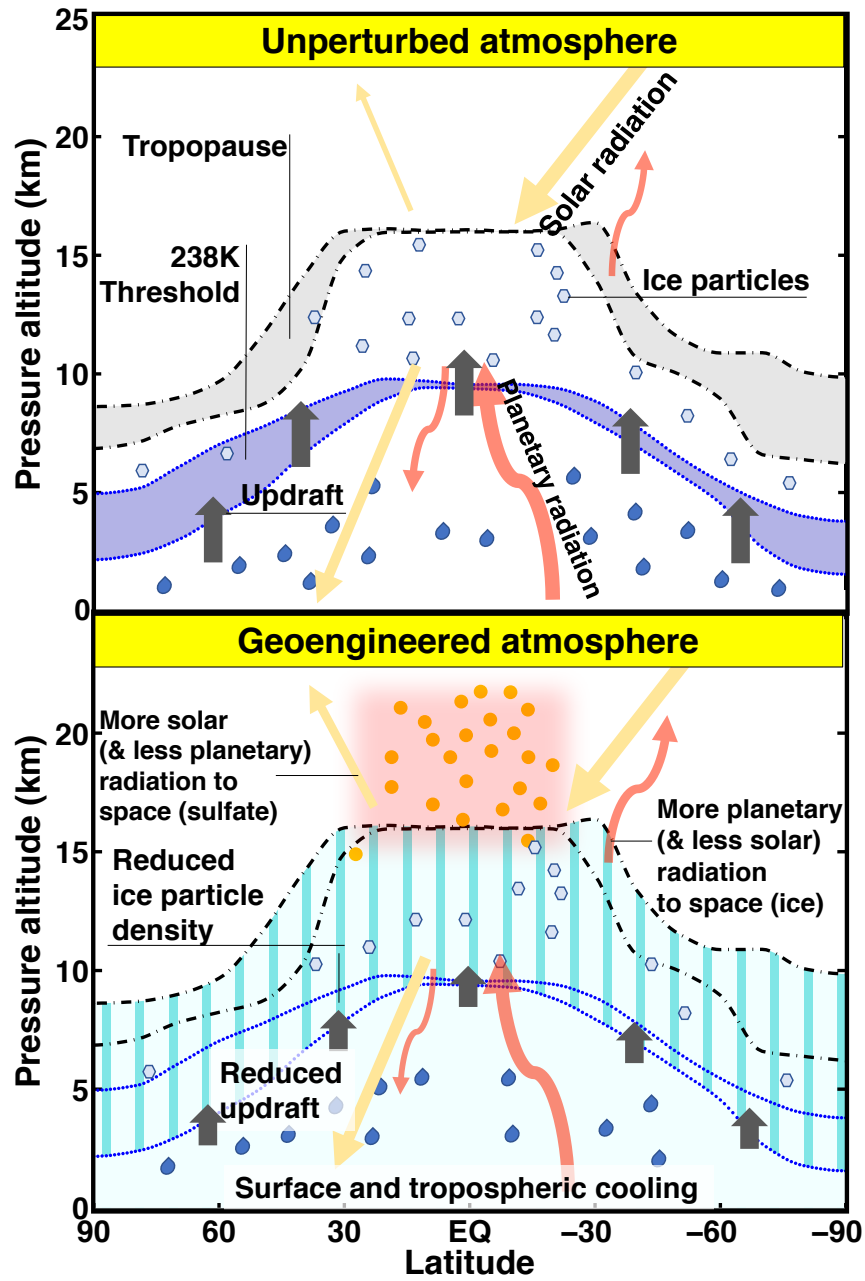


**Figure 16.** Cartoon of the sulfate geoengineering impact on cirrus ice particles formed through freezing and schematic representation of [ice-induced-ice and aerosol](#) changes in radiative fluxes.

*Acknowledgements.* Some of the analyses and visualizations used in this study were produced with the Giovanni online data system, developed and maintained by the NASA GES DISC. We also acknowledge the MODIS mission scientists and associated NASA personnel for the production of the data used in this research effort. One of the authors (GP) would like to thank Bernd Karcher for helpful discussions on the physical processes behind aerosol-ice interactions and for providing the heterogeneous freezing numerical code used in the ULAQ-CCM.

- 5 Finally, the authors are indebted with ~~two~~four anonymous reviewers for their helpful suggestions that improved this study in a significant way.

## References

- Aquila, V., Garfinkel, C., Newman, P., Oman, L., and Waugh, D.: Modifications of the quasi-biennial oscillation by a geoengineering perturbation of the stratospheric aerosol layer, *Geophysical Research Letters*, 41, 1738–1744, 2014.
- Barahona, D., Molod, A., and Kalesse, H.: Direct estimation of the global distribution of vertical velocity within cirrus clouds, *Scientific Reports*, 7, 6840, doi:10.1038/s41598-017-07038-6, <https://doi.org/10.1038/s41598-017-07038-6>, 2017.
- 5 Bosilovich, M. G., Robertson, F. R., Takacs, L., Molod, A., and Mocko, D.: Atmospheric Water Balance and Variability in the MERRA-2 Reanalysis, *Journal of Climate*, 30, 1177–1196, doi:10.1175/JCLI-D-16-0338.1, <https://doi.org/10.1175/JCLI-D-16-0338.1>, 2017.
- Budyko, M. I.: *The Climate of the Future*, American Geophysical Union, doi:10.1002/9781118665251.ch7, <http://dx.doi.org/10.1002/9781118665251.ch7>, 1974.
- 10 Canty, T., Mascioli, N. R., Smarte, M. D., and Salawitch, R. J.: An empirical model of global climate - Part 1: A critical evaluation of volcanic cooling, *Atmospheric Chemistry and Physics*, 13, 3997–4031, doi:10.5194/acp-13-3997-2013, <http://www.atmos-chem-phys.net/13/3997/2013/>, 2013.
- Chen, T., Zhang, Y., and Rossow, W. B.: Sensitivity of Atmospheric Radiative Heating Rate Profiles to Variations of Cloud Layer Overlap, *Journal of Climate*, 13, 2941–2959, doi:10.1175/1520-0442(2000)013<2941:SOARHR>2.0.CO;2, [https://doi.org/10.1175/1520-0442\(2000\)013<2941:SOARHR>2.0.CO;2](https://doi.org/10.1175/1520-0442(2000)013<2941:SOARHR>2.0.CO;2), 2000.
- 15 Chipperfield, M. P., Liang, Q., Strahan, S. E., Morgenstern, O., Dhomse, S. S., Abraham, N. L., Archibald, A. T., Bekki, S., Braesicke, P., Di Genova, G., Fleming, E. L., Hardiman, S. C., Iachetti, D., Jackman, C. H., Kinnison, D. E., Marchand, M., Pitari, G., Pyle, J. A., Rozanov, E., Stenke, A., and Tummon, F.: Multimodel estimates of atmospheric lifetimes of long-lived ozone-depleting substances: Present and future, *Journal of Geophysical Research: Atmospheres*, 119, 2555–2573, doi:10.1002/2013JD021097, <http://dx.doi.org/10.1002/2013JD021097>, 2014.
- 20 Chou, M. M. J. S. X. L.: A thermal infrared radiation parameterization for atmospheric studies, Tech. Rep. TM-2001-104606, NASA, NASA Goddard Space Flight Cent., Greenbelt, MD, 2001.
- Cirisan, A., Spichtinger, P., Luo, B. P., Weisenstein, D. K., Wernli, H., Lohmann, U., and Peter, T.: Microphysical and radiative changes in cirrus clouds by geoengineering the stratosphere, *Journal of Geophysical Research: Atmospheres*, 118, 4533–4548, doi:10.1002/jgrd.50388, <http://dx.doi.org/10.1002/jgrd.50388>, 2013.
- 25 Clegg, S. M. and Abbatt, J. P. D.: Oxidation of SO<sub>2</sub> by H<sub>2</sub>O<sub>2</sub> on ice surfaces at 228 K: a sink for SO<sub>2</sub> in ice clouds, *Atmospheric Chemistry and Physics*, 1, 73–78, doi:10.5194/acp-1-73-2001, <https://www.atmos-chem-phys.net/1/73/2001/>, 2001.
- Crutzen, P. J.: Albedo Enhancement by Stratospheric Sulfur Injections: A Contribution to Resolve a Policy Dilemma?, *Climatic Change*, 77, 211–220, doi:10.1007/s10584-006-9101-y, <http://dx.doi.org/10.1007/s10584-006-9101-y>, 2006.
- 30 Curtis, D. B., Rajaram, B., Toon, O. B., and Tolbert, M. A.: Measurement of the temperature-dependent optical constants of water ice in the 15–200 μm range, *Appl. Opt.*, 44, 4102–4118, doi:10.1364/AO.44.004102, <http://ao.osa.org/abstract.cfm?URI=ao-44-19-4102>, 2005.
- Cziczko, D. J., Froyd, K. D., Gallavardin, S. J., Moehler, O., Benz, S., Saathoff, H., and Murphy, D. M.: Deactivation of ice nuclei due to atmospherically relevant surface coatings, *Environmental Research Letters*, 4, 044 013, <http://stacks.iop.org/1748-9326/4/i=4/a=044013>, 2009.
- 35 Cziczko, D. J., Froyd, K. D., Hoose, C., Jensen, E. J., Diao, M., Zondlo, M. A., Smith, J. B., Twohy, C. H., and Murphy, D. M.: Clarifying the Dominant Sources and Mechanisms of Cirrus Cloud Formation, *Science*, 340, 1320–1324, doi:10.1126/science.1234145, <http://science.sciencemag.org/content/340/6138/1320>, 2013.

- Delanoe, J. and Hogan, R. J.: A variational scheme for retrieving ice cloud properties from combined radar, lidar, and infrared radiometer, *Journal of Geophysical Research: Atmospheres*, 113, doi:10.1029/2007JD009000, <https://agupubs.onlinelibrary.wiley.com/doi/abs/10.1029/2007JD009000>, 2008.
- Duncan, D. I. and Eriksson, P.: An update on global atmospheric ice estimates from satellite observations and reanalyses, *Atmospheric Chemistry and Physics Discussions*, 2018, 1–20, doi:10.5194/acp-2018-275, <https://www.atmos-chem-phys-discuss.net/acp-2018-275/>, 2018.
- Eyring, V., Butchart, N., Waugh, D. W., Akiyoshi, H., Austin, J., Bekki, S., Bodeker, G. E., Boville, B. A., Bruhl, C., Chipperfield, M. P., Cordero, E., Dameris, M., Deushi, M., Fioletov, V. E., Frith, S. M., Garcia, R. R., Gettelman, A., Giorgetta, M. A., Grewe, V., Jourdain, L., Kinnison, D. E., Mancini, E., Manzini, E., Marchand, M., Marsh, D. R., Nagashima, T., Newman, P. A., Nielsen, J. E., Pawson, S., Pitari, G., Plummer, D. A., Rozanov, E., Schraner, M., Shepherd, T. G., Shibata, K., Stolarski, R. S., Struthers, H., Tian, W., and Yoshiki, M.: Assessment of temperature, trace species, and ozone in chemistry-climate model simulations of the recent past, *Journal of Geophysical Research: Atmospheres*, 111, n/a–n/a, doi:10.1029/2006JD007327, d22308, 2006.
- Feichter, J., Kjellstram, E., Rodhe, H., Dentener, F., Lelieveld, J., and Roelofs, G.-J.: Simulation of the tropospheric sulfur cycle in a global climate model, *Atmospheric Environment*, 30, 1693 – 1707, doi:[https://doi.org/10.1016/1352-2310\(95\)00394-0](https://doi.org/10.1016/1352-2310(95)00394-0), <http://www.sciencedirect.com/science/article/pii/1352231095003940>, joint 8th CAGCP and 2nd IGAC Conference on Global Atmospheric Chemistry, 1996.
- Friberg, J., Martinsson, B. G., Sporre, M. K., Andersson, S. M., Brenninkmeijer, C. A. M., Hermann, M., Velthoven, P. F. J., and Zahn, A.: Influence of volcanic eruptions on midlatitude upper tropospheric aerosol and consequences for cirrus clouds, *Earth and Space Science*, 2, 285–300, doi:10.1002/2015EA000110, <https://agupubs.onlinelibrary.wiley.com/doi/abs/10.1002/2015EA000110>, 2005.
- Fusina, F., Spichtinger, P., and Lohmann, U.: Impact of ice supersaturated regions and thin cirrus on radiation in the midlatitudes, *Journal of Geophysical Research: Atmospheres*, 112, n/a–n/a, doi:10.1029/2007JD008449, <http://dx.doi.org/10.1029/2007JD008449>, d24S14, 2007.
- Gasparini, B. and Lohmann, U.: Why cirrus cloud seeding cannot substantially cool the planet, *Journal of Geophysical Research: Atmospheres*, 121, 4877–4893, doi:10.1002/2015JD024666, <https://agupubs.onlinelibrary.wiley.com/doi/abs/10.1002/2015JD024666>, 2016.
- Gasparini, B., Munch, S., Poncet, L., Feldmann, M., and Lohmann, U.: Is increasing ice crystal sedimentation velocity in geoengineering simulations a good proxy for cirrus cloud seeding?, *Atmospheric Chemistry and Physics*, 17, 4871–4885, doi:10.5194/acp-17-4871-2017, <https://www.atmos-chem-phys.net/17/4871/2017/>, 2017.
- Gelaro, R., McCarty, W., Suárez, M. J., Todling, R., Molod, A., Takacs, L., Randles, C. A., Darmenov, A., Bosilovich, M. G., Reichle, R., Wargan, K., Coy, L., Cullather, R., Draper, C., Akella, S., Buchard, V., Conaty, A., da Silva, A. M., Gu, W., Kim, G.-K., Koster, R., Lucchesi, R., Merkova, D., Nielsen, J. E., Partyka, G., Pawson, S., Putman, W., Rienecker, M., Schubert, S. D., Sienkiewicz, M., and Zhao, B.: The Modern-Era Retrospective Analysis for Research and Applications, Version 2 (MERRA-2), *Journal of Climate*, 30, 5419–5454, doi:10.1175/JCLI-D-16-0758.1, <https://doi.org/10.1175/JCLI-D-16-0758.1>, 2017.
- Gettelman, A., Liu, X., Ghan, S. J., Morrison, H., Park, S., Conley, A. J., Klein, S. A., Boyle, J., Mitchell, D. L., and Li, J.-L. F.: Global simulations of ice nucleation and ice supersaturation with an improved cloud scheme in the Community Atmosphere Model, *Journal of Geophysical Research: Atmospheres*, 115, n/a–n/a, doi:10.1029/2009JD013797, <http://dx.doi.org/10.1029/2009JD013797>, d18216, 2010.
- Hegglin, M. I., Gettelman, A., Hoor, P., Krichevsky, R., Manney, G. L., Pan, L. L., Son, S.-W., Stiller, G., Tilmes, S., Walker, K. A., Eyring, V., Shepherd, T. G., Waugh, D., Akiyoshi, H., Anel, J. A., Austin, J., Baumgaertner, A., Bekki, S., Braesicke, P., Bruhl, C., Butchart, N., Chipperfield, M. P., Dameris, M., Dhomse, S., Frith, S., Garny, H., Hardiman, S. C., Jockel, P., Kinnison, D. E., Lamarque, J. F., Mancini, E., Michou, M., Morgenstern, O., Nakamura, T., Olivie, D., Pawson, S., Pitari, G., Plummer, D. A., Pyle, J. A., Rozanov, E., Scinocca, J. F., Shibata, K., Smale, D., Teyssedre, H., Tian, W., and Yamashita, Y.: Multimodel assessment of the upper troposphere

- and lower stratosphere: Extra-tropics, *Journal of Geophysical Research: Atmospheres*, 115, D00M09, doi:10.1029/2010JD013884, <https://hal.archives-ouvertes.fr/hal-00510687>, 2010.
- Hendricks, J., Karcher, B., and Lohmann, U.: Effects of ice nuclei on cirrus clouds in a global climate model, *Journal of Geophysical Research: Atmospheres*, 116, doi:10.1029/2010JD015302, <http://dx.doi.org/10.1029/2010JD015302>, d18206, 2011.
- 5 Karcher, B. and Lohmann, U.: A parameterization of cirrus cloud formation: Homogeneous freezing of supercooled aerosols, *Journal of Geophysical Research: Atmospheres*, 107, doi:10.1029/2001JD000470, <http://dx.doi.org/10.1029/2001JD000470>, 2002.
- Kleinschmitt, C., Boucher, O., and Platt, U.: Sensitivity of the radiative forcing by stratospheric sulfur geoengineering to the amount and strategy of the SO<sub>2</sub> injection studied with the LMDZ-S3A model, *Atmospheric Chemistry and Physics Discussions*, 2017, 1–34, doi:10.5194/acp-2017-722, <https://www.atmos-chem-phys-discuss.net/acp-2017-722/>, 2017.
- 10 Kravitz, B., Robock, A., Boucher, O., Schmidt, H., Taylor, K. E., Stenchikov, G., and Schulz, M.: The Geoengineering Model Intercomparison Project (GeoMIP), *Atmospheric Science Letters*, 12, 162–167, doi:10.1002/asl.316, <http://dx.doi.org/10.1002/asl.316>, 2011.
- Kravitz, B., Robock, A., and Irvine, P.: Robust Results From Climate Model Simulations of Geoengineering, *Eos, Transactions American Geophysical Union*, 94, 292–292, doi:10.1002/2013EO330005, <http://dx.doi.org/10.1002/2013EO330005>, 2013.
- Kravitz, B., MacMartin, D. G., Mills, M. J., Richter, J. H., Tilmes, S., Lamarque, J.-F., Tribbia, J. J., and Vitt, F.: First Simulations of Design-  
15 ing Stratospheric Sulfate Aerosol Geoengineering to Meet Multiple Simultaneous Climate Objectives, *Journal of Geophysical Research: Atmospheres*, 122, 12,616–12,634, doi:10.1002/2017JD026874, <http://dx.doi.org/10.1002/2017JD026874>, 2017JD026874, 2017.
- Kuebbeler, M., Lohmann, U., and Feichter, J.: Effects of stratospheric sulfate aerosol geo-engineering on cirrus clouds, *Geophysical Research Letters*, 39, doi:10.1029/2012GL053797, <http://dx.doi.org/10.1029/2012GL053797>, l23803, 2012.
- Lamarque, J.-F., Emmons, L. K., Hess, P. G., Kinnison, D. E., Tilmes, S., Vitt, F., Heald, C. L., Holland, E. A., Lauritzen, P. H.,  
20 Neu, J., Orlando, J. J., Rasch, P. J., and Tyndall, G. K.: CAM-chem: description and evaluation of interactive atmospheric chemistry in the Community Earth System Model, *Geoscientific Model Development*, 5, 369–411, doi:10.5194/gmd-5-369-2012, <https://www.geosci-model-dev.net/5/369/2012/>, 2012.
- Lohmann, U. and Karcher, B.: First interactive simulations of cirrus clouds formed by homogeneous freezing in the ECHAM general circulation model, *Journal of Geophysical Research: Atmospheres*, 107, AAC 8–1–AAC 8–13, doi:10.1029/2001JD000767, <http://dx.doi.org/10.1029/2001JD000767>,  
25 <http://dx.doi.org/10.1029/2001JD000767>, 2002.
- Long, C. S. and Stowe, L. L.: using the NOAA/AVHRR to study stratospheric aerosol optical thicknesses following the Mt. Pinatubo Eruption, *Geophysical Research Letters*, 21, 2215–2218, doi:10.1029/94GL01322, <http://dx.doi.org/10.1029/94GL01322>, 1994.
- MacMartin, D. G., Kravitz, B., Long, J. C. S., and Rasch, P. J.: Geoengineering with stratospheric aerosols: What do we not know after a decade of research?, *Earth's Future*, 4, 543–548, doi:10.1002/2016EF000418, <http://dx.doi.org/10.1002/2016EF000418>, 2016EF000418,  
30 2016.
- MacMartin, D. G., Kravitz, B., Tilmes, S., Richter, J. H., Mills, M. J., Lamarque, J.-F., Tribbia, J. J., and Vitt, F.: The Climate Response to Stratospheric Aerosol Geoengineering Can Be Tailored Using Multiple Injection Locations, *Journal of Geophysical Research: Atmospheres*, 122, 12,574–12,590, doi:10.1002/2017JD026868, <http://dx.doi.org/10.1002/2017JD026868>, 2017JD026868, 2017.
- Meyer, K., Platnick, S., and Zhang, Z.: Simultaneously inferring above-cloud absorbing aerosol optical thickness and underlying liquid phase cloud optical and microphysical properties using MODIS, *Journal of Geophysical Research: Atmospheres*, 120, 5524–5547, doi:10.1002/2015JD023128, <https://agupubs.onlinelibrary.wiley.com/doi/abs/10.1002/2015JD023128>, 2015.

- Mitchell, D. L., Rasch, P., Ivanova, D., McFarquhar, G., and Nousiainen, T.: Impact of small ice crystal assumptions on ice sedimentation rates in cirrus clouds and GCM simulations, *Geophysical Research Letters*, 35, n/a–n/a, doi:10.1029/2008GL033552, <http://dx.doi.org/10.1029/2008GL033552>, 109806, 2008.
- Morgenstern, O., Giorgetta, M. A., Shibata, K., Eyring, V., Waugh, D. W., Shepherd, T. G., Akiyoshi, H., Austin, J., Baumgaertner, A., J. G., Bekki, S., Braesicke, P., Bruhl, C., Chipperfield, M. P., Cugnet, D., Dameris, M., Dhomse, S., Frith, S. M., Garny, H., Gettelman, A., Hardiman, S. C., Hegglin, M. I., Jockel, P., Kinnison, D. E., Lamarque, J.-F., Mancini, E., Manzini, E., Marchand, M., Michou, M., Nakamura, T., Nielsen, J. E., Olivie, D., Pitari, G., Plummer, D. A., Rozanov, E., Scinocca, J. F., Smale, D., Teyssedre, H., Toohey, M., Tian, W., and Yamashita, Y.: Review of the formulation of present-generation stratospheric chemistry-climate models and associated external forcings, *Journal of Geophysical Research: Atmospheres*, 115, n/a–n/a, doi:10.1029/2009JD013728, <http://dx.doi.org/10.1029/2009JD013728>, d00M02, 2010.
- Morgenstern, O., Hegglin, M. I., Rozanov, E., O'Connor, F. M., Abraham, N. L., Akiyoshi, H., Archibald, A. T., Bekki, S., Butchart, N., Chipperfield, M. P., Deushi, M., Dhomse, S. S., Garcia, R. R., Hardiman, S. C., Horowitz, L. W., Jockel, P., Josse, B., Kinnison, D., Lin, M., Mancini, E., Manyin, M. E., Marchand, M., Marecal, V., Michou, M., Oman, L. D., Pitari, G., Plummer, D. A., Revell, L. E., Saint-Martin, D., Schofield, R., Stenke, A., Stone, K., Sudo, K., Tanaka, T. Y., Tilmes, S., Yamashita, Y., Yoshida, K., and Zeng, G.: Review of the global models used within phase 1 of the Chemistry–Climate Model Initiative (CCMI), *Geoscientific Model Development*, 10, 639–671, doi:10.5194/gmd-10-639-2017, <https://www.geosci-model-dev.net/10/639/2017/>, 2017.
- Neale, R. B., Richter, J., Park, S., Lauritzen, P. H., Vavrus, S. J., Rasch, P. J., and Zhang, M.: The Mean Climate of the Community Atmosphere Model (CAM4) in Forced SST and Fully Coupled Experiments, *Journal of Climate*, 26, 5150–5168, doi:10.1175/JCLI-D-12-00236.1, <https://doi.org/10.1175/JCLI-D-12-00236.1>, 2013.
- Niemeier, U. and Schmidt, H.: Changing transport processes in the stratosphere by radiative heating of sulfate aerosols, *Atmospheric Chemistry and Physics*, 17, 14 871–14 886, doi:10.5194/acp-17-14871-2017, <https://www.atmos-chem-phys.net/17/14871/2017/>, 2017.
- Niemeier, U. and Tilmes, S.: Sulfur injections for a cooler planet, *Science*, 357, 246–248, doi:10.1126/science.aan3317, <http://science.sciencemag.org/content/357/6348/246>, 2017.
- Pitari, G.: A Numerical Study of the Possible Perturbation of Stratospheric Dynamics Due to Pinatubo Aerosols: Implications for Tracer Transport, *Journal of the Atmospheric Sciences*, 50, 2443–2461, doi:10.1175/1520-0469(1993)050<2443:ANSOTP>2.0.CO;2, [https://doi.org/10.1175/1520-0469\(1993\)050<2443:ANSOTP>2.0.CO;2](https://doi.org/10.1175/1520-0469(1993)050<2443:ANSOTP>2.0.CO;2), 1993.
- Pitari, G., Mancini, E., Rizi, V., and Shindell, D. T.: Impact of Future Climate and Emission Changes on Stratospheric Aerosols and Ozone, *Journal of the Atmospheric Sciences*, 59, 414–440, doi:10.1175/1520-0469(2002)059<0414:IOFCAE>2.0.CO;2, [https://doi.org/10.1175/1520-0469\(2002\)059<0414:IOFCAE>2.0.CO;2](https://doi.org/10.1175/1520-0469(2002)059<0414:IOFCAE>2.0.CO;2), 2002.
- Pitari, G., Aquila, V., Kravitz, B., Robock, A., Watanabe, S., Cionni, I., De Luca, N., Di Genova, G., Mancini, E., and Tilmes, S.: Stratospheric ozone response to sulfate geoengineering: Results from the Geoengineering Model Intercomparison Project (GeoMIP), *Journal of Geophysical Research: Atmospheres*, 119, 2629–2653, 2014.
- Pitari, G., Cionni, I., Di Genova, G., Visionsi, D., Gandolfi, I., and Mancini, E.: Impact of Stratospheric Volcanic Aerosols on Age-of-Air and Transport of Long-Lived Species, *Atmosphere*, 7, <http://www.mdpi.com/2073-4433/7/11/149>, 2016a.
- Pitari, G., Di Genova, G., Mancini, E., Visionsi, D., Gandolfi, I., and Cionni, I.: Stratospheric Aerosols from Major Volcanic Eruptions: A Composition-Climate Model Study of the Aerosol Cloud Dispersal and e-folding Time, *Atmosphere*, 7, 75, doi:10.3390/atmos7060075, <http://dx.doi.org/10.3390/atmos7060075>, 2016b.

- Pitari, G., Visionsi, D., Mancini, E., Cionni, I., Di Genova, G., and Gandolfi, I.: Sulfate Aerosols from Non-Explosive Volcanoes: Chemical-Radiative Effects in the Troposphere and Lower Stratosphere, *Atmosphere*, 7, doi:10.3390/atmos7070085, <http://www.mdpi.com/2073-4433/7/7/85>, 2016c.
- Randles, C. A., Kinne, S., Myhre, G., Schulz, M., Stier, P., Fischer, J., Doppler, L., Highwood, E., Ryder, C., Harris, B., Huttunen, J., Ma, Y., Pinker, R. T., Mayer, B., Neubauer, D., Hitzenberger, R., Oreopoulos, L., Lee, D., Pitari, G., Di Genova, G., Quaas, J., Rose, F. G., Kato, S., Rumbold, S. T., Vardavas, I., Hatzianastassiou, N., Matsoukas, C., Yu, H., Zhang, F., Zhang, H., and Lu, P.: Intercomparison of shortwave radiative transfer schemes in global aerosol modeling: results from the AeroCom Radiative Transfer Experiment, *Atmospheric Chemistry and Physics*, 13, 2347–2379, doi:10.5194/acp-13-2347-2013, <http://www.atmos-chem-phys.net/13/2347/2013/>, 2013.
- Robock, A.: Volcanic eruptions and climate, *Reviews of Geophysics*, 38, 191–219, doi:10.1029/1998RG000054, <http://dx.doi.org/10.1029/1998RG000054>, 2000.
- Sanderson, B. M., Piani, C., Ingram, W. J., Stone, D. A., and Allen, M. R.: Towards constraining climate sensitivity by linear analysis of feedback patterns in thousands of perturbed-physics GCM simulations, *Climate Dynamics*, 30, 175–190, doi:10.1007/s00382-007-0280-7, <https://doi.org/10.1007/s00382-007-0280-7>, 2008.
- Sassen, K., Starr, D. O., Mace, G. G., Poellot, M. R., Melfi, S., Eberhard, W. L., Spinhirne, J. D., Eloranta, E., Hagen, D. E., and Hallett, J.: The 5–6 December 1991 FIRE IFO II Jet Stream Cirrus Case Study: Possible Influences of Volcanic Aerosols, *Journal of the Atmospheric Sciences*, 52, 97–123, doi:10.1175/1520-0469(1995)052<0097:TDFIJI>2.0.CO;2, 1995.
- Schulz, M., Textor, C., Kinne, S., Balkanski, Y., Bauer, S., Berntsen, T., Berglen, T., Boucher, O., Dentener, F., Guibert, S., Isaksen, I. S. A., Iversen, T., Koch, D., Kirkevåg, A., Liu, X., Montanaro, V., Myhre, G., Penner, J. E., Pitari, G., Reddy, S., Seland, Ø., Stier, P., and Takemura, T.: Radiative forcing by aerosols as derived from the AeroCom present-day and pre-industrial simulations, *Atmospheric Chemistry and Physics*, 6, 5225–5246, doi:10.5194/acp-6-5225-2006, <https://www.atmos-chem-phys.net/6/5225/2006/>, 2006.
- Schumann, U., Mayer, B., Graf, K., and Mannstein, H.: A Parametric Radiative Forcing Model for Contrail Cirrus, *Journal of Applied Meteorology and Climatology*, 51, 1391–1406, doi:10.1175/JAMC-D-11-0242.1, <https://doi.org/10.1175/JAMC-D-11-0242.1>, 2012.
- SPARC: Chapter 5: Model Estimates of Lifetimes in SPARC Report on Lifetimes of Stratospheric Ozone-Depleting Substances, Their Replacements, and Related Species. Chipperfield, M. and Q. Liang, et al., Tech. rep., SPARC, <http://www.sparc-climate.org/publications/sparc-reports/>, 2013.
- Stephens, G., Benedetti, A., Gabriel, P., and Vane, D.: Cloud assimilation in the era of CLOUDSAT, in: ECMWF/EuroTRMM Workshop on the Assimilation of Clouds and Precipitation, 6–9 November 2000, pp. 19–34, ECMWF, ECMWF, Shinfield Park, Reading, 2000.
- Stier, P., Schutgens, N. A. J., Bellouin, N., Bian, H., Boucher, O., Chin, M., Ghan, S., Huneeus, N., Kinne, S., Lin, G., Ma, X., Myhre, G., Penner, J. E., Randles, C. A., Samset, B., Schulz, M., Takemura, T., Yu, F., Yu, H., and Zhou, C.: Host model uncertainties in aerosol radiative forcing estimates: results from the AeroCom Prescribed intercomparison study, *Atmospheric Chemistry and Physics*, 13, 3245–3270, doi:10.5194/acp-13-3245-2013, <https://www.atmos-chem-phys.net/13/3245/2013/>, 2013.
- Storelvmo, T. and Herger, N.: Cirrus cloud susceptibility to the injection of ice nuclei in the upper troposphere, *Journal of Geophysical Research: Atmospheres*, 119, 2375–2389, doi:10.1002/2013JD020816, <https://agupubs.onlinelibrary.wiley.com/doi/abs/10.1002/2013JD020816>, 2014.
- Strom, J., Strauss, B., Anderson, T., Schrader, F., Heintzenberg, J., and Wendling, P.: In Situ Observations of the Microphysical Properties of Young Cirrus Clouds, *Journal of the Atmospheric Sciences*, 54, 2542–2553, doi:10.1175/1520-0469(1997)054<2542:ISOOTM>2.0.CO;2, [http://dx.doi.org/10.1175/1520-0469\(1997\)054<2542:ISOOTM>2.0.CO;2](http://dx.doi.org/10.1175/1520-0469(1997)054<2542:ISOOTM>2.0.CO;2), 1997.

- Taylor, K. E., Stouffer, R. J., and Meehl, G. A.: An overview of CMIP5 and the experiment design, *Bulletin of the American Meteorological Society*, 93, 485, 2012.
- Thomason, L. W., Poole, L. R., and Deshler, T.: A global climatology of stratospheric aerosol surface area density deduced from Stratospheric Aerosol and Gas Experiment II measurements: 1984–1994, *Journal of Geophysical Research: Atmospheres*, 102, 8967–8976, doi:10.1029/96JD02962, <http://dx.doi.org/10.1029/96JD02962>, 1997.
- 5 Tilmes, S., Muller, R., and Salawitch, R.: The Sensitivity of Polar Ozone Depletion to Proposed Geoengineering Schemes, *Science*, 320, 1201–1204, doi:10.1126/science.1153966, <http://science.sciencemag.org/content/320/5880/1201>, 2008.
- Tilmes, S., Garcia, R. R., Kinnison, D. E., Gettelman, A., and Rasch, P. J.: Impact of geoengineered aerosols on the troposphere and stratosphere, *Journal of Geophysical Research: Atmospheres*, 114, doi:10.1029/2008JD011420, <http://dx.doi.org/10.1029/2008JD011420>, d12305, 2009.
- 10 Tilmes, S., Mills, M. J., Niemeier, U., Schmidt, H., Robock, A., Kravitz, B., Lamarque, J.-F., Pitari, G., and English, J. M.: A new Geoengineering Model Intercomparison Project (GeoMIP) experiment designed for climate and chemistry models, *Geoscientific Model Development*, 8, 43–49, doi:10.5194/gmd-8-43-2015, <https://www.geosci-model-dev.net/8/43/2015/>, 2015.
- Tilmes, S., Lamarque, J.-F., Emmons, L. K., Kinnison, D. E., Marsh, D., Garcia, R. R., Smith, A. K., Neely, R. R., Conley, A., Vitt, F., Val Martin, M., Tanimoto, H., Simpson, I., Blake, D. R., and Blake, N.: Representation of the Community Earth System Model (CESM1) CAM4-chem within the Chemistry-Climate Model Initiative (CCMI), *Geoscientific Model Development*, 9, 1853–1890, doi:10.5194/gmd-9-1853-2016, <https://www.geosci-model-dev.net/9/1853/2016/>, 2016.
- 15 Tilmes, S., Richter, J. H., Mills, M. J., Kravitz, B., MacMartin, D. G., Vitt, F., Tribbia, J. J., and Lamarque, J.-F.: Sensitivity of Aerosol Distribution and Climate Response to Stratospheric SO<sub>2</sub> Injection Locations, *Journal of Geophysical Research: Atmospheres*, pp. n/a–n/a, doi:10.1002/2017JD026888, <http://dx.doi.org/10.1002/2017JD026888>, 2017JD026888, 2017.
- 20 Visioni, D., Pitari, G., and Aquila, V.: Sulfate geoengineering: a review of the factors controlling the needed injection of sulfur dioxide, *Atmos. Chem. Phys.*, 17, 3879–3889, doi:10.5194/acp-17-3879-2017, <http://www.atmos-chem-phys.net/17/3879/2017/>, 2017a.
- Visioni, D., Pitari, G., Aquila, V., Tilmes, S., Cionni, I., Di Genova, G., and Mancini, E.: Sulfate geoengineering impact on methane transport and lifetime: results from the Geoengineering Model Intercomparison Project (GeoMIP), *Atmospheric Chemistry and Physics*, 17, 11 209–11 226, doi:10.5194/acp-17-11209-2017, <https://www.atmos-chem-phys.net/17/11209/2017/>, 2017b.
- 25 Visioni, D., Pitari, G., Tuccella, P., and Curci, G.: Sulfur deposition changes under sulfate geoengineering conditions: quasi-biennial oscillation effects on the transport and lifetime of stratospheric aerosols, *Atmospheric Chemistry and Physics*, 18, 2787–2808, doi:10.5194/acp-18-2787-2018, <https://www.atmos-chem-phys.net/18/2787/2018/>, 2018.
- Warren, S. G.: Optical constants of ice from the ultraviolet to the microwave, *Appl. Opt.*, 23, 1206–1225, doi:10.1364/AO.23.001206, <http://ao.osa.org/abstract.cfm?URI=ao-23-8-1206>, 1984.
- 30 Warren, S. G. and Brandt, R. E.: Optical constants of ice from the ultraviolet to the microwave: A revised compilation, *Journal of Geophysical Research: Atmospheres*, 113, doi:10.1029/2007JD009744, <https://agupubs.onlinelibrary.wiley.com/doi/abs/10.1029/2007JD009744>, 2008.
- Wu, D. L., Jiang, J. H., Read, W. G., Austin, R. T., Davis, C. P., Lambert, A., Stephens, G. L., Vane, D. G., and Waters, J. W.: Validation of the Aura MLS cloud ice water content measurements, *Journal of Geophysical Research: Atmospheres*, 113, doi:10.1029/2007JD008931, <https://agupubs.onlinelibrary.wiley.com/doi/abs/10.1029/2007JD008931>, 2008.
- 35

Xia, L., Nowack, P. J., Tilmes, S., and Robock, A.: Impacts of Stratospheric Sulfate Geoengineering on Tropospheric Ozone, *Atmospheric Chemistry and Physics Discussions*, 2017, 1–38, doi:10.5194/acp-2017-434, <http://www.atmos-chem-phys-discuss.net/acp-2017-434/>, 2017.

5 Yang, P., Zhang, L., Hong, G., Nasiri, S. L., Baum, B. A., Huang, H. L., King, M. D., and Platnick, S.: Differences Between Collection 4 and 5 MODIS Ice Cloud Optical/Microphysical Products and Their Impact on Radiative Forcing Simulations, *IEEE Transactions on Geoscience and Remote Sensing*, 45, 2886–2899, doi:10.1109/TGRS.2007.898276, 2007.

Zhang, Z., Platnick, S., Yang, P., Heidinger, A. K., and Comstock, J. M.: Effects of ice particle size vertical inhomogeneity on the passive remote sensing of ice clouds, *Journal of Geophysical Research: Atmospheres*, 115, doi:10.1029/2010JD013835, <https://agupubs.onlinelibrary.wiley.com/doi/abs/10.1029/2010JD013835>, 2010.